

**FACTORS AFFECTING PROPERTIES OF RICE HUSK  
SILICA/POLY(BUTYLENE ADIPATE-CO-  
TEREPHTHALATE) COMPOSITES**

**Jirapa Phosee**

**A Thesis Submitted in Partial Fulfillment of the Requirements for the  
Degree of Master of Engineering in Polymer Engineering**

**Suranaree University of Technology**

**Academic Year 2011**

ตัวแปรที่มีผลต่อสมบัติของวัสดุเชิงประกอบระหว่างซีลิกาจากแกลบข้าว  
และพอลิบิวทีลีนอะดิเพตเทอเรพธาลเตต

นางสาวจิรภา โปธิศรี

วิทยานิพนธ์นี้เป็นส่วนหนึ่งของการศึกษาตามหลักสูตรปริญญาวิศวกรรมศาสตรมหาบัณฑิต  
สาขาวิชาวิศวกรรมพอลิเมอร์  
มหาวิทยาลัยเทคโนโลยีสุรนารี  
ปีการศึกษา 2554

**FACTORS AFFECTING PROPERTIES OF RICE HUSK  
SILICA/POLY (BUTYLENE ADIPATE-CO-  
TEREPHTHALATE) COMPOSITES**

Suranaree University of Technology has approved this thesis submitted in partial fulfillments of the requirements for a Master's Degree.

Thesis Examining Committee

---

(Asst. Prof. Dr. Wimonlak Sutapun)

Chairperson

---

(Asst. Prof. Dr. Nitinat Suppakarn)

Member (Thesis Advisor)

---

(Assoc. Prof. Dr. Jatuporn Wittayakun)

Member

---

(Asst. Prof. Dr. Kasama Jarukumjorn)

Member

---

(Asst. Prof. Dr. Pranee Chumsumrong)

Member

---

(Prof. Dr. Sukit Limpijumnong)

Vice Rector for Academic Affairs

---

(Assoc. Prof. Flt.Lt.Dr. Kontorn Chamniprasart)

Dean of Institute of Engineering



จิรภา โปธิศรี : ตัวแปรที่มีผลต่อสมบัติของวัสดุเชิงประกอบระหว่างซิลิกาจากแกลบข้าว และพอลิเมอร์ที่ลีนอะดิเพตเทอเรพธาลेट (FACTORS AFFECTING PROPERTIES OF RICE HUSK SILICA/POLY (BUTYLENE ADIPATE-CO-TEREPHTHALATE) COMPOSITES) อาจารย์ที่ปรึกษา : ผู้ช่วยศาสตราจารย์ ดร. นิธินาถ ศุกกาญจน์, 130 หน้า.

ในการศึกษานี้ ซิลิกาจากแกลบข้าวในรูปของอสัณฐานซิลิกามีความบริสุทธิ์ประมาณร้อยละ 97 โดยน้ำหนัก ซึ่งได้จากการปรับสภาพแกลบข้าวถูกใช้เป็นสารเสริมแรงสำหรับการเตรียมพอลิเมอร์เชิงประกอบระหว่างซิลิกาจากแกลบข้าวและพอลิเมอร์ที่ลีนอะดิเพตเทอเรพธาลेट

เพื่อศึกษาผลของปริมาณซิลิกาจากแกลบข้าวต่อสมบัติต่าง ๆ ของวัสดุเชิงประกอบระหว่างระหว่างซิลิกาจากแกลบข้าวและพอลิเมอร์ที่ลีนอะดิเพตเทอเรพธาลेट ซิลิกาจากแกลบข้าวปริมาณต่างๆ (ร้อยละ 10-60 โดยน้ำหนัก) ถูกนำไปผสมกับพอลิเมอร์ที่ลีนอะดิเพตเทอเรพธาลेटในเครื่องบดผสม การใส่ซิลิกาจากแกลบข้าวในพอลิเมอร์ที่ลีนอะดิเพตเทอเรพธาลेटเมทริกซ์ช่วยเพิ่มปริมาณความเป็นผลึก ความหนืด ความแข็งแรงต่อแรงดึง ณ จุดครากและ โมดูลัสของการดึง ของพอลิเมอร์เชิงประกอบ อย่างไรก็ตามการยืดตัว ณ จุดแตกหักและ ค่าความแข็งแรงต่อการกระแทก ลดลง นอกจากนี้ สันฐานวิทยาจาก SEM แสดงให้เห็นถึงการยึดติดที่ไม่ดีระหว่างซิลิกาจากแกลบข้าวและพอลิเมอร์ที่ลีนอะดิเพตเทอเรพธาลेटเมทริกซ์

เพื่อเพิ่มสมบัติต่างๆ ของพอลิเมอร์เชิงประกอบระหว่างซิลิกาจากแกลบข้าวกับพอลิเมอร์ที่ลีนอะดิเพตเทอเรพธาลेट ผิวหน้าซิลิกาจากแกลบข้าวถูกปรับเปลี่ยนด้วย  $\gamma$ -เมทาคริลอซีโพลีฟิไตรเมทอซีไซเลน (MPS) หรือ กรดอะคริลิก (AA) ซิลิกาจากแกลบข้าวที่ไม่ได้ถูกปรับเปลี่ยนและถูกปรับเปลี่ยน ถูกเรียกว่า U-RHS, MPS-RHS and AA-RHS ตามลำดับ วัสดุเชิงประกอบของพอลิเมอร์ที่ลีนอะดิเพตเทอเรพธาลेटถูกเตรียมโดยใช้ซิลิกาจากแกลบข้าวที่ปริมาณคงที่ที่ ร้อยละ 30 โดยน้ำหนัก MPS-RHS ที่ MPS ปริมาณต่าง ๆ (ร้อยละ 0.5-5 โดยน้ำหนัก) สามารถปรับปรุงสมบัติทางกลต่าง ๆ ของพอลิเมอร์เชิงประกอบพอลิเมอร์ที่ลีนอะดิเพตเทอเรพธาลेटและ เปลี่ยนอุณหภูมิการสลายตัวและ ความหนืดของพอลิเมอร์เชิงประกอบพอลิเมอร์ที่ลีนอะดิเพตเทอเรพธาลेटเล็กน้อย ความแข็งแรงต่อแรงดึง ค่าแข็งแรงต่อการกระแทกและอุณหภูมิการสลายตัวของพอลิเมอร์เชิงประกอบเสริมแรงด้วยซิลิกาจากแกลบข้าวที่ถูกปรับปรุงผิวหน้าด้วย MPS2-RHS ให้ค่ามากที่สุด AA-RHS ที่เวลาการเกิดปฏิกิริยาต่าง (6-24 ชั่วโมง) สามารถปรับปรุงสมบัติทางกลต่าง ๆ ของ พอลิเมอร์เชิงประกอบพอลิเมอร์ที่ลีนอะดิเพตเทอเรพธาลेटและ เปลี่ยนอุณหภูมิการสลายตัวและความหนืดของพอลิเมอร์เชิงประกอบพอลิเมอร์ที่ลีนอะดิเพตเทอเรพธาลेटเล็กน้อย สมบัติทางกลต่าง ๆ

ของพอลิเมอร์เชิงประกอบเสริมแรงด้วยซิลิกาจากแคลบข้าวที่ถูกปรับปรุงผิวหน้าด้วย AA24-RHS มีค่าสูงสุดท่ามกลางวัสดุเชิงประกอบเสริมแรงด้วยซิลิกาจากแคลบข้าวที่ถูกปรับปรุงผิวหน้าด้วยกรดอะคริลิก ยิ่งกว่านั้น สันฐานวิทยาจาก SEM แสดงให้เห็นถึงการยึดติดระหว่าง MPS-RHS หรือ AA-RHS และ พอลิบิวทีลีนอะดิเพตเทอเรพธาลเตดเมทริกซ์ที่ดีกว่าการยึดติดระหว่าง U-RHS และ พอลิบิวทีลีนอะดิเพตเทอเรพธาลเตดเมทริกซ์

การดูดซึมน้ำและการย่อยสลายทางชีวภาพของพอลิบิวทีลีนอะดิเพตเทอเรพธาลเตดและวัสดุเชิงประกอบระหว่างพอลิบิวทีลีนอะดิเพตเทอเรพธาลเตดและซิลิกาจากแคลบข้าวถูกศึกษา พบว่าการเติม U-RHS ในพอลิบิวทีลีนอะดิเพตเทอเรพธาลเตดเพิ่มการดูดซึมน้ำและการย่อยสลายทางชีวภาพของพอลิเมอร์เชิงประกอบ อย่างไรก็ตาม การปรับเปลี่ยนผิวหน้าของ U-RHS ด้วย MPS หรือ AA จะลดการดูดซึมน้ำและการย่อยสลายทางชีวภาพของพอลิเมอร์เชิงประกอบ

จากการเปรียบเทียบระหว่างพอลิบิวทีลีนอะดิเพตเทอเรพธาลเตดที่เสริมแรงด้วย MPS-RHS และ พอลิบิวทีลีนอะดิเพตเทอเรพธาลเตดที่เสริมแรงด้วย AA-RHS พบว่าสมบัติทางกลของ พอลิบิวทีลีนอะดิเพตเทอเรพธาลเตดเสริมแรงด้วย MPS-RHS มีค่าสูงกว่าพอลิบิวทีลีนอะดิเพตเทอเรพธาลเตดเสริมแรงด้วย AA-RHS แต่อย่างไรก็ตาม การดูดซึมน้ำ และการย่อยสลายทางชีวภาพของพอลิบิวทีลีนอะดิเพตเทอเรพธาลเตดเสริมแรงด้วย AA-RHS มีค่าสูงกว่าพอลิบิวทีลีนอะดิเพตเทอเรพธาลเตดเสริมแรงด้วย MPS-RHS

สาขาวิชา วิศวกรรมพอลิเมอร์  
ปีการศึกษา 2554

ลายมือชื่อนักศึกษา \_\_\_\_\_  
ลายมือชื่ออาจารย์ที่ปรึกษา \_\_\_\_\_  
ลายมือชื่ออาจารย์ที่ปรึกษาร่วม \_\_\_\_\_

JIRAPA PHOSEE : FACTORS AFFECTING PROPERTIES OF RICE  
HUSK SILICA/POLY(BUTYLENE ADIPATE-*CO*-TEREPHTHALATE)  
COMPOSITES. THESIS ADVISOR : ASST. PROF. NITINAT SUPPAKARN,  
Ph.D., 130 PP.

RICE HUSK SILICA/POLY (BUTYLENE ADIPATE-*CO*-TEREPHTHALATE)  
/SILANE COUPLING AGENT/ACRYLIC ACID

In this work, rice husk silica (RHS), amorphous silica with approximate purity of 97 wt% obtained from treated rice husk waste, was used as a reinforcing filler for preparing RHS/poly (butylenes adipate-*co*-terephthalate) (PBAT) composites.

To study effect of RHS content on properties of RHS/PBAT composites, various RHS contents (10-60 wt%) were mixed with PBAT in an internal mixer. The incorporation of RHS into PBAT matrix increased crystallinity, viscosity, yield strength and tensile modulus of the PBAT composites. However, elongation at break and impact strength of the PBAT composites decreased with the addition of RHS. Moreover, SEM morphologies revealed a weak surface adhesion between RHS and PBAT matrix.

To improve properties of RHS/PBAT composites, RHS surface was modified by either  $\gamma$ -methacryloxypropyltrimethoxysilane (MPS) or acrylic acid (AA). The untreated RHS and treated RHS were referred to as U-RHS, MPS-RHS and AA-RHS, respectively. The RHS content of 30 wt% was selected for fabricating RHS/PBAT composites. The MPS-RHS at various MPS content (0.5-5 wt%) improved mechanical properties of PBAT composites and slightly changed  $T_d$  and viscosity of PBAT composites. In addition, tensile strength, impact strengths and  $T_d$  of the MPS2-RHS/PBAT composites

were the highest. The AA-RHS at various reaction times (6-24 h) improved mechanical properties and slightly changed  $T_d$  and viscosity of PBAT composites. Among the AA-RHS/PBAT composites, the mechanical properties of AA24-RHS/PBAT composites were the highest. Additionally, SEM morphologies of PBAT composites confirmed that the surface adhesion between MPS-RHS or AA-RHS and PBAT were better than that of U-RHS and PBAT.

Water absorption and biodegradability of PBAT and PBAT composites were determined. The addition of U-RHS into PBAT increased water absorption and biodegradability of PBAT composites. Nevertheless, treating U-RHS surface with MPS or AA delayed water absorption and biodegradability of the PBAT composites.

In comparison between MPS-RHS/PBAT and AA-RHS/PBAT composites, the mechanical properties of MPS-RHS/PBAT composites were higher than those of AA-RHS/PBAT composites. However, water absorption and biodegradability of MPS-RHS/PBAT composites were lower than those of AA-RHS/PBAT composites.

School of Polymer Engineering

Academic Year 2011

Student's Signature \_\_\_\_\_

Advisor's Signature \_\_\_\_\_

Co-advisor's Signature \_\_\_\_\_





## ACKNOWLEDGEMENTS

I wish to acknowledge the funding support from Suranaree University of Technology and National Center of Excellence for petroleum, Petrochemicals, and Advanced Materials.

The grateful thanks and appreciation are given to the thesis advisor, Asst. Prof. Dr. Nitinat Suppakarn for her consistent supervision, advice and support throughout this project. Special thanks are also extended to Assoc. Prof. Dr. Jatuporn Wittayakun for his valuable suggestion and guidance given as thesis *co*-advisor.

Special note of thanks to Asst. Prof. Dr. Wimonlak Sutapun, Asst. Prof. Dr. Kasama Jarukumjorn, and Asst. Prof. Dr. Pranee Chumsumrong for their valuable suggestion and guidance given as committee members. I am also grateful to all the faculty and staff members of the School of Polymer Engineering, Suranaree University of Technology for their help and assistance throughout the period of this study.

I would especially like to thank Mr. Sangey Pasang, Mr. Suriyan Rakmae, and Mr. Chalermpan Keawkumay for their support and help during the course of this research and always cheer me up whenever I got problems in the work. Finally, I would like to express my deep sense of gratitude to my parents, teachers and friends who support and encourage me throughout the course of this study at the Suranaree University of Technology.

Jirapa Phosee

# TABLE OF CONTENTS

	<b>Page</b>
ABSTRACT (THAI) .....	I
ABSTRACT (ENGLISH).....	III
ACKNOWLEDGEMENTS.....	V
TABLE OF CONTENTS.....	VI
LIST OF TABLES.....	XII
LIST OF FIGURES .....	XIII
SYMBOLS AND ABBREVIATIONS.....	XIX
<b>CHAPTER</b>	
<b>I INTRODUCTION</b> .....	<b>1</b>
1.1 Background.....	1
1.2 Research objective .....	3
1.3 Scope and limitation of the study .....	3
<b>II LITERATURE REVIEW</b> .....	<b>5</b>
2.1 Poly (butylene adipate - <i>co</i> -terephthalate).....	6
2.2 Silica from rice husk (RHS) .....	8



## TABLE OF CONTENTS (Continued)

	<b>Page</b>
3.2.5.1 Rheological properties .....	26
3.2.5.2 Thermal properties .....	26
3.2.5.3 Mechanical properties.....	27
3.2.5.4 Morphological properties.....	27
3.2.5.5 Water absorption.....	27
3.2.5.6 Biodegradability.....	28
<b>IV RESULTS AND DISCUSSION .....</b>	<b>28</b>
4.1 Effect of rice husk silica (RHS) content on rheological, thermal, mechanical and morphological properties of RHS/PBAT composites .....	30
4.1.1 Characterization of RHS .....	30
4.1.2 Rheological properties of neat PBAT and RHS/PBAT composites.....	34
4.1.3 Thermal properties of neat PBAT and RHS/PBAT composites.....	35
4.1.4 Mechanical properties of neat PBAT and RHS/PBAT Composites.....	37
4.1.5 Morphological properties of RHS/PBAT composites.....	43

## TABLE OF CONTENTS (Continued)

	<b>Page</b>
4.2 Effect of $\gamma$ -methacryloxypropyltrimethoxysilane (MPS) content on rheological, mechanical, thermal and morphological properties of MPS treated RHS/PBAT composites.....	47
4.2.1 Characterization of MPS treated RHS .....	47
4.2.2 Rheological properties of MPS treated RHS/PBAT composites.....	56
4.2.3 Thermal properties of MPS treated RHS/PBAT composites.....	57
4.2.4 Mechanical properties of MPS treated RHS/PBAT composites.....	59
4.2.5 Morphological properties of U-RHS/PBAT and MPS-RHS/PBAT composites.....	65
4.3 Effect of acrylic acid (AA) content on rheological, mechanical, thermal and morphological properties of RHS/PBAT composites .....	68
4.3.1 Characterization of AA treated RHS.....	68
4.3.2 Rheological properties of AA treated RHS/PBAT composites.....	73
4.3.3 Thermal properties of AA treated RHS/PBAT composites.....	75

## TABLE OF CONTENTS (Continued)

	<b>Page</b>
4.3.4 Mechanical properties of AA treated RHS/PBAT composites.....	77
4.3.5 Morphological properties of AA treated RHS/PBAT composites.....	81
4.4 Water absorption of PBAT and RHS/PBAT composites.....	84
4.4.1 Water absorption of PBAT and RHS/PBAT composites.....	84
4.4.2 Dimension stability of PBAT and RHS/PBAT composites after water absorption.....	86
4.4.3 Impact property of PBAT and RHS/PBAT composites after water absorption .....	88
4.5 Biodegradability of PBAT and RHS/PBAT composites.....	91
4.5.1 Weight loss of PBAT and RHS/PBAT composites .....	91
4.5.2 Tensile properties of PBAT and PBAT composites after soil-burial tests .....	94
4.5.3 Morphological properties of PBAT and RHS/PBAT composites after soil-burial tests.....	98
<b>V CONCLUSIONS .....</b>	<b>104</b>

**TABLE OF CONTENTS (Continued)**

	<b>Page</b>
REFERENCES .....	107
APPENDICES	
APPENDIX A. PARTICLE SIZE DISTRIBUTION OF U-RHS .....	116
APPENDIX B. MECHANICAL PROPERTIES OF PBAT AND PBAT COMPOSITES .....	118
APPENDIX C. PUBLICATIONS .....	125
BIOGRAPHY .....	130

## LIST OF TABLES

Table	Page
4.1	Chemical compositions of rice husk ash ..... 33
4.2	Properties of rice husk ash..... 33
4.3	Melting temperature and crystallinity of neat PBAT and PBAT composites at various RHS contents. .... 37
4.4	Average diameter, surface area and pore characteristics of U-RHS and MPS-RHS at various MPS content..... 50
4.5	Decomposition temperatures and residue weight at 600°C of physically mixed MPS/RHS, U-RHS and MPS-RHS at various MPS content. .... 55
4.6	Decomposition temperatures and residue weight at 600°C of neat PBAT, U-RHS/PBAT and MPS-RHS/PBAT composites at various MPS contents ..... 59
4.7	Average diameter, surface area and pore characteristics of U-RHS and AA-RHS at various reaction times ..... 70
4.8	Decomposition temperatures and residue weight at 600°C of physically mixed AA/RHS, U-RHS and AA-RHS at various reaction times..... 73
4.9	Decomposition temperatures and residue weight at 600°C of neat PBAT, U-RHS/PBAT and AA-RHS/PBAT composites at various reaction times..... 76



## LIST OF FIGURES

Figure	Page
2.1	Chemical formula of aliphatic–aromatic copolyesters with Terephthalic acid, adipic acid and 1, 4-butanediol ..... 6
3.1	Chemical structures of (a) $\gamma$ -Methacryloxypropyltrimethoxysilane (MPS) and (b) acrylic acid (AA) .....21
4.1	Photographs of (a) as-received rice husk (b) HCl treated rice husk and (c) white rice husk ash ..... 30
4.2	XRD pattern of rice husk ash..... 31
4.3	FTIR spectrum of rice husk ash.....32
4.4	Shear viscosity as a function of shear rate of neat PBAT and RHS/PBAT composites at various RHS contents.....35
4.5	DSC thermograms of neat PBAT and PBAT composites at various RHS contents ..... 36
4.6	Stress-strain curves of neat PBAT and PBAT composites at various RHS contents. .... 38
4.7	Tensile modulus and elongation at break of neat PBAT and PBAT composites at various RHS contents ..... 39
4.8	Tensile strength of neat PBAT and PBAT composites at various RHS contents. ....41

## LIST OF FIGURES (Continued)

	<b>Page</b>
4.9 Yield strength of neat PBAT and PBAT composites at various RHS contents.....	42
4.10 Impact strength of PBAT and PBAT composites at various RHS contents. ....	43
4.11 SEM micrographs of tensile fracture surfaces of (a) neat PBAT and PBAT composites at various RHS contents: (b) 20 wt%, (c) 30 wt%, (d) 40 wt%, (e) 50 wt% and (f) 60 wt%. ....	45
4.12 SEM micrographs of impact fracture surfaces of neat PBAT composites at various RHS contents: (a) 30 wt% (b) 40 wt% (c) 50 wt% and (d) 60 wt% .....	46
4.13 Schematic illustration of silane treated rice hush silica.....	48
4.14 Photographs of RHS particles in water (a) MPS-RHS and (b) U-RHS. ....	49
4.15 SEM micrographs of (a) U-RHS and (b) MPS-RHS.....	50
4.16 FTIR spectra of U-RHS and MPS-RHS at various MPS contents (a) wavenumber 4000-400 cm <sup>-1</sup> and (b) wavenumber 1800-1500 cm <sup>-1</sup> . ....	52
4.17 Simplified illustrative molecular structures of (a) random and (b) parallel monomolecular MPS molecules .....	53

## LIST OF FIGURES (Continued)

	<b>Page</b>
4.18 TGA thermograms of (a) U-RHS, MPS-RHS at various MPS content and (b) physically mixed MPS/RHS. ....	55
4.19 Shear viscosity as a function of shear rate of neat PBAT, U-RHS and MPS RHS/PBAT composites at various MPS contents. ....	57
4.20 TGA and DTG thermograms of neat PBAT, U-RHS/PBAT and MPS-RHS/PBAT composites at various MPS contents ....	58
4.21 Tensile modulus of U-RHS/PBAT and MPS-RHS/PBAT composites at various MPS contents ....	60
4.22 Elongation at break of U-RHS/PBAT and MPS-RHS/PBAT composites at various MPS contents ....	62
4.23 Tensile strength of U-RHS/PBAT and MPS-RHS at various MPS contents. ....	63
4.24 Impact strength of U-RHS/PBAT and MPS-RHS at various MPS contents ....	64
4.25 Simplified illustrative molecular structures of multilayer MPS molecules ....	65
4.26 SEM micrographs of tensile fracture surfaces of (a) U-RHS/PBAT composite and MPS-RHS/PBAT composites at various MPS contents: (b) 1 wt%, (c) 2 wt% and (d) 3 wt% ....	67

## LIST OF FIGURES (Continued)

	<b>Page</b>
4.27 Photographs of (a) AA-RHS particles and (b) U-RHS particles .....	69
4.28 SEM micrographs of (a) U-RHS particles and (c) AA-RHS particles .....	70
4.29 FTIR spectra of U-RHS and AA-RHS at various reaction times .....	71
4.30 TGA thermograms of U-RHS and AA-RHS at various reaction times.....	73
4.31 Shear viscosity as a function of shear rate of neat PBAT, U- RHS/PBAT and AA RHS/PBAT composites at various reaction times.....	74
4.32 TGA and DTG thermograms of neat PBAT, U-RHS/PBAT and AA-RHS/PBAT composites at various reaction times.....	76
4.33 Tensile modulus of U-RHS/PBAT and AA-RHS/PBAT composites at various reaction times .....	78
4.34 Elongation at break of U-RHS/PBAT and AA-RHS/PBAT composites at various reaction times .....	79
4.35 Tensile strength of U-RHS/PBAT and AA-RHS/PBAT composites at various reaction times .....	80
4.36 Impact strength of U-RHS/PBAT and AA-RHS/PBAT composites at various reaction times .....	81

## LIST OF FIGURES (Continued)

	<b>Page</b>
4.37 SEM micrographs of impact fracture surfaces of (a) U-RHS/PBAT composite and AA-RHS/PBAT composites at various reaction times: (b) 6 h, (c) 12 h and (d) 24 h.....	83
4.38 Plots of Percentage of absorbed water against immersion time for neat PBAT, U-RHS/PBAT, MPS-RHS/PBAT and AA-RHS/PBAT composites .....	86
4.39 Plots of width and thickness changes against immersion time for neat PBAT, U-RHS/PBAT, MPS-RHS/PBAT and AA-RHS/PBAT composites .....	88
4.40 Impact strength of neat PBAT, U-RHS/PBAT, MPS-RHS/PBAT and AA-RHS/PBAT composites .....	89
4.41 Plots of weight loss after soil-burial tests against burial time for neat PBAT, U-RHS/PBAT, MPS-RHS/PBAT and AA-RHS/PBAT composites .....	90
4.42 Tensile modulus of neat PBAT, U-RHS/PBAT, MPS-RHS/PBAT and AA-RHS/PBAT composites at various composting times .....	95
4.43 Elongation at break of neat PBAT, U-RHS/PBAT, MPS-RHS/PBAT and AA-RHS/PBAT composites at various composting times .....	96

## LIST OF FIGURES (Continued)

	<b>Page</b>
4.44 Tensile strength of neat PBAT, U-RHS/PBAT, MPS-RHS/PBAT and AA-RHS/PBAT composites at various composting times .....	97
4.45 SEM micrographs of surfaces fragmentation of (a) neat PBAT, (b) U-RHS/PBAT, (c) MPS2-RHS/PBAT and (d) AA24-RHS/PBAT composites after soil-burial tests .....	100
4.46 SEM micrographs of cryofracture of (a) neat PBAT, (b) U-RHS/PBAT, (c) MPS2-RHS/PBAT and (d) AA24-RHS/PBAT composites after soil-burial tests .....	101
4.47 SEM micrographs of impact fracture surfaces of (a) U-RHS/PBAT, (b) MPS2-RHS/PBAT and (c) AA24-RHS/PBAT composites before soil-burial tests.....	102



## SYMBOLS AND ABBREVIATIONS

%	=	Percent
°	=	Degree
°C	=	Degree Celsius
AA	=	Acrylic acid
cm <sup>-1</sup>	=	Reciprocal centrimeter
cm <sup>3</sup>	=	Cubic centrimeter
FTIR	=	Fourier Transform Infrared Spectrometer
g	=	Gram
GPa	=	Gigapascal
h	=	hours
J	=	Joule
keV	=	Kilo electron volt
kN	=	Kilo Newton
kN/m	=	Kilo Newton per meter
kV	=	Kilo volt
M	=	Molar (mol/L)
m <sup>2</sup>	=	Square meter
m <sup>3</sup>	=	Cubic meter
min	=	Minute

**SYMBOLS AND ABBREVIATIONS (Continued)**

ml	=	Milliliter
mm	=	Millimeter
mol	=	Mole
mol%	=	Percent by mole
MPa	=	Mega Pascal
MPS	=	$\gamma$ -methacryloxypropyltrimethoxysilane
PBAT	=	Poly (butylene adipate- <i>co</i> -terephthalate)
phr	=	Part per hundred of rubber
psi	=	Pound per square inch
RHS	=	Rice husk silica
rpm	=	Round per minute
SEM	=	Scanning electron microscope
U-RHS	=	Untreated rice husk silica
v/v	=	Volume by volume
wt%	=	Percent by weight
wt/v	=	Weight by volume
wt/wt	=	Weight by weight
XRD	=	X-ray diffraction

# CHAPTER I

## INTRODUCTION

### 1.1 Background

Plastic materials are vastly used for various applications in daily basis but not many of them are biodegradable, leading to tons of plastic waste left in landfill. Thus, it is necessary to develop biodegradable polymers with acceptable properties and reasonable cost.

Aliphatic polyesters are currently one of the most important commercial biodegradable plastics, *e.g.* poly(lactic acid) (PLA), poly( $\epsilon$ -caprolactone) (PCL), poly( $\epsilon$ -hydroxybutyrate) (PHB). However, these materials still have high cost and lack of important properties for applications. On the other hand, aromatic polyesters such as poly(ethylene terephthalate) (PET), poly(butylene terephthalate) (PBT), exhibit excellent properties and have relatively inexpensive cost. However, they are resistant to microbial attack and not degradable under normal environmental conditions (Muller, Kleeberg, and Deckwer, 2001; Van de Velde and Kiekens, 2002).

To combine good material properties with biodegradability, a special type of biodegradable polymer, poly(butylene adipate-*co*-terephthalate) (PBAT), was developed by BASF company under the trade name of Ecoflex. PBAT is a random aliphatic–aromatic copolyester of butylene adipate and terephthalate which has shown to be completely biodegradable when it is composted (Muller *et al.*, 2001; Witt *et al.*, 2001).

PBAT is a large scale polymer products used extensively to produce fibers, films and packaging materials due to its high ultimate elongation, good optical properties, resistance to creep fracture and resistance to fatigue and wear. Nonetheless, its properties such as modulus of elasticity have to be improved to suit applications (Signori, Coltelli, and Bronco, 2009; Tan, Cooper, Maric, and Nicell, 2008; Van de Velde *et al.*, 2002). The modulus of elasticity of PBAT can be enhanced by either blending it with other biodegradable or non-biodegradable polymers (Martin and Averous, 2001), such as PLA, or mixing with a reinforcing filler such as montmorillonite (MMT), silica (SiO<sub>2</sub>) (Jiang, Zhang, and Wolcott, 2007; Martin and Averous, 2001).

An approach to enhance the mechanical properties is the combination of biodegradable polymers with inorganic or organic fillers. Rice husk is a byproduct from rice milling process and abundantly available in Thailand. Moreover, it is an excellent natural source of high purity and low cost silica, namely rice husk silica (RHS) (Wittayakun, Khemthong, and Prayoonpokarach, 2008; Della, Kuhn, and Hotza, 2002). In addition to other applications of RHS, *e.g.* as a support material for metal catalysts and in thin film, coatings for electronic and optical materials, it can be one attractive filler for producing polymer composites (Chandrasekhar, Pramada, and Praveen, 2005; Kalapathy, Proctor, and Shultz, 2000).

However, direct mixing of hydrophilic RHS particles with hydrophobic PBAT often leads to RHS agglomeration within PBAT matrix and deterioration of mechanical properties and load bearing ability of the composites. This is because RHS particle has silanol (Si-OH) groups on the surface, which can form hydrogen bonds between RHS particles, leading to agglomeration and low filler-polymer interaction. Compatibility and

adhesion between RHS and PBAT can be enhanced by introducing appropriate interfacial interaction between the surface of the RHS and the PBAT matrix (Wu, Cao, and Huang, 2008; Yan *et al.*, 2007).

In this work, in order to encourage the use of PBAT and other biodegradable plastics as well as to find alternative approach of using rice husk, RHS was prepared from rice husk and incorporated into PBAT matrix to fabricate RHS/PBAT composites. Effect of RHS surface modification on rheological properties, thermal properties, mechanical properties, water absorption, biodegradability and morphological properties of RHS/PBAT composites were determined.

## 1.2 Research objectives

The main objectives of this research are as follows:

- i) To determine the filler characteristics of RHS powder prepared from rice husk.
- ii) To determine effect of RHS content on mechanical properties of RHS/PBAT composites.
- iii) To determine effect of RHS surface modification on the rheological properties, thermal properties, mechanical properties, water absorption, biodegradability and morphological properties of RHS/PBAT composites.

## 1.3 Scope and limitation of the study

In this study, RHS was prepared by treating rice husk with HCl and heating the HCl treated rice husk to remove organic residues. Then, the RHS surface was modified by either  $\gamma$ -methacryloxypropyltrimethoxysilane (MPS) or acrylic acid (AA). The

untreated RHS (U-RHS), MPS treated RHS (MPS-RHS) and AA treated RHS (AA-RHS) were characterized before fabricating RHS/PBAT composites.

To determine effect of RHS content on mechanical properties of RHS/PBAT composites, various contents of U-RHS, *i.e.* 10, 20, 30, 40, 50 and 60 wt% based on weight of PBAT, were mixed with PBAT using an internal mixer. Then, composite specimens were prepared using a compression molding machine. The RHS/PBAT composites were characterized. The RHS content that gave optimal mechanical properties of PBAT composites was selected for using in experimental steps.

Effect of RHS surface modifications (MPS-RHS or AA-RHS) on properties of PBAT composites was determined. The MPS-RHS was prepared using various contents of MPS, *i.e.* 0.5, 1, 2, 3 and 5 based on weight of RHS. The AA-RHS was prepared by various reaction times, *i.e.* 3, 6, 12 and 24 h. Then, the MPS-RHS/PBAT composites and the AA-RHS/PBAT composites were fabricated at the fixed content of the filler. Effect of MPS content and effect of reaction time of AA treating RHS on rheological properties, thermal properties, mechanical properties, water absorption, biodegradability and morphological properties of RHS/PBAT composites were determined.

## **CHAPTER II**

### **LITERATURE REVIEW**

With the increase in the demand of biodegradable polymers, PBAT an aliphatic aromatic copolyester has become an interesting candidate. However, its price is quite expensive as compared with other commodity plastics of similar properties. In order to encourage the uses of PBAT as well as other biodegradable plastics, the properties such as mechanical properties still need to be improved to fulfil applications at the competitive cost. Thus, it is necessary to add a reinforcing filler into PBAT matrix to enhance mechanical properties of the matrix.

Rice husk is an agricultural waste which is abundantly available in Thailand. These husks are byproducts from rice milling process with no commercial interest and low cost. However, rice husk is an excellent natural source of high purity and low cost silica. Rice husk silica (RHS) is one of attractive filler for PBAT matrix since it can improve thermal, mechanical and gas barrier properties of PBAT matrix (Someya, Kondo, and Shibata, 2007). However, the compatibility and adhesion between hydrophilic RHS and hydrophobic PBAT matrix is rather poor, leading to RHS agglomeration within PBAT matrix and deterioration of mechanical properties of the composites. Various methods such as filler surface treatment, polymer matrices modification, and addition of compatibilizer can be used to introduce appropriate interfacial interaction between the surface of the inorganic particles and the organic matrix.

## 2.1 Poly (butylene adipate -*co*-terephthalate) (PBAT)

PBAT is an aliphatic-aromatic copolyester based on terephthalic acid, adipic acid, and 1, 4- butanediol (Figure 2.1). PBAT has been developed by BASF Company under the trade name of Ecoflex.

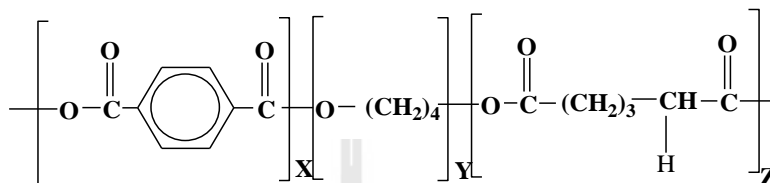


**Figure 2.1** Chemical formula of aliphatic–aromatic copolyesters with terephthalic acid, adipic acid and 1, 4-butanediol (Witt *et al.* 2001).

Muller, Kleeberg, and Deckwer (2001) investigated the degradation of PBAT containing various contents of terephthalic acid. The data were obtained from degradation tests on agar plates, where PBAT films (2.5 cm diameter) were inoculated with a pre-screened mixed microbial culture from compost at 60°C test (mineral salt medium). The results demonstrated that the biological degradation rate decreased continuously with increasing the fraction of terephthalic acid in the copolymer. Beyond 60 mol% of terephthalic acid content, the degradation rate of PBAT became so small that such materials were not suitable for degradation in a composting process. In contrast, the water uptake and hydrolytic chain scission of PBAT were significantly increased by introducing aliphatic acid components.

Witt *et al.* (2001) studied the degradation of aliphatic–aromatic copolyesters with regard to the degree of degradation and the intermediates formed during the degradations process. The strain *Thermomonospora fusca* DSM43793 isolated from compost material

was used for degradation experiments in a defined medium. During the degradation run for 21 days at 55°C, various aliphatic and aromatic oligomers could be determined and identified. The result showed that only the monomers, adipic acid, terephthalic acid and 1, 4-butanediol were observed. No other ester compounds, which could not be related to medium components, were detected. With the synthetic degradation medium containing a high concentration of the degradation intermediates, ecotoxicological test were performed (test with daphnia and luminescent bacteria test). The results indicated that no acute toxicological effect was caused by monomeric or oligomeric intermediates, even at the concentrations of the intermediates that was higher than those detected in real compost environment.

Marten, Muller, and Deckwer (2005) investigated the dependence of the enzymatic degradation of aliphatic-aromatic copolyesters on the polymer structure. A number of defined model copolyesters containing terephthalate units as aromatic component were synthesized. The model polymers included random copolyesters, block copolyesters and also strictly alternating copolyesters, which were made from especially synthesized and purified pre-building blocks. The biodegradability was evaluated using a laboratory degradation test under well-defined conditions with a lipase from *Pseudomonas sp.* It was proven that the selectivity of the lipase concerning the aliphatic or aromatic environment near the ester bonds was not the predominant factor controlling the biodegradability of the copolyesters. As already described for aliphatic homopolyesters, the biodegradation rate of the copolyesters was mainly controlled by the chain mobility of the polymers, being correlated with the difference between the melting point of the polyester, and the degradation temperature. The presence of longer aliphatic

domains in block copolyesters did not facilitate the hydrolytic attack by the lipase. However, the long aromatic sequences controlled the melting point of the crystalline regions and reduced the biodegradation rate.

Tan, Cooper, Maric, and Nicell (2008) studied biological degradation of the synthetic aliphatic–aromatic co-polyester using different enzyme from bacteria, yeasts and fungi grown on various media in the presence of the aliphatic–aromatic copolyester at moderate environmental conditions. The amounts of weight loss in polymer films of control samples versus those exposed to pure cultures of various bacteria and fungi and yeasts over 21 days period were measured. Qualitative assessments of biodegradation by visual inspection were also performed. Results showed that the aliphatic–aromatic copolyester could be degraded by a number of different microorganisms. After 21 days exposure to the most promising cultures of pure microorganisms, only partial degradation of the Ecoflex was accomplished and only a few samples showed visible signs of degradation as loosely defined by the mechanical weakening of the films. The bacteria studied preferentially degraded the bonds between aliphatic components of the copolymer. In addition, GPC experiments suggested that the rate of biodegradation of oligomers was faster than that of the polymer chains.

## **2.1 Silica from rice husk (RHS)**

Rice husk is an abundantly available agricultural waste in Thailand and can be used as a silica ( $\text{SiO}_2$ ) source with high  $\text{SiO}_2$  content and low cost. Therefore, reinforcing PBAT matrix with RHS filler can reduce the cost of PBAT and also improve some mechanical properties of the matrix. However, RHS carries too many impurities and

exhibits some inferior properties. Therefore, researchers have investigated several methods to purify the product obtained.

Yalcin and Sevinc (2001) investigated effect of chemical treatments on properties of obtained RHS, in terms of SiO<sub>2</sub> content, particle size distribution and morphology, specific surface area and porosity. Rice husk was leached in the chemical solutions using HCl, H<sub>2</sub>SO<sub>4</sub> and NaOH solutions, before (pre-) or after (post-) incineration at 600°C for 4 h. XRD diagrams of all RHS showed only a broad peak position at  $2\theta = 22^\circ$ , indicating that samples were amorphous SiO<sub>2</sub>. The results indicated that the rice husk leached with HCl solution gave the highest content of SiO<sub>2</sub>. Moreover, SEM and TEM micrographs of the RHS obtained from HCl pretreatment presented homogeneous particle distribution and small average particle size compared with those obtained from other preparation techniques. The HCl pretreated RHS also showed the highest BET specific surface area and specific pore volume with SiO<sub>2</sub> purity of 99.66%.

Della, Kuhn, and Hotza (2002) studied effect of burning temperature (400, 500, 600 and 700°C) and burning time (1, 3 and 6 h) on purity of SiO<sub>2</sub>. The result showed that the relative amount of SiO<sub>2</sub> was increased by heat treatment. A 95% SiO<sub>2</sub> powder was produced after heat-treating at 700°C for 6 h. The specific surface area of particles was increased after wet milling from 54 to 81 m<sup>2</sup>/g.

Liou (2004) studied effect of burning rate on SiO<sub>2</sub> content, specific surface area, pore volume, particle size and pore size distribution of obtained silica. The experiment conducted included treating rice husk with HCl and burning at 700°C with heating rates of 5–20°C/min. The result showed that nano-structured SiO<sub>2</sub> powders with high specific surface area were obtained at a heating rate of 5 K/min. About 95% of the impurities were

extracted. The specific surface area of the SiO<sub>2</sub> powder was 235 m<sup>2</sup>/g, the average pore diameter was 5.4 nm, and the average particle size was 60 nm.

## 2.2 Properties of silica (SiO<sub>2</sub>)/polymer composites

Silica (SiO<sub>2</sub>) is the most abundant mineral in the Earth's crust as sand or quartz, as well as in the cell walls of diatoms. SiO<sub>2</sub> also resides in certain plants and whole grains, but usually as insoluble compounds. Moreover, SiO<sub>2</sub> is widely used in various applications in electronics, ceramic, and polymer material industries because it has good abrasion resistance, electrical insulation and high thermal stability. Moreover, SiO<sub>2</sub> has been proposed as attractive filler for biodegradable polymer matrices because it can improve thermal and mechanical properties and increase gas barrier properties of the polymer composites (Yan *et al.*, 2007).

Ismail, Nasaruddin, and Ishiaku (1999) investigated effect of RHS loading on mechanical properties of natural rubber composites. The results showed that the optimum loading of RHS was 10 phr since the maximum tensile strength of the composites was obtained. In addition, tensile modulus and hardness of the composites increased with increasing RHS loading.

Chuayjuljit, Eiumnoh, and Potiyaraj (2001) studied the use of RHS and commercial SiO<sub>2</sub> as reinforcing fillers in natural rubber. Curing characteristics and mechanical properties of natural rubber composites were determined. The results indicated that rubber reinforced with RHS had shorter curing times as compared with those reinforced with commercial SiO<sub>2</sub>. Overall mechanical properties (*i.e.* tensile strength, tear strength, abrasion resistance, compression set and resilience) of rubber reinforced with RHS were better than those of rubber reinforced with commercial SiO<sub>2</sub>.

However, the hardness of the natural rubber containing RHS composites was inferior compared with that of the composites containing commercial SiO<sub>2</sub>. Therefore, the natural rubber containing RHS was suitable for applications where hardness was not the major concern but other mechanical properties were desirable.

Wu, Zhang, Rong, and Friedrich (2002) studied effect of silica content on mechanical properties of SiO<sub>2</sub>/polypropylene (PP) nanocomposites. PP was compounded with nano-SiO<sub>2</sub> by twin screw extruder and injection molding machine. Tensile testing results indicated that the nano-SiO<sub>2</sub> can simultaneously provide PP with stiffening, strengthening and toughening effects at rather low filler content (typically 0.5% by volume). Moreover, increasing crosshead speed of the tensile tests, the dominant failure mode of the PP composites changed from plastic yielding to brittle cleavage.

Lin (2008) studied effect of SiO<sub>2</sub> content on structure, mechanical properties and interaction between SiO<sub>2</sub> and polyacrylate (PA) of SiO<sub>2</sub>/PA nanocomposites. The composites with various SiO<sub>2</sub> content from 10 to 50 wt% were used to investigate their mechanical and morphological properties. The results showed that all SiO<sub>2</sub> filled composites reduced the interfacial crack area in low energy impact. The maximum stress intensity factor of the PA nanocomposites was significantly enhanced as compared with that of neat PA. The PA composite with 30 wt% SiO<sub>2</sub> showed the best structural stiffness and the steady state fracture toughness ( $K_{IS}$ ) was approximately 45%, higher than that of PA. SEM micrographs of the composites revealed that a strong correlation was established between the fracture toughness and the percolation network of the particle agglomeration.

Yao *et al.* (2009) investigated the interface structure of the SiO<sub>2</sub>/poly(ethylene terephthalate) (PET) nanocomposites during the polymerization of terephthalic acid (TPA), ethylene glycol (EG) and pure SiO<sub>2</sub>. The result showed that PET chains were grafted onto surface of SiO<sub>2</sub> particles and formed branched and lightly crosslinking structures during the polycondensation. Moreover, nanocomposites attributed to the interaction of an entanglement network with SiO<sub>2</sub> surfaces which led to improve shear storage modulus, shear loss modulus and complex viscosity values of the SiO<sub>2</sub>/PET nanocomposites.

## **2.3 Improvement of compatibility between polymer matrix and filler**

### **2.4.1 Filler surface modification**

Fuad, Ismail, Ishak, and Omar (1995) used silanes coupling agents, PROSIL 9234 (n-octyltriethoxysilane) and PROSIL 2020 (a proprietary silane containing the peroxide bis (t-butyl peroxy) di-siopropyl benzene), to treat rice husk silica (RHS) surface and investigated mechanical properties of RHS/PP composites. PP composites with 10-40 wt% RHS were compounded using a twin screw extruder. The results showed that flexural modulus of the composites increased with filler content while their tensile strength, elongation at break and Izod impact strength decreased. Melt flow index of PP filled with PROSIL treated RHS 9234 decreased with increasing filler content. In contrast, for PP containing RHS treated with a silane containing peroxide functional groups (PROSIL 2020), melt flow index increased with increasing filler content. Incorporating of PROSIL 2020 treated RHS improved tensile strength of PP composites. However, impact property of the composites was enhanced with the addition of treating RHS with PROSIL 9234 coupling agent.

Hong *et al.* (2004) modified surface of hydroxyapatite nano-particles (n-HAP) by grafting ring-opening polymerization of L-lactide (LLA) onto n-HAP.  $^{31}\text{P}$  NMR and FTIR results showed that PLLA was chemical bonded onto the n-HAP surface. The amount of grafted polymer determined by thermal gravimetric analysis (TGA) was about 6 wt%. Tensile strength and elongation at break of the PLLA-g-HAP/PLLA composite containing 8 wt% of PLLA-g-HAP were 55 MPa and about 10–13%, respectively, while those of the n-HAP/PLLA composites were 40 MPa and 3–5%, respectively. The PLLA-g-HAP particles were more uniformly dispersed in chloroform and showed much improved adhesion with PLLA matrix than the non-grafted n-HAP. Therefore, the PLLA-g-HAP/PLLA composites exhibited better mechanical properties than the simple n-HAP/PLLA composites.

Sun, Li, Zhang, Du, and Burnell-Gray (2006) studied effect of surface modification of nano-SiO<sub>2</sub> particles with dimethyldichlorosilane (DMCS) and methylacryloxypropyltrimethoxy silane (KH570) on interfacial structures and mechanical properties of poly (vinyl chloride) (PVC) composites. The results showed that nano-SiO<sub>2</sub> treated with KH570 or DMCS significantly reinforced and toughened the PVC composites. The tensile yield stress of the composites increased with increasing content of treated nano-SiO<sub>2</sub>. The interfacial interaction calculated from tensile yield stress and loss modulus of SiO<sub>2</sub>/PVC nanocomposites were employed to quantitatively characterize the effective interfacial interaction between the nano-SiO<sub>2</sub> and PVC matrix. It was demonstrated that the nano-SiO<sub>2</sub> treated with KH570 had stronger effective interfacial interaction with PVC matrix than those treated with DMCS. However, nano-SiO<sub>2</sub>

particles treated with DMCS had stronger effective interfacial interaction with PVC matrix than the untreated nano-SiO<sub>2</sub>.

Yan *et al.* (2007) investigated the surface modification of SiO<sub>2</sub> particle by grafting L-lactic acid oligomer onto the surface silanol groups of the SiO<sub>2</sub> particles. The results showed that L-lactic acid oligomers were successfully grafted onto SiO<sub>2</sub> surface. Moreover, grafted SiO<sub>2</sub> had a novel core-shell structure with the inner SiO<sub>2</sub> core and outside L-lactic acid oligomer shell. The modified SiO<sub>2</sub> particles were comparatively homogeneously dispersed in chloroform or PLLA matrix in contrast to the severe aggregation of ungrafted SiO<sub>2</sub> particles. The tensile strength of materials was greatly improved upon increasing grafted SiO<sub>2</sub> particles loading. In addition, the morphology of grafted SiO<sub>2</sub>/PLLA nanocomposites implied the tough characteristics and great interfacial strength of the nanocomposites. However, the incorporation of ungrafted SiO<sub>2</sub> particle in PLLA led to the deterioration of mechanical properties of PLLA nanocomposites.

Abdelmouleh, Boufi, Belgacem, and Dufresne (2007) studied effect of silane coupling agent type on mechanical properties and water absorbance behavior of cellulose fibers reinforced thermoplastic polymer composites, *i.e.* low density polyethylene and natural rubber. Three silane coupling agents, namely methacryloxypropyltrimethoxy (MPS), mercaptoproyltrimethoxy (MRPS) and hexadecyltrimethoxy-silanes (HDS) were used to modify cellulose fibers. The results showed that fiber treated with HDS modestly enhanced composite mechanical properties. On the other hand, adding cellulose fiber treated with MPS and MRPS for both matrices revealed good mechanical performances of the composites. The treatment of the fibers

with HDS did not significantly reduce water absorption compared with those with MPS or MRPS. This was because, both MPS and MRPS contained functional groups which can react with radical species to generate a covalent bond with matrices during the processing of the composites. The resulting reaction gave rise to chemical bonding between the fibers and the matrices which enhanced the interfacial adhesion leading to good mechanical performances and significant reduction of water absorption.

Lin, Akil, and Ishak (2008) studied effect of coupling agents namely 3-aminopropyl triethoxysilane (APTES) and neopentyl (diallyl) oxytri (dioctyl) phosphate titanate (Lica 12) on the properties of SiO<sub>2</sub>/PP nanocomposites. Prior to compounding, nanosilica was subjected to surface activation using sodium hydroxide (NaOH) solution. The effectiveness of the activation process was evaluated by measuring the amount of hydroxyl groups on the surface of nano-SiO<sub>2</sub> via titration method and supported by FTIR analysis. Then, the two coupling agents were used for nano-SiO<sub>2</sub> surface treatment after activation process. Treated nanosilica (1 wt%) was mixed with PP to prepare the composites by melt mixing in an internal mixer. The result showed that hydroxyl groups on the nano-SiO<sub>2</sub> surface played an important role in enhancing the treatment with silane coupling agents. Tensile strength, tensile modulus, and impact strength of SiO<sub>2</sub>/PP nanocomposites improved with activation process. With regards to the coupling agent, APTES coupling agent was more pronounced in enhancing the mechanical properties of the composites as compared with Lica 12 coupling agent.

Hsiang, Chang, Chen, and Yen (2009) studied effect of MPS content on rheological behavior, optical and abrasion resistance properties of transparent UV-curable nanocomposites coatings consisting of nano-SiO<sub>2</sub> and acrylate resin. The nano-SiO<sub>2</sub> was

surface modified using various amounts of MPS (weight ratio of MPS to SiO<sub>2</sub> = 0.1, 0.2, 0.4, 0.6, 1.0, and 1.5). The results showed that the MPS modified nano-SiO<sub>2</sub> in acrylate solutions exhibited Newtonian behavior in the low shear rate range, followed by shear thinning flow behaviors. As the MPS/SiO<sub>2</sub> weight ratio increased from 0.2 to above 0.6, the abrasion resistance was significantly improved and the pencil hardness increased from 4H to 6H. These were because MPS formed steric-hinderance between SiO<sub>2</sub> particle leading to the improvement of dispersibility of SiO<sub>2</sub> particle in acrylate suspensions and the enhancement of the compatibility between SiO<sub>2</sub> and acrylate resin.

Sideridou and Karabela (2009) studied effect of MPS treated nano-SiO<sub>2</sub> on some physical–mechanical properties of Bis-GMA/TEGDMA resin matrix reinforced with nano-SiO<sub>2</sub>. The nano-SiO<sub>2</sub> was silanized with 5 different amounts of MPS, *i.e.* 1.0, 2.5, 5.0, 7.5 and 10 wt% relative to SiO<sub>2</sub> weight. Then the silanized nano-SiO<sub>2</sub> of 60 wt% was mixed with a Bis-GMA/TEGDMA (50/50 wt/wt) matrix. The results showed that the flexural strength and flexural modulus of the composites containing various MPS contents were not significantly different. Dynamic elastic modulus showed a maximum value for the composite containing 5 wt% MPS. The composites with the higher amounts of MPS showed lower values of  $\tan \delta$  at the  $T_g$ , indicating that these composites had better interfacial adhesion between filler and matrix.

#### **2.4.2 Polymer matrix modification**

Bailly and Kontopoulou (2009) studied effects of vinyltriethoxysilane (VTEOS) treatment of PP matrix on morphology and mechanical properties of SiO<sub>2</sub>/PP nanocomposites (SiO<sub>2</sub>/PP-g-VTEOS). The experimental started from grafting PP with 5 wt% of VTEOS by using dicumyl peroxide (DCP) as an initiator content of 0.1 wt%.

Amounts of nanosilica ranging from 2 to 7 wt% were used. TEM micrograph of the PP composites containing up to 7 wt% of the nano-SiO<sub>2</sub> showed good dispersion of the nano-SiO<sub>2</sub> and encapsulation/core-shell structure. Tensile and flexural properties of the composites were improved upon adding rigid nano-SiO<sub>2</sub>, whereas the impact strength decreased. These improvements in properties of the composites were attributed to covalent bonding of VTEOS onto PP matrix. The presence of covalent bonding primarily reduced nanosilica polar nature. This was responsible for good dispersion of nano-SiO<sub>2</sub> in the matrix and strengthened the interface between polymer and nano-SiO<sub>2</sub>.

### 2.4.3 Addition of compatibilizer

Ismail, Nasaruddin, and Ishiaku (1999) investigated effect of n-tallow-1-3-propane diamine of general structure  $[\text{RNH}_2^+(\text{CH}_2)_3\text{NH}_3^+][\text{R}'\text{COO}^-]_2$ , referred to as a multifunctional additive (MFA), on mechanical properties of RHS filled natural rubber compounds. The result showed that optimum loading of RHS to obtain maximum tensile and tear strength of the composites was achieved at 10 phr of RHS after which there was deterioration in properties of the composites. However, tensile modulus and hardness of the composites increased with increasing RHS loading. The incorporation of multifunctional additive (MFA) improved the curing characteristics and mechanical properties of RHS filled natural rubber compounds. At 10 phr of RHS and 3 phr of MFA, tensile strength, tensile modulus, tear strength and hardness of the composites showed the maximum values. SEM micrographs indicated that the incorporation of MFA improved filler dispersion. Ismail, Nasaruddin, and Ishiaku (1999) also studied effect of Bis(3-triethoxysilylpropyl) tetrasulfide (Si-69) silane coupling agent and combination of MFA/Si-69 on the properties of RHS filled natural rubber compounds. The incorporation

of these additives increased the cure rate and improved the mechanical properties of RHS filled natural rubber vulcanizates. These were because the addition of these additives improved the functionality of the filler surface leading to the chemical bonding of the treated RHS to a rubber matrix. SEM micrographs indicated that these additives enhanced filler dispersion in the rubber matrix. Overall studies showed that MFA can be partially used to replace the Si-69 without much effect on curing characteristics and mechanical properties.

Ismail, Nizam, and Abdul Khalil (2001) investigated effect of compatibilizer, poly (propylene-ethylene-acrylic acid) (PPEAA), on properties of natural rubber (NR)/linear low density polyethylene (LLDPE) blends reinforced with RHS. The composites with and without PPEAA were prepared using an internal mixer. The result showed that tensile strength, elongation at break and mass swell of the composites decreased with increasing RHS loading. However, tensile modulus and hardness of the composites increased with increasing RHS loading. At an equal filler loading, the presence of PPEAA increased the tensile strength, tensile modulus, hardness, and elongation at break but reduced the mass swell of the composites.

Nabar, Raquez, Dubois, and Narayan (2005) studied effect of compatibilizer, maleic anhydride (MA) grafted PBAT (MA-g-PBAT), on physicomechanical and hydrophobic properties of starch foams/PBAT. 2, 5-dimethyl-2, 5-di (*tert*-butylperoxy) hexane was used as the free radical initiator for reactive grafting of MA onto PBAT. The experimental variables were investigated. Firstly, the initiator concentration was varied from 0.0 to 0.5 wt% and MA content was fixed at 3.0 wt%. Secondly, the MA concentration was varied from 1.0 to 5.0 wt% and initiator content was

fixed at 0.5 wt%. The results showed that the increase in initiator and MA content increased the grafting percentage of MA onto the polyester backbone. However, an increase in initiator content resulted in reduction of molecular weight of the polymer foam. MA-g-PBAT was proved to be very efficient in promoting strong interfacial adhesion between PBAT and starch. Incorporation of MA-g-PBAT reduced the density of starch foams and improved resilience of starch foams. Moreover, its dimensional stability and moisture absorption of starch foams was also improved.

Yang *et al.* (2007) studied effect of maleated polypropylene (MAPP) as a compatibilizing agent on mechanical properties and morphology of rice husk flour/PP composites. In PP composites preparation, the various amounts of MAPP (1, 3 and 5 wt%) were mixed with 0 to 40 wt% of rice husk flour and PP in a single screw extruder. The results showed that when the filler loading was increased, the composites without compatibilizing agent showed a decrease in tensile strength and a more brittleness due to poor interfacial adhesion between the rice husk flour and the PP matrix. However, the tensile strength and the modulus of the composites were greatly improved by incorporating the compatibilizing agent. Impact strength of the composites with and without compatibilizing decreased with increasing fillers. In contrast, the composites with compatibilizing agent presented higher impact strength than those without compatibilizing agent for all fillers loading.

Tan, Xu, Cai, and Jia (2009) studied effect of a compatibilizer, poly(propylene-*g*-maleic anhydride) (PP-*g*-MAH), on mechanical properties and filler dispersion of SiO<sub>2</sub>/PP nanocomposites. PP-*g*-MAH at 0.5 wt% based on SiO<sub>2</sub> content was mixed with 3 wt% nano-SiO<sub>2</sub> loading and PP in the melt process. The reaction of

maleic anhydride groups with the hydroxyl groups on the surface of nano-SiO<sub>2</sub> was characterized by FTIR. The results showed that PP-g-MAH played an important role in nanosilica dispersion in PP matrix and interface interaction. Therefore, the enhancement in mechanical properties of nanocomposites was because of the reduction in SiO<sub>2</sub> agglomeration and the improvement of interface adhesion between SiO<sub>2</sub> and PP matrix.

Castel, Barbosa, Liberman, and Mauler (2010) studied effect of vinyltriethoxysilane modified polypropylene (PP-g-VTES) as a compatibilizing agent on mechanical properties and morphologies of montmorillonite (OMMT)/PP nanocomposites. PP pellets were premixed with 5 wt% of organoclay and 0, 10 and 20 wt% of PP-g-VTES in a tumbling mixer, and then they were mixed in an internal mixer. The results showed that the incorporation of PP-g-VTES into OMMT/PP nanocomposites improved clay dispersion and interaction between OMMT and PP matrix leading to an increase in tensile modulus by 50%. Moreover, the maximum Izod impact strength was achieved with addition of 10% of PP-g-VTES. Moreover, PP-g-VTES presented an easily noticeable nucleating activity of OMMT by shifting the crystallization temperatures of PP composites to the higher temperatures.

# CHAPTER III

## EXPERIMENTAL

### 3.1 Materials

Rice husk was obtained from a local rice mill in Nakhon Ratchasima, Thailand. Poly(butylene adipate-*co*-terephthalate) (PBAT), P(BA-*co*-44mol%BT) with the trademark Ecoflex F BX 7011 was purchased from BASF. Hydrochloric acid (37 wt%, HCl), ethanol and methanol were purchased from Carlo-Erba.  $\gamma$ -Methacryloxypropyltrimethoxysilane (MPS), acrylic acid (AA), benzoyl peroxide (BPO) and N,N dimethylformamide (DMF) were bought from Sigma-Aldrich Chemical. The chemical structures of MPS and AA are shown in Figure 3.1.

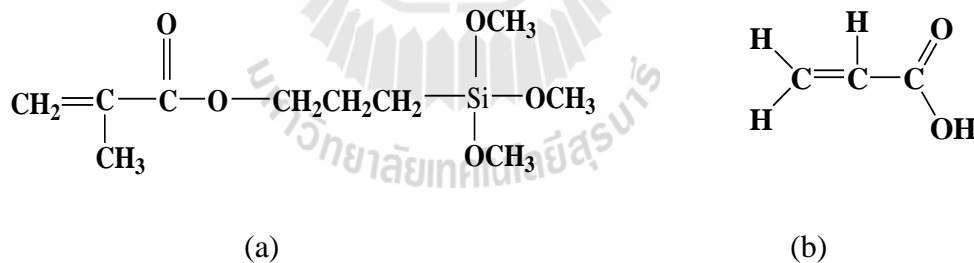


**Figure 3.1** Chemical structures of (a)  $\gamma$ -methacryloxypropyltrimethoxysilane (MPS) and (b) acrylic acid (AA).

## **3.2 Experimental**

### **3.2.1 Preparation of RHS**

RHS was prepared from rice husk as described by Wittayakun, Khemthong, and Prayoonpokarach (2008). Rice husk was washed thoroughly with water to remove the adhered soil and dust, and then dried in open air. The dried rice husk was refluxed in 3M HCl solution for 3 h, filtered and then washed repeatedly with water until the filtrate was neutral. After the HCl treatment, the rice husk was dried at 100°C overnight and heated in a muffle furnace at 550°C for 5 h to remove the organic contents. The obtained ash was called rice husk silica (RHS). The RHS was ground using with mortar and pestle and kept for further uses.

### **3.2.2 Surface modifications of RHS**

#### **3.2.2.1 Treating of MPS onto the surface of RHS particles**

MPS was pre-hydrolyzed for 30 min in a solution of ethanol/water (3/7, v/v) at a pH of 3.5. Then, RHS was immersed in the solution at a RHS to solution ratio of 3/100 (g/ml) and left under agitation for 3 h. After that the mixture was filtered, washed with the ethanol/water solution and dried at 80°C for 24 h. The amounts of MPS used were 0.5, 1.0, 2.0, 3.0 and 5.0% based on weight of RHS. Accordingly, the MPS treated RHS (MPS-RHS) particles were designated as MPS0.5-RHS, MPS1-RHS, MPS2-RHS, MPS3-RHS and MPS5-RHS based on the treated MPS content.

#### **3.2.2.2 Treating of AA onto the surface of RHS particles**

In the order to treat AA onto RHS surface, the number of hydroxyl group (OH) on the surface of RHS before treating AA onto RHS surface was determined by a titration method as described by Ong Hui Lin and Mohd Ishak (2009). RHS 2 g was

weighed and charged into an Erlenmeyer flask (100 ml), where 80 ml of 0.05 M aqueous solution of NaOH was added. The flask was capped and stirred using a magnetic stirrer for 24 h at ambient temperature. The mixture was then separated by centrifugation and 10 ml of the solution was sampled. Prior to titration, 0.5 g of phenolphthalein was added into a mixture of 50 ml ethanol and 50 ml distilled water. Phenolphthalein solution as an indicator was added into the solution and further titrated until neutralization (color changes from purple to transparent) with a 0.05 M aqueous solution of HCl (A ml). The above procedures were repeated with a blank solution (0.05 M NaOH without RHS sample). The amount of the solution of HCl for neutralization is B (ml). The amount of the surface OH groups on RHS surface can be obtained as follows.

$$X = \frac{(B-A) \times 0.05 \times 80}{W \times 10} \quad (3.1)$$

Where X (mM/g) is the amount of OH group milli-molar per unit weight of the RHS particles (g). W is mass of RHS. 80 (ml) is amount of NaOH solution and 0.05 (M) is concentration of NaOH aqueous solution. 10 (ml) is amount of the sampling NaOH solution after centrifugation. From the titration method, the amount of OH groups result was 1.714 mM/g. Then, it was used to determine the amount of AA treating on RHS surface. The ratio of AA to RHS was 0.3 g of AA to 1 g of RHS.

In the order to treat AA onto RHS surface, 16 g of AA was dissolved in 200 ml of DMF in dried glass ampoule. Then, 50 g of RHS was added into this solution after that the mixture was slowly heated to 140°C and maintained at this temperature for various time periods. Then the reaction mixture was cooled down to

room temperature. After that the mixture was filtered, washed with excessive amount of methanol for five times and dried at 80°C for 24 h. The reaction time used was 3, 6, 12 and 24 h. Accordingly, the AA treated RHS (AA-RHS) particles were designated as AA3-RHS, AA6-RHS, AA12-RHS and AA24-RHS based on the reaction time.

### 3.2.3 Characterization of RHS and surface modified RHS

Chemical compositions of untreated RHS (U-RHS), calculated as major oxides, were analyzed using an X-ray fluorescence (XRF) (EDS Oxford Instrument, model ED 2000) with an array of 16 anodes analyzing crystals and Rh X-ray tube as target with a vacuum medium.

Density ( $\rho$ ) of U-RHS was determined by using a pycnometer with known volume, filled with a distilled water with known density, Firstly, the pycnometer was filled with distilled water and weighed. The density of the sample can be determined from the known density of the water, the weight of the pycnometer filled only with the liquid, the weight of the pycnometer containing both sample and liquid, and the weight of the sample (ASTM D792).

Phase and crystallinity of U-RHS was determined by an X-ray diffraction (XRD) (Bruker AXS diffractometer, model D5005) with Cu-K $\alpha$  radiation.

Specific surface areas (BET), pore volumes and pore sizes of U-RHS, MPS-RHS and AA-RHS were determined by a nitrogen adsorption analyzer (Micrometrics, model ASAP 2010). The sample was degassed at 300°C for 3 h before measurement.

Particle size distribution of U-RHS, MPS-RHS and AA-RHS was determined by a diffraction particle size analyzer (DPSA) (Malvern Instruments, model

Mastersizer 2000). The RHS was dispersed in ethanol/water (3/7, v/v) and analyzed by He-Ne laser. The average particle size distribution was determined from the standard volume percentiles at 10, 50 and 90% and was denoted as  $d(v,0.1)$ ,  $d(v,0.5)$  and  $d(v,0.9)$ , respectively. The average particle size was defined from the average volume weighted diameter and denoted as  $d(4,3)$ .

Functional groups of U-RHS, MPS-RHS and AA-RHS were characterized by a Fourier transform infrared (FTIR) spectroscope (Perkin Elmer, model spectrum GX). Each sample was mixed with KBr powder and pressed into a disk. Then, its spectrum was recorded from 4000 to 400  $\text{cm}^{-1}$  with a resolution of 4  $\text{cm}^{-1}$ .

Thermal degradation of U-RHS, MPS-RHS and AA-RHS was determined using a thermogravimetric analyzer (TGA) (TA Instrument, model SDT 2960). To obtain a TGA thermogram, a sample was heated from 40 to 700°C at a heating rate of 10°C/min under nitrogen atmosphere.

### **3.2.4 Preparation of RHS/PBAT composites**

The RHS particle that passed through a 63  $\mu\text{m}$  mesh sieve was selected and used for preparing RHS/PBAT composites. The RHS/PBAT composites were prepared using an internal mixer (Haake, model Rheomix 3000P) with a mixing temperature of 150°C, a rotor speed of 50 rpm and a mixing time of 15 min. PBAT pellets and RHS were dried at 100°C for 4 h before mixing. Formulations for preparing RHS/PBAT composites are as follows:

- (i) U-RHS contents used to determine the optimum RHS content in PBAT composites were 10, 20, 30, 40, 50 and 60 wt% based on weight of PBAT.

- (ii) According to the optimum RHS content obtained from the previous experimental part, MPS-RHS/PBAT composites were prepared. RHS-MPS0.5, RHS-MPS1, RHS-MPS2, RHS-MPS3 and RHS-MPS5 were used to investigate effect of MPS content on properties of PBAT composites.
- (iii) By using the optimum RHS content obtained from the experimental part (i), AA-RHS/PBAT composites were prepared. RHS-AA3, RHS-AA6, RHS-AA12 and RHS-AA24 were used to fabricate the AA-RHS/PBAT composites.

Then, composite specimens were prepared using a compression molding machine (Scientific, model LP20-30) at a temperature of 170°C.

### **3.2.5 Characterization of RHS/PBAT Composites**

#### **3.2.5.1 Rheological properties**

Rheological properties of neat PBAT and PBAT composites were obtained using the Kayeness capillary rheometer (Kayeness, model D5052m) at 150°C. The viscosity of neat PBAT and PBAT composites at various shear rates (shear rate ranges 10-1000 s<sup>-1</sup>) were measured.

#### **3.2.5.2 Thermal properties**

Thermal degradation of neat PBAT and PBAT composites was determined using a thermogravimetric analyzer (TGA) (TA Instrument, model SDT 2960). To obtain a TGA thermogram, a sample was heated from 40 to 700°C at a heating rate of 10°C/min under nitrogen atmosphere as described in section 3.2.3.

Melting and crystallization behaviors of the U-RHS/PBAT composites were determined using a differential scanning calorimeter (DSC) (TA Instrument, model SDT 2920). The sample weight of approximately 10 mg was crimp-sealed in 40  $\mu\text{L}$  aluminum crucibles and scanned from 30 to 200 at 5°C/min. The melting temperature ( $T_m$ ) was measured from the thermograms (from mid-point of the endothermic peak) during the heating process. The percentage of crystallinity can be determined using Equation 3.2.

$$\text{Crystallinity (\%)} = \frac{\Delta H_{\text{sample}}}{\Delta H_f^\circ \times W} \times 100 \quad (3.2)$$

Where  $\Delta H_{\text{sample}}$  is the heat of fusion of sample (J/g) obtained from the heating scan by integration of the melting temperature.  $\Delta H_f^\circ$  is the heat of fusion of pure crystalline PBAT equal to 114 J/g (Madera-Santana, Misra, Drzal, Robledo, and Freile-Pelegrin, 2009).  $W$  is mass fraction of the PBAT in the composite.

### 3.2.5.3 Mechanical properties

Impact properties of neat PBAT and PBAT composites were tested by an impact testing machine (Atlas, model BPI) following ASTM D256. Tensile properties of neat PBAT and PBAT composites were carried out using a universal testing machine (Instron, model 5569) with a load cell of 5 kN, a crosshead speed of 50 mm/min, and a gauge length of 7.62 mm.

### 3.2.5.4 Morphological properties

Dispersion of RHS in RHS/PBAT composites and surface morphologies of tensile fracture surfaces, impact fracture surfaces and cryofracture

surfaces of the composites were obtained from a scanning electron microscope (SEM) (JEOL, model JSM 6400) at 10 kV. Samples were coated with gold before analysis.

### 3.2.5.5 Water absorption

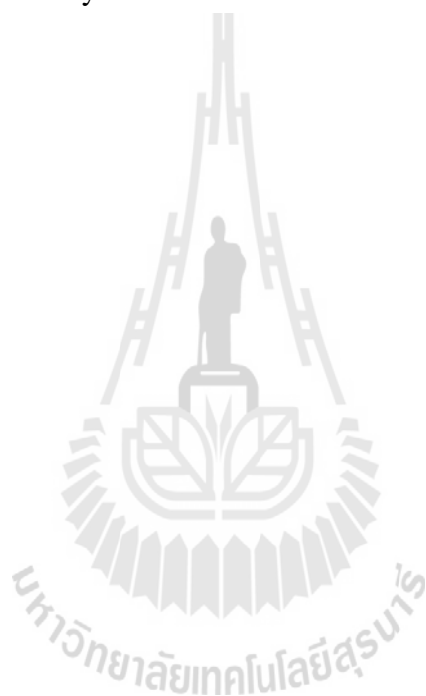
Water absorption of neat PBAT and PBAT composites was determined by measuring weight of immersion the samples in water as a function of immersion time. The specimens were prepared by compression molding. The dimension of specimen was 12.7 x 64 x 3.5 mm<sup>3</sup>. The test specimens were immersed in distilled water at room temperature for 4 months. The weight of each specimen was recorded before immersion ( $W_i$ ). During this period, the specimens were removed from water at specific intervals, gently blotted with tissue paper to remove excess water on the surface, and the specimen weight was recorded ( $W_f$ ). The water absorption was calculated by Equation 3.3. The test specimen weight before immersed in distilled water was 3.6 g for neat PBAT and 4.2 g for PBAT composites.

$$\text{Water absorption (\%)} = \frac{W_i - W_f}{W_f} \times 100 \quad (3.3)$$

### 3.2.5.6 Biodegradability

Biodegradability of neat PBAT and PBAT composites was determined by measuring weight, tensile properties and morphologies of the samples buried in soil as a function of burial time. Soil used in the test was 1:1:1 mixture of black soil, muck and burned rice husk used for gardening. Each sample was buried in the soil in planters and incubated in plant growth chamber machine (Convicon, model E7/2). The environmental chamber was employed at temperature of 30°C, 90% of humidity and fluorescent lights on for 12 h. Water was provided for every 2 days and the soil moisture

was kept 40-60% of the soil's maximum water holding capacity. The samples were removed from the soil every 20 days. The total sample incubation time was 4 months. The debris on the specimens was removed by washing with water. After that, the samples were dried in an oven at 80°C for 24 h. Then the samples were weighed using an electronic balance. Tensile properties and morphologies of the neat PBAT and the PBAT composites were investigated using the instrument and methods described in section 3.2.5.3 and 3.2.5.4, respectively.



## CHAPTER IV

### RESULTS AND DISCUSSION

#### 4.1 Effect of rice husk silica content on rheological, thermal, mechanical and morphological properties of RHS/PBAT composites

##### 4.1.1 Characterization of RHS

The photographs of as-received rice husk, HCl treated rice husk and white rice husk ash after heat treating are shown in Figure 4.1. The obtained white rice husk ash was characterized before using as a filler for fabricating PBAT composites. The results are as follows.



**Figure 4.1** Photographs of (a) as-received rice husk (b) HCl treated rice husk and (c) white rice husk ash.

XRD pattern of rice husk ash is shown in Figure 4.2. Only a broad peak at  $2\theta = 22^\circ$  was observed. This indicated the appearance of amorphous  $\text{SiO}_2$  (Kalapathy, Proctor, and Shultz, 2000).

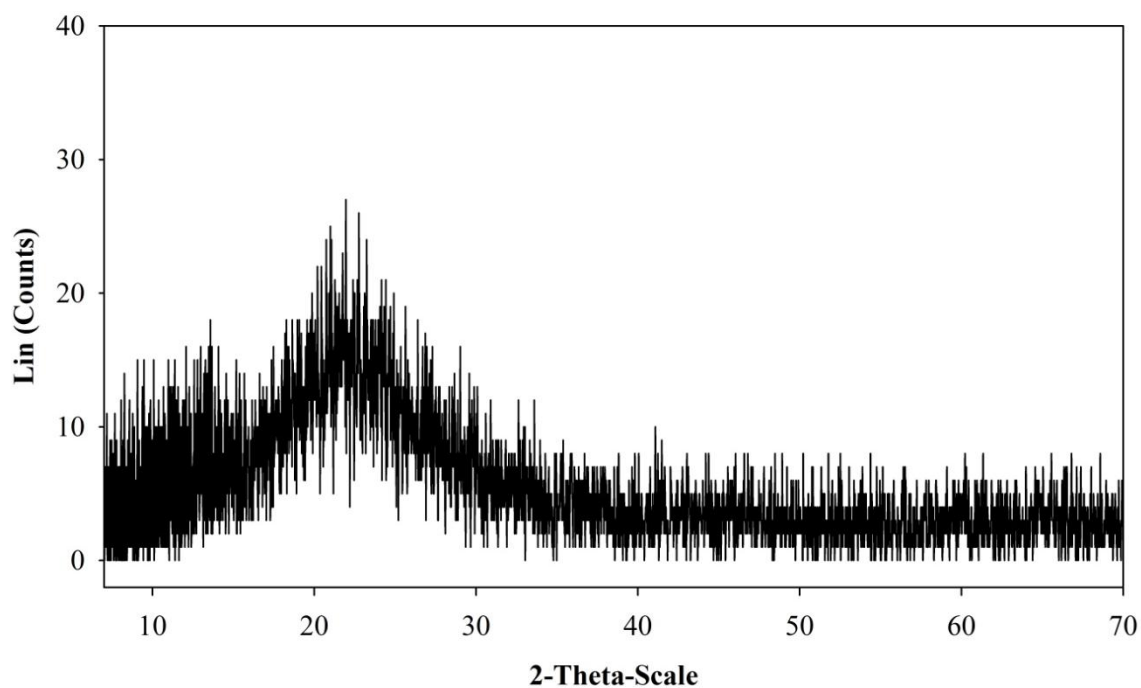


**Figure 4.2** XRD pattern of rice husk ash.

FTIR spectrum of rice husk ash is shown in Figure 4.3. The appearance of peaks at  $1090$ ,  $802$  and  $464\text{ cm}^{-1}$  were attributed to the stretching and the bending vibrations of Si-O-Si bonds (Lu, Hu, Li, Chen, and Fan, 2006). The presence of band at  $3450\text{ cm}^{-1}$  was due to the stretching vibrations of hydroxyl groups. Additionally, absorption peak observed at  $1632\text{ cm}^{-1}$  was due to the adsorbed water on rice husk ash surface (Si-H<sub>2</sub>O) (Stojanovic *et al.*, 2010).

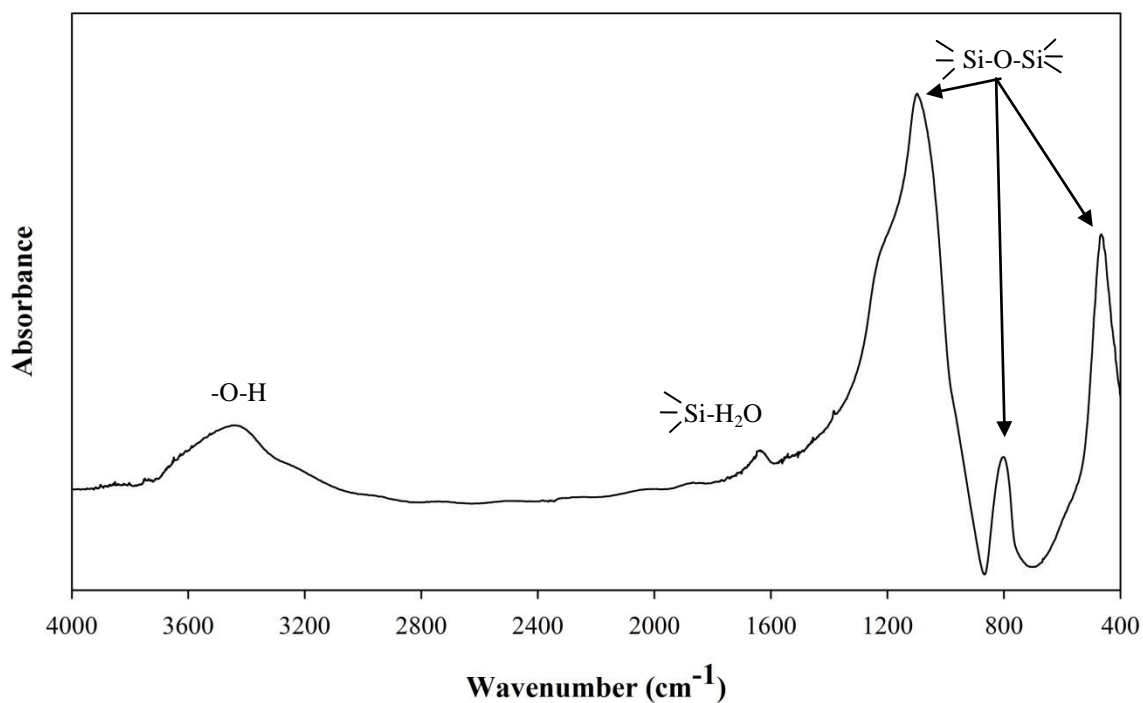


**Figure 4.3** FTIR spectrum of rice husk ash.

Chemical compositions of rice husk ash in forms of stable oxide are shown in Table 4.1. The major component of rice husk ash was SiO<sub>2</sub> with approximate purity of 97 wt% along with small amounts of other inorganic oxides including aluminum oxide (Al<sub>2</sub>O<sub>3</sub>), potassium oxide (K<sub>2</sub>O), calcium oxide (CaO) and iron oxide (Fe<sub>2</sub>O<sub>3</sub>). In addition, other physical properties of rice husk ash, *i.e.* density, BET specific surface area, average pore diameter, pore specific volume, average diameter and size distribution were also determined and reported in Table 4.2.

**Table 4.1** Chemical compositions of rice husk ash.

Component	(wt%)
SiO <sub>2</sub>	97.08
CaO	0.89
Al <sub>2</sub> O <sub>3</sub>	0.40
K <sub>2</sub> O	0.07
Fe <sub>2</sub> O <sub>3</sub>	0.03

**Table 4.2** Properties of rice husk ash.

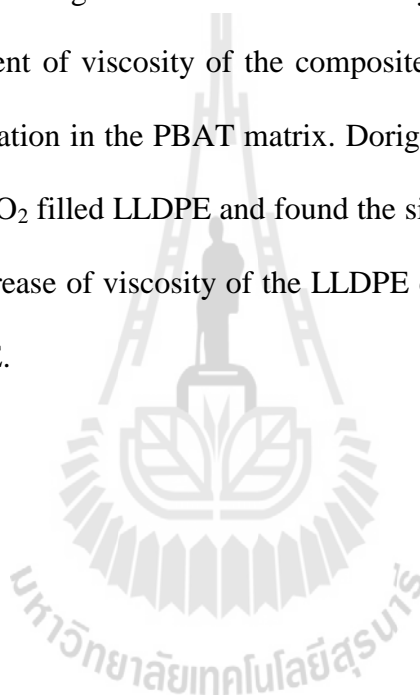
Property	Value
Density (g/cm <sup>3</sup> )	1.80
BET specific surface area (m <sup>2</sup> /g)	278.76
Average pore diameter (nm)	0.59
Pore specific volume (cm <sup>3</sup> /g)	0.41
Average diameter, d (4,3) (μm)	46.20
Particle size distribution (μm)	
d (v,0.1)	8.80
d (v,0.5)	44.48
d (v,0.9)	84.87

From the characterization results, it can be concluded that the obtained white rice husk ash was amorphous silica with approximate purity of 97 wt% which was called rice husk silica (RHS) for the rest of this work.

Since mechanical and physical properties of PBAT are similar to LDPE, HDPE and PP (Madera-Santana *et al.*, 2009) and there are only a few works reported about properties of inorganic particle reinforced PBAT matrix, the present study reported and compared the observed properties of PBAT composites with other particulate filled polyester or the mentioned polyolefin system.

#### 4.1.2 Rheological properties of neat PBAT and RHS/PBAT composites

Shear viscosities as a function of shear rate of neat PBAT and RHS/PBAT composites at various RHS contents are shown in Figure 4.4. Neat PBAT and PBAT composites showed shear thinning behavior and their viscosity increased with increasing RHS content. These results were similar to the study of Madera-Santana, Misra, Drzal, Robledo, and Freile-Pelegrin (2009). They found that the PBAT reinforced with agar particle showed shear thinning behavior and its viscosity increased with increasing agar content. The enhancement of viscosity of the composites was because the agar particle increased viscous dissipation in the PBAT matrix. Dorigato, Pegoretti, and Penati (2010) studied properties of  $\text{SiO}_2$  filled LLDPE and found the similar results, in which the  $\text{SiO}_2$  particle induced the increase of viscosity of the LLDPE composite as compared with the viscosity of neat LLDPE.



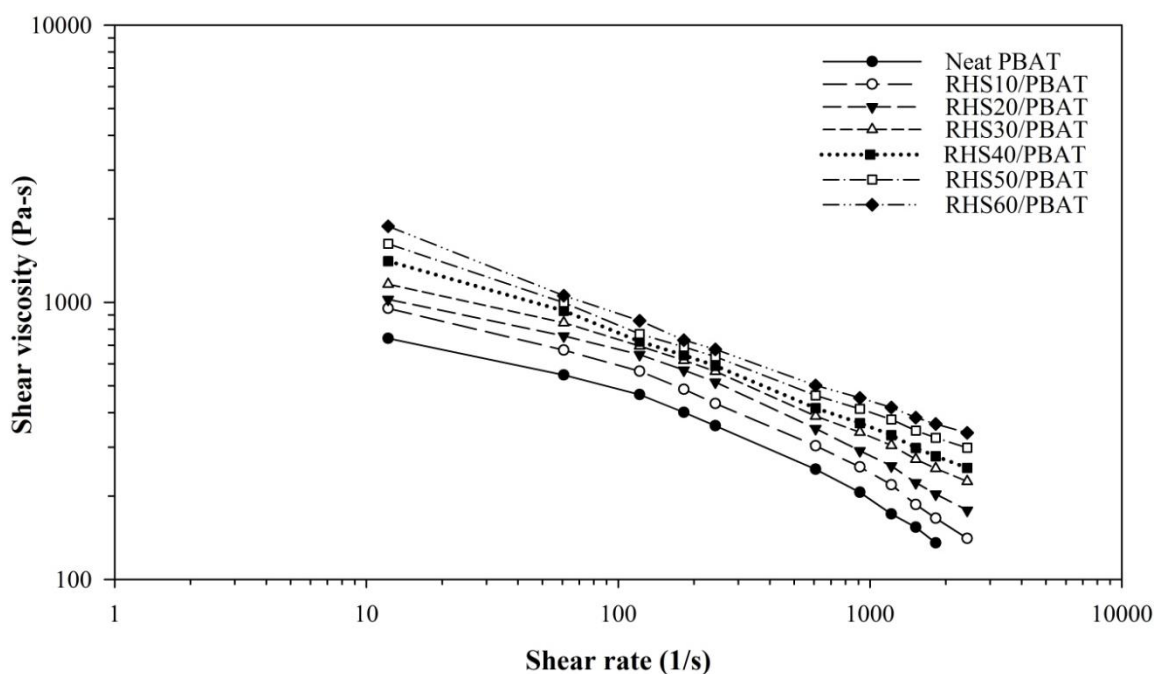


**Figure 4.4** Shear viscosity as a function of shear rate of neat PBAT and RHS/PBAT composites at various RHS contents.

#### 4.1.3 Thermal properties of neat PBAT and RHS/PBAT composites

DSC thermograms of neat PBAT and PBAT composites at various RHS contents are shown in Figure 4.5. The DSC thermograms showed single endothermic peak within the testing temperature range of 30-200°C. Their melting temperatures ( $T_m$ ) (determined from the mid-point of the endothermic peak) and percentages of crystallinity are summarized in Table 4.3. The  $T_m$  of neat PBAT was observed at 119°C while those of PBAT composites were slightly lower. Furthermore, the percentage of crystallinity in PBAT composites was higher than that of neat PBAT and increased with increasing RHS content. This indicated that RHS served as a nucleating agent and made crystallization easier for PBAT matrix. Liu *et al.* (2003) studied SiO<sub>2</sub>/PET composites systems and observed the similar results. They found that the SiO<sub>2</sub> served as the nucleating agent and

enhanced the crystallization rate of the PET. Also, this phenomenon was similar to that found in SiO<sub>2</sub> filled PP systems, in which the percentage of crystallinity in PP composites was higher than that of neat PP and increased with increasing SiO<sub>2</sub> content (Bikiaris, *et al.*, 2006).

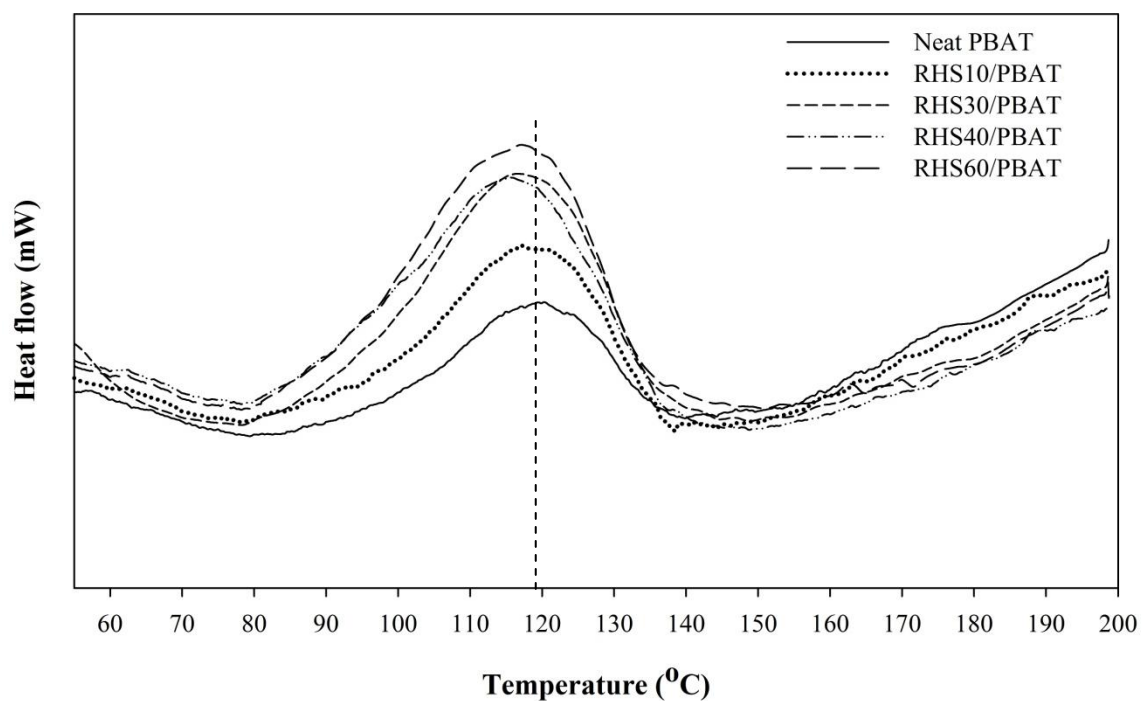


**Figure 4.5** DSC thermograms of neat PBAT and PBAT composites at various RHS contents.

**Table 4.3** Melting temperature and crystallinity of neat PBAT and PBAT composites at various RHS contents.

<b>Materials</b>	<b>T<sub>m</sub> (°C)</b>	<b>Crystallinity (%)</b>
Neat PBAT	119.34	4.58
RHS10/PBAT	115.46	12.19
RHS30/PBAT	116.50	18.48
RHS40/PBAT	117.04	30.48
RHS60/PBAT	117.12	38.27

#### **4.1.4 Mechanical properties of neat PBAT and RHS/PBAT composites**

The influence of RHS content on mechanical properties of PBAT composites are displayed in Figure 4.6-4.9.

A gradual change in stress-strain behavior of neat PBAT and PBAT composites with increasing RHS content was observed in Figure 4.6. The stress-strain curves of neat PBAT and the PBAT composites at 10-30 wt% of RHS showed a proportional limit (stress is proportional to strain) followed by abrupt yielding with necking and strain hardening. On the other hand, the stress-strain curves of PBAT composites at RHS beyond 30 wt% showed a proportional limit followed by abrupt yielding with small elongation before breaking. It was noticed that the elongation at break of the RHS10/PBAT composite tremendously decreased as compared with that of the neat PBAT. Moreover, the elongation at break of the PBAT composites further decreased with increasing RHS content.

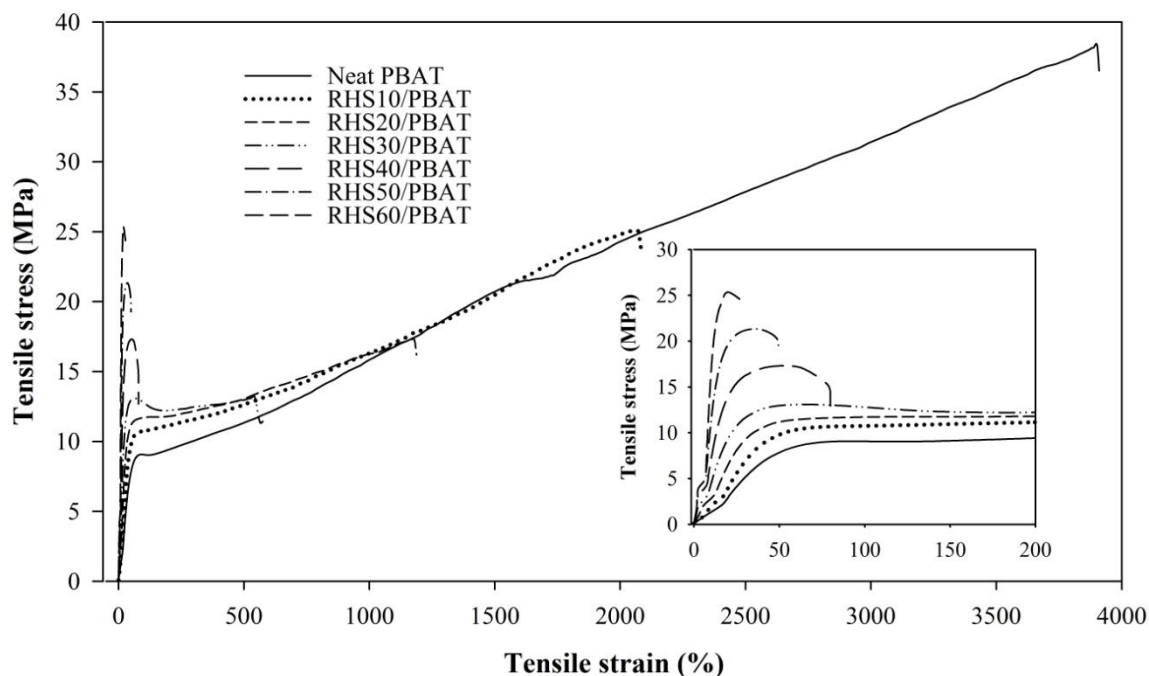


**Figure 4.6** Stress-strain curves of neat PBAT and PBAT composites at various RHS contents.

Tensile modulus and elongation at break of neat PBAT and RHS/PBAT composites various RHS contents are shown in Figure 4.7. Tensile modulus of the PBAT composites significantly increased with increasing RHS content. In contrast, a rather precipitous drop of elongation at break of the PBAT composites was observed with the addition of RHS between 10 to 40 wt%. This was because the rigid filler in the polymer matrix restrained mobility and stretching ability of the polymer chains (Nurdina, Mariatti, and Samayamutthirian, 2011). Another factor affecting tensile modulus and elongation at break of the polymer composites was the degree of crystallinity of polymer component (Galeski, 2003; Someya, Sugahara, and Shibata, 2005). The crystallinity of PBAT composites as shown in Table 4.3 increased with the addition of RHS.

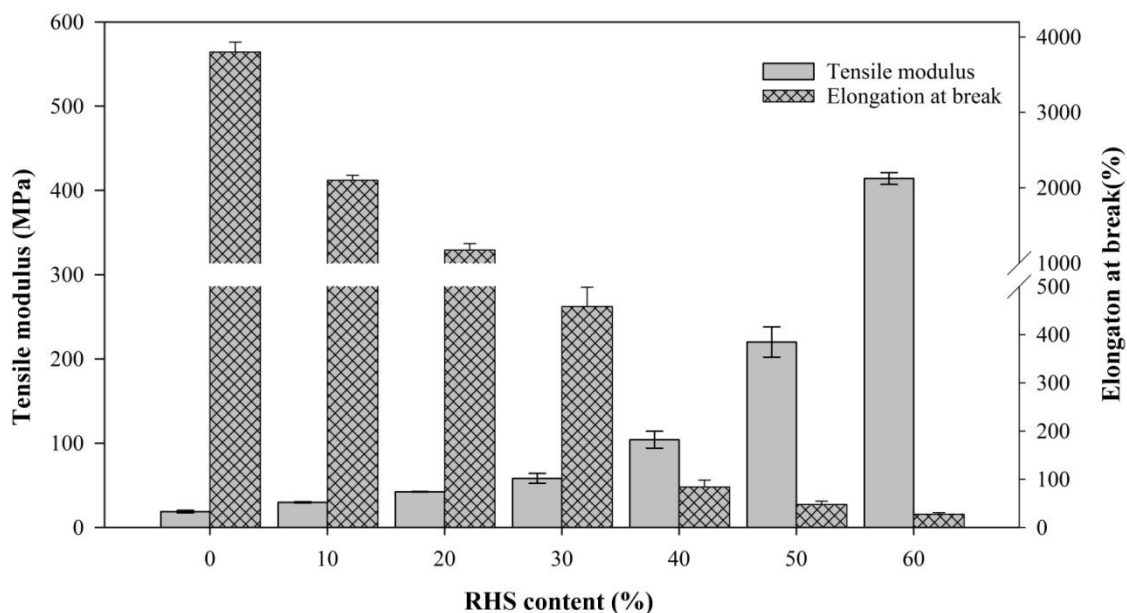
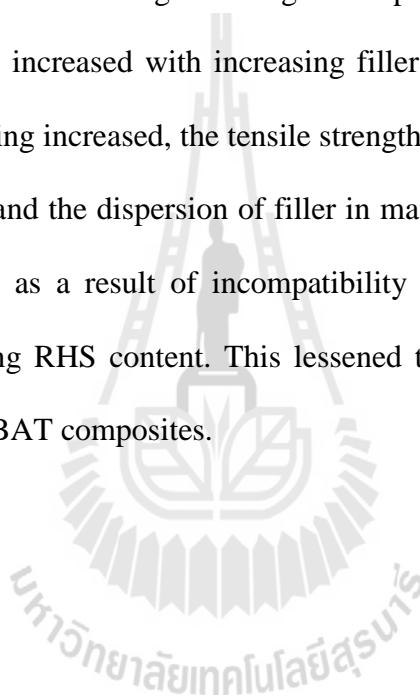


**Figure 4.7** Tensile modulus and elongation at break of neat PBAT and PBAT composites at various RHS contents.

Tensile strength of neat PBAT and RHS/PBAT composites were obtained from the ultimate load divided by the cross sectional area of the sample. Tensile strength of neat PBAT and RHS/PBAT composites at various RHS contents is shown in Figure 4.8. As seen in the figure, the PBAT composites with 30 wt% of RHS had the lowest tensile strength. A gradual increase in tensile strength of the PBAT composites was noticed with RHS content diverting either ways from 30 wt%.

At RHS content of 30 wt% or lower, the PBAT composites showed strain hardening after yielding and high value of elongation at break as seen in Figure 4.6. This was because PBAT composites at low RHS content had low resistance to the PBAT deformation under tension and, therefore, the stress-stain behaviors of the PBAT composites were governed by behavior of PBAT matrix.

As RHS content in PBAT composites was beyond 30 wt%, the PBAT composites showed small value of elongation at break and their tensile strength increased with increasing RHS content. This was probably because the tensile strength of the PBAT composites was governed by the properties of RHS filler. Theoretically, in the case of varying filler content, the mechanical properties of the composites depended on not only the content of the filler in the matrix but also the properties of the filler and the matrix. Generally, the inorganic filler had higher strength than polymer matrix and the strength of the polymer composites increased with increasing filler content (Arencon and Velasco, 2009). As the filler loading increased, the tensile strength of the composites compromised between filler property and the dispersion of filler in matrix. However, the micro-void at RHS-PBAT interphases as a result of incompatibility between those two phases also increased with increasing RHS content. This lessened the effect of filler properties on tensile strength of the PBAT composites.



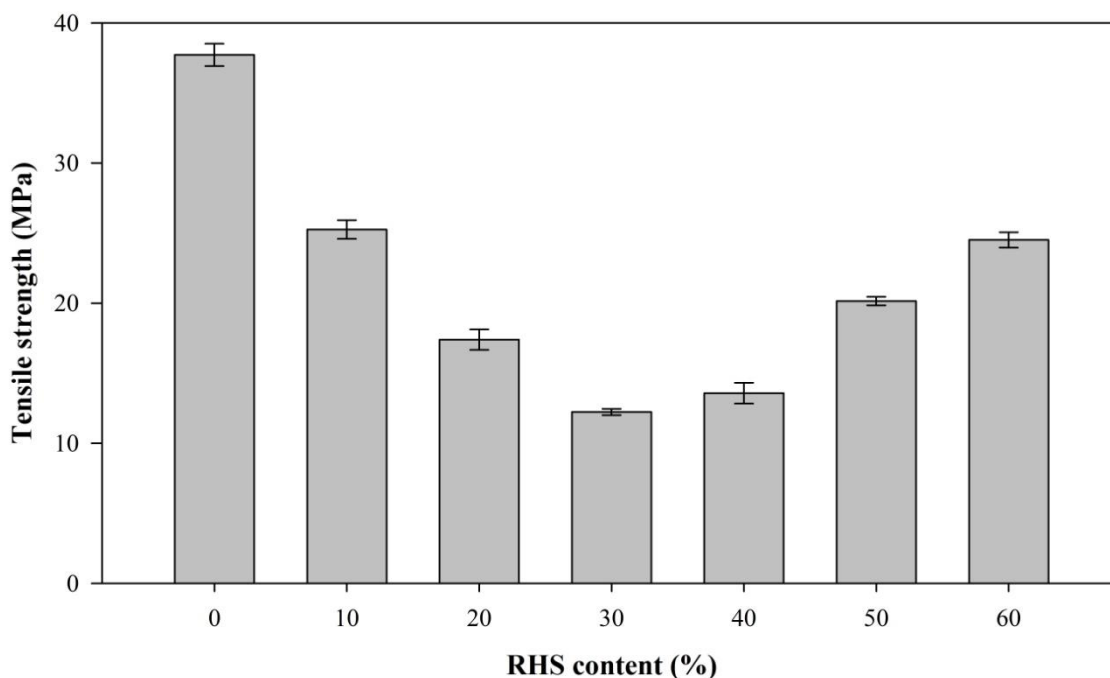


**Figure 4.8** Tensile strength of neat PBAT and PBAT composites at various RHS contents.

Yield strength of neat PBAT and RHS/PBAT composites were obtained from the maximum stress a material can withstand without permanent deformation. Yield strength of neat PBAT and RHS/PBAT composites at various RHS contents is shown in Figure 4.9. Yield strength of neat PBAT composites increased with increasing RHS content. The increase in yield strength of polymer was a linear function of the increasing of polymer crystallinity (Galeski, 2003). Bikiaris *et al.* (2006) observed the similar results in SO<sub>2</sub>/PP composite system. It was explained that the increase in yield strength of the PP composites was due to an increase in crystallinity of the PP matrix. The SO<sub>2</sub> acted as a nucleating agent for PP matrix and retarded the mobility of the PP chains resulting in a higher yield strength and modulus under tensile.

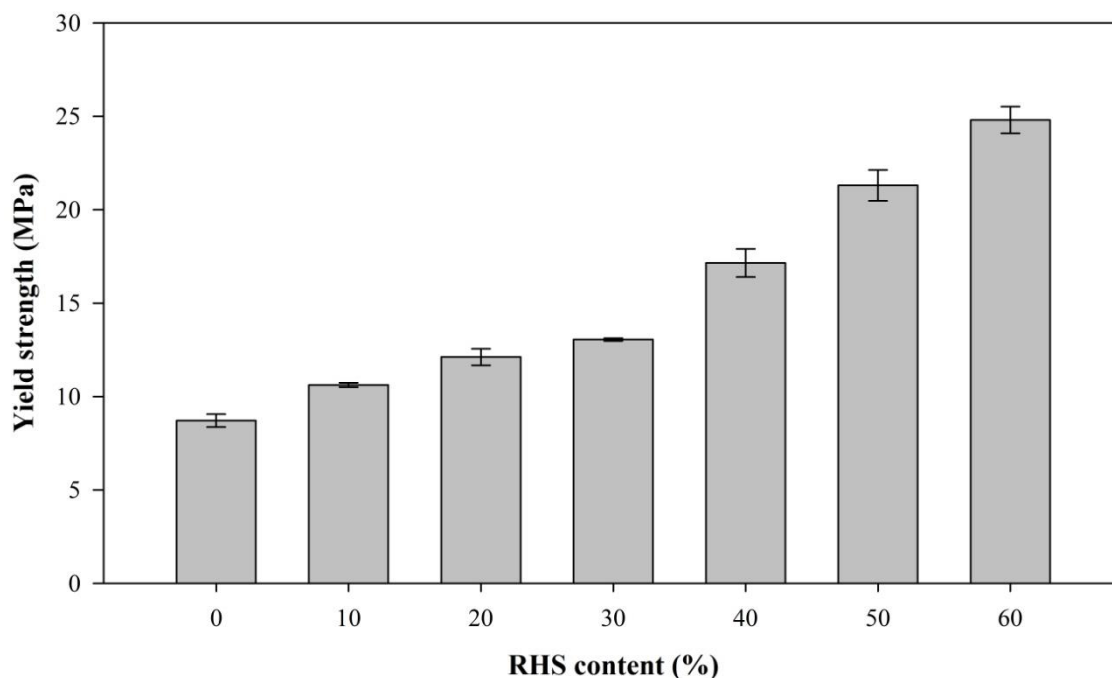


**Figure 4.9** Yield strength of neat PBAT and PBAT composites at various RHS contents.

Impact strength of PBAT composites at various RHS contents is shown in Figure 4.10. The specimens containing RHS between 0 to 20 wt% did not break at the striking impact energy of 2.7 J indicating that their impact strength, calculated from maximum energy divided by the cross sectional area of the specimens, was higher than  $144 \text{ kJ/m}^2$ . Figure 4.10 revealed that impact strength of the composites decreased with increasing RHS content. Basically, the impact strength of the PBAT composites is influenced by the filler fraction and the interfacial adhesion between filler and matrix. RHS particles in the PBAT matrix acted as micro-crack initiator. With increasing RHS content in PBAT, the rate of crack propagation increased and the impact strength of PBAT composites decreased. In addition, impact behaviors of polymer composites also related to crystallinity and the crystalline size of polymer matrix. The crystallinity of

PBAT composites as shown in Table 4.3 increased with the addition of RHS. The increase in values of crystallinity led to the decrease in impact strength of the polymer composites (Wang, Wu, Ye, Zeng, and Cai, 2003).

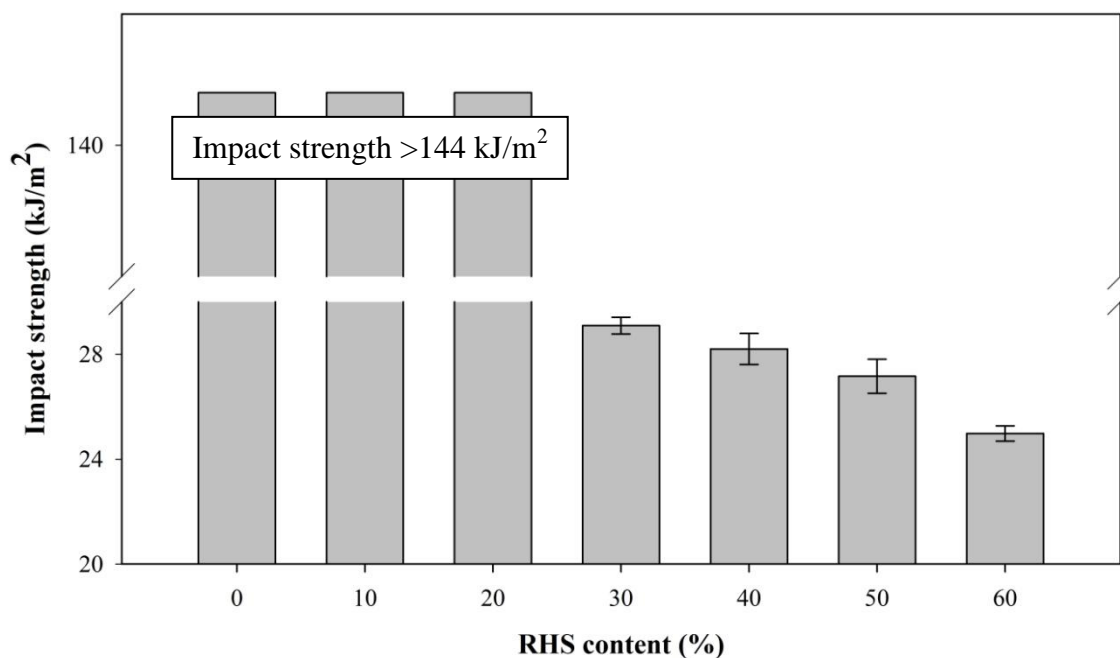
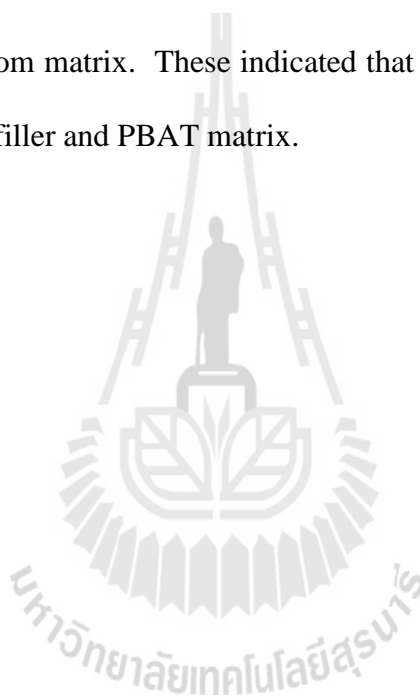


**Figure 4.10** Impact strength of PBAT and PBAT composites at various RHS contents.

#### 4.1.5 Morphological properties of RHS/PBAT composites

SEM micrographs of tensile fracture surfaces and impact fracture surfaces of neat PBAT and PBAT composites at various RHS contents are shown in Figure 4.11 and Figure 4.12, respectively. The micrographs in Figure 4.11(a-f) clearly revealed that the extended fibrils of PBAT composites were shorter than those of the neat PBAT. Moreover, the extended fibrils of PBAT composites decreased with the addition of RHS. This was because the existence of RHS in PBAT matrix restrained the mobility of the PBAT chains and made the PBAT matrix brittle. These tensile fracture surface

morphologies supported the observed stress-strain behaviors of PBAT composites (Figure 4.6). In addition, SEM micrographs of impact fracture surfaces of PBAT composites at various RHS contents are shown in Figure 4.12. The PBAT composite at 30 wt% of RHS in Figure 4.12(a) revealed a gap between RHS–PBAT interphase and a cleaned RHS surface without the adhered PBAT ligaments on the RHS surface. In Figure 4.12 (b-d), the PBAT reinforced with RHS beyond 30 wt% showed not only the debonding between RHS–PBAT and the cleaned RHS surface but also the hole of missing RHS particle from matrix. These indicated that the PBAT composites had weak adhesion between RHS filler and PBAT matrix.



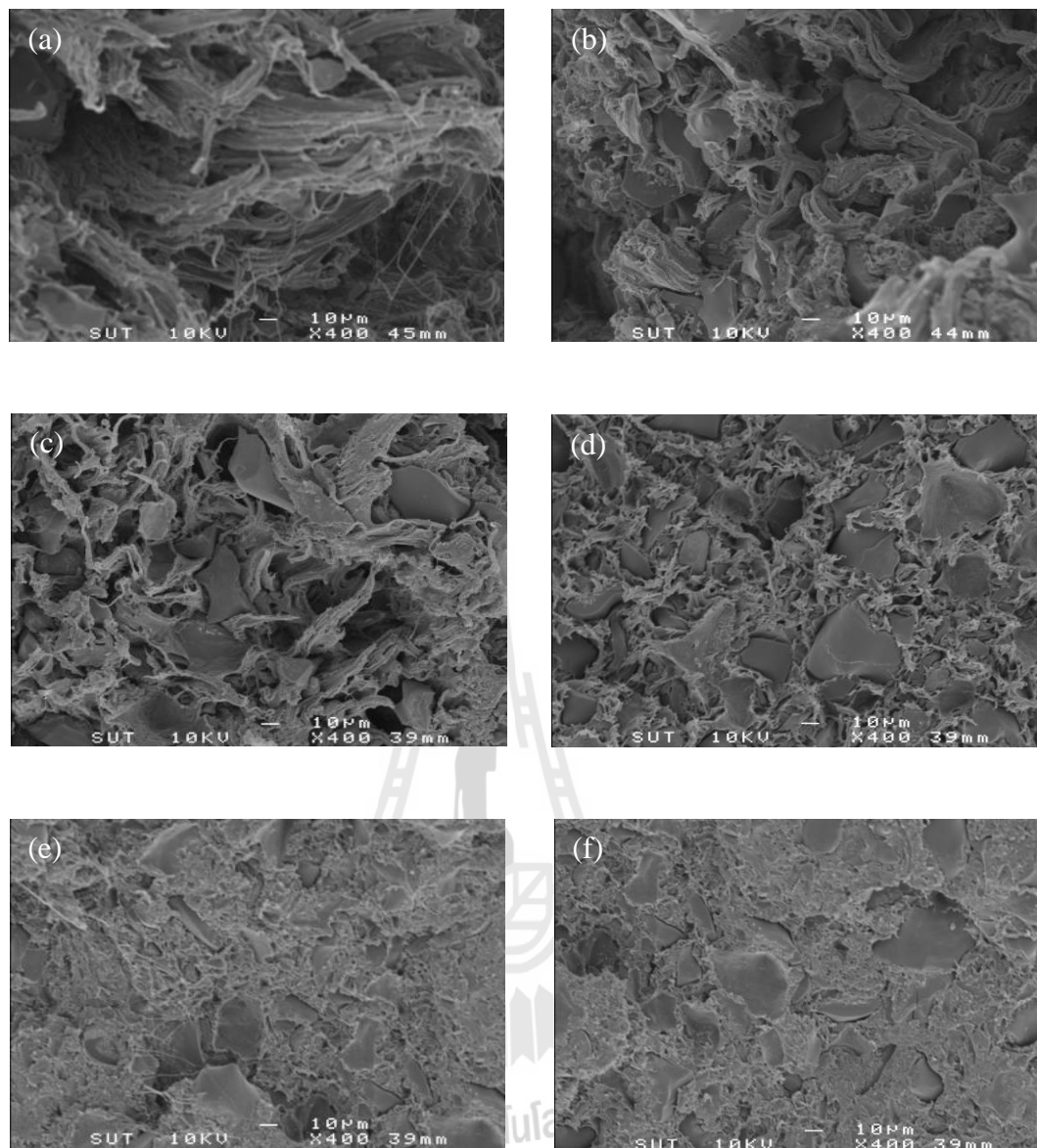


**Figure 4.11** SEM micrographs of tensile fracture surfaces of (a) neat PBAT and PBAT composites at various RHS contents: (b) 20 wt%, (c) 30 wt%, (d) 40 wt%, (e) 50 wt% and (f) 60 wt%.

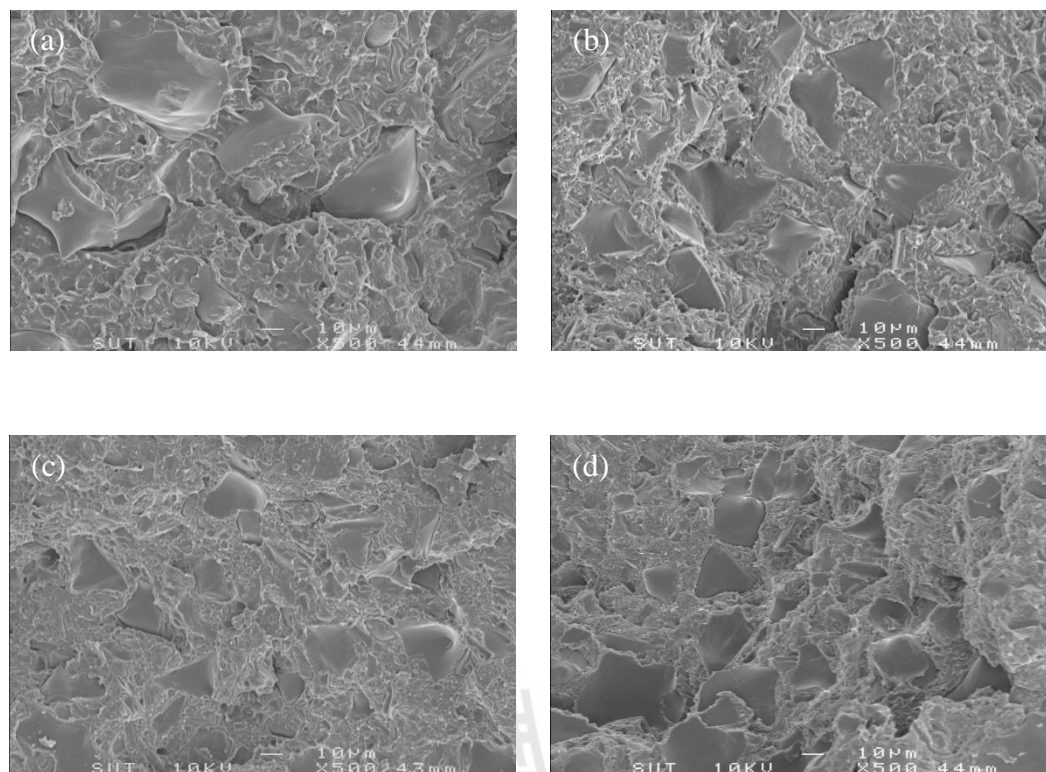


**Figure 4.12** SEM micrographs of impact fracture surfaces of neat PBAT composites at various RHS contents: (a) 30 wt%, (b) 40 wt%, (c) 50 wt% and (d) 60 wt%.

In this part of the study, amorphous silica with 97% purity was prepared and used as filler for PBAT matrix. The effects of RHS content on rheological, thermal, mechanical and morphological properties of the PBAT composites were studied. The incorporation of RHS into PBAT matrix increased tensile modulus and yield strength while decreased elongation at break and impact strength of the PBAT composites. The stress-strain behaviors of PBAT composites become less ductile at RHS content beyond 30 wt%. The increase in tensile modulus and the improved stiffness of PBAT matrix were because RHS had high tensile modulus compared with PBAT matrix. In addition,

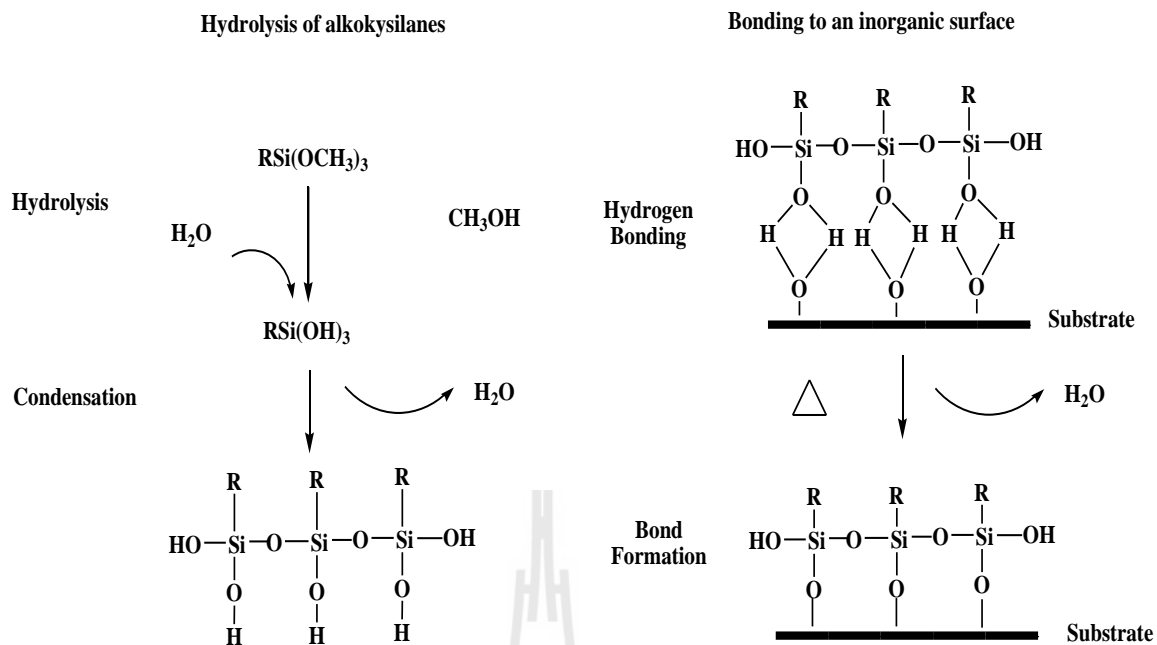
the added RHS acted as nucleating agent for the PBAT matrix, restrained PBAT chains mobility and limited elongation at break of the PBAT matrix. Moreover, the SEM morphologies revealed a weak surface adhesion between RHS and PBAT matrix which caused the decrease in impact strength and tensile strength of the PBAT composites.

Therefore, the following section reported approaches to improve the properties of RHS/PBAT composites. The MPS silane coupling agent and acrylic acid (AA) were used to modify surface of RHS before mixing with PBAT. The RHS content of 30 wt% was selected for fabricating RHS/PBAT composites. This was because the composite at this RHS content had optimum mechanical properties and showed plastic deformed behavior.

## **4.2 Effect of $\gamma$ -methacryloxypropyltrimethoxysilane (MPS) content on rheological, mechanical, thermal and morphological properties of MPS treated RHS/PBAT composites**

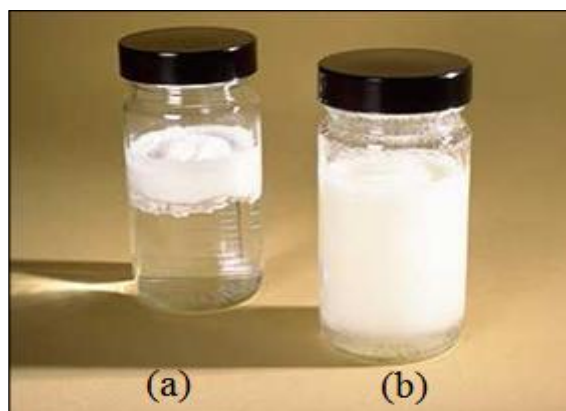
### **4.2.1 Characterization of MPS treated RHS**

Chemical structure of MPS is shown in Figure 3.1. In order to modify RHS surface, MPS must be chemically activated as proposed in Figure 4.13. Firstly, methacryloxypropyl groups of MPS are hydrolyzed to obtain hydroxyl groups. Secondly, hydroxy groups from each MPS molecules are condensed to form silane oligomers. Then, these oligomers are formed hydrogen bonds with hydroxyl groups on RHS surface. These physical bonds can be converted to covalent bonds during drying RHS particles (Kanani, Krishnan, and Narayan, 1997).



**Figure 4.13** Schematic illustration of silane treated rice hush silica (Kanani, Krishnan, and Narayan, 1997).

The photographs of untreated RHS (U-RHS) and MPS treated RHS (MPS-RHS) particles immersed in water at equal time period are shown in Figure 4.14. As seen, U-RHS was homogeneously dispersed in water while MPS-RHS was obviously separated from water. These suggested that surfaces of MPS-RHS had lower hydrophilicity compared with those of U-RHS. The obtained MPS-RHS was further characterized before using it as a filler for fabricating RHS/PBAT composites. The results were reported as follows.



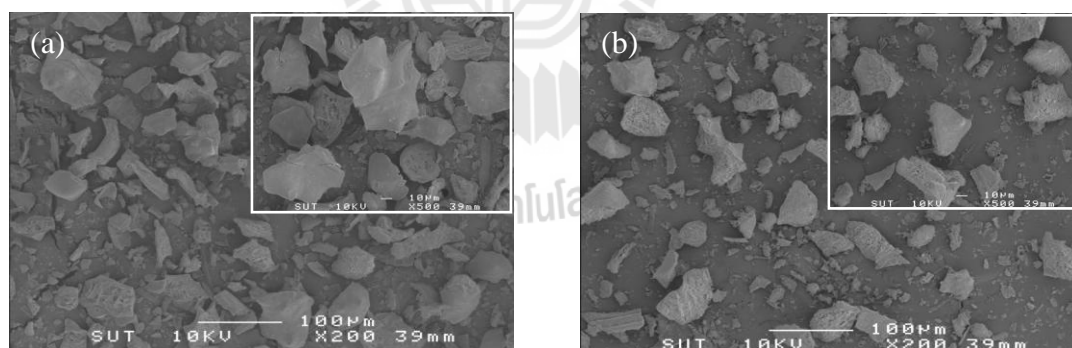
**Figure 4.14** Photographs of RHS particles in water (a) MPS-RHS and (b) U-RHS.

Table 4.4 shows the summarized results of particle size distribution, specific surface area and pore characteristic of U-RHS and MPS-RHS particles. In comparison between U-RHS and MPS-RHS, U-RHS showed the highest particle size distribution while the particle size distribution of MPS-RHS decreased with increasing MPS content up to 2 wt%. This may be due to the breaking up of RHS agglomerates during MPS treating process that led to the smaller RHS particles. The specific surface area of U-RHS particles showed the highest value while the specific surface area of the MPS-RHS decreased with increasing MPS content. Also, the pore volumes of U-RHS were the highest while those of the MPS-RHS decreased with increasing MPS content. The decrease in specific surface area and pore volumes of MPS-RHS particles were because the MPS molecules were planted on RHS particles (Wu, Zhang, Rong, and Friedrich, 2005). The pore diameters of the U-RHS were the lowest whereas the pore diameters of MPS-RHS increased with increasing MPS content.

**Table 4.4** Average diameter, surface area and pore characteristics of U-RHS and MPS-RHS at various MPS contents.

Material	Average diameter, $d(4,3)$ ( $\mu\text{m}$ )	Total pore volume ( $\text{ml/g}$ )	Average pore diameter ( $\text{nm}$ )	BET surface area ( $\text{m}^2/\text{g}$ )
U-RHS	46.20	0.41	0.59	278.76
MPS1-RHS	44.26	0.32	0.73	181.76
MPS2-RHS	39.18	0.29	0.76	149.68
MPS5-RHS	36.29	0.28	0.79	146.90

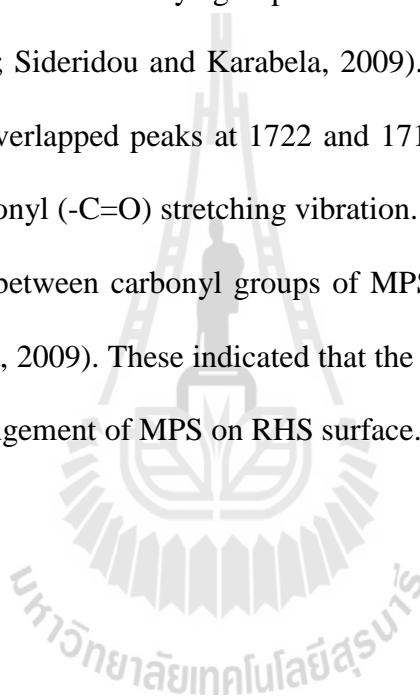
SEM micrographs of U-RHS and MPS-RHS particles are shown in Figure 4.15. The micrograph of U-RHS in Figure 4.15(a) showed an irregular geometry and a large scale of particle size distribution. On the other hand, the micrograph of MPS-RHS in Figure 4.15(b) showed the reduction in particles size distribution of RHS after treating with MPS. The SEM micrographs were in agreement with the data reported in Table 4.4.

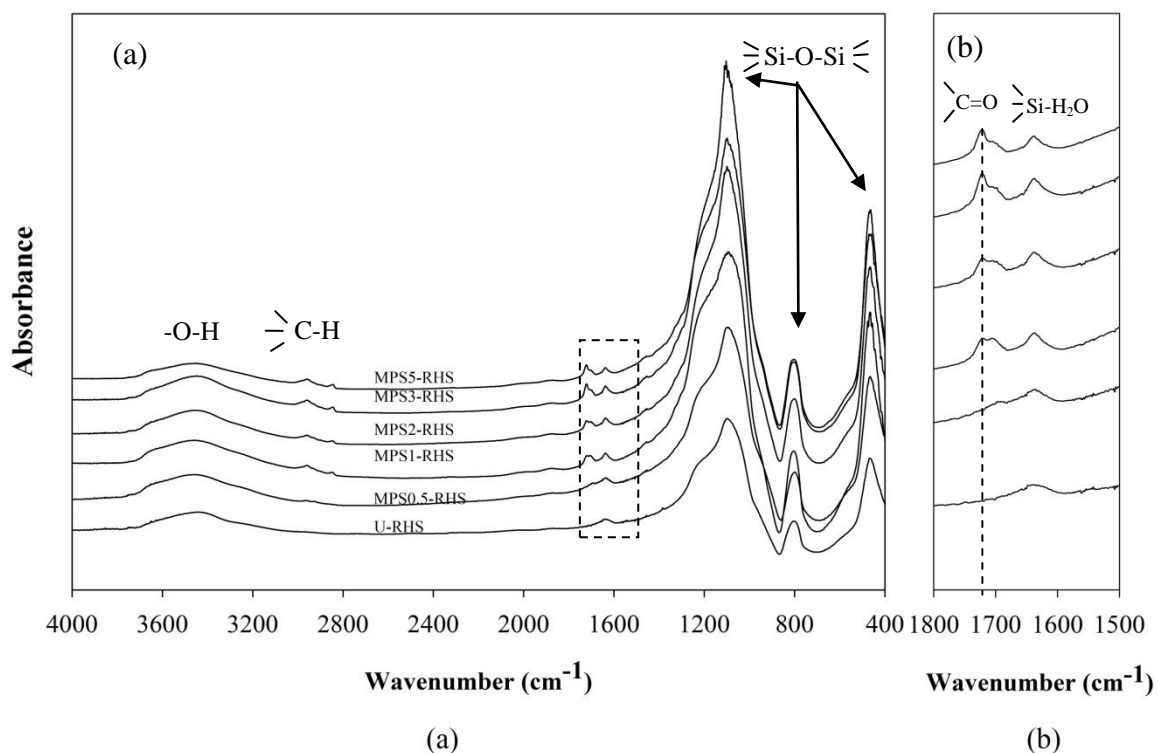


**Figure 4.15** SEM micrographs of (a) U-RHS and (b) MPS2-RHS.

FTIR spectra of U-RHS and MPS-RHS at various MPS contents are shown in Figure 4.16. The absorption bands of U-RHS were described in section 4.1. The additional absorption bands of MPS-RHS were observed around 2968, 2857 and

1452  $\text{cm}^{-1}$ . These bands belonged to C-H asymmetrical stretching, C-H symmetrical stretching and C-H scissoring vibrations, respectively (Lu, Hu, Li, Chen, and Fan, 2006). In addition, the bands around 1717-1722  $\text{cm}^{-1}$  belonged to carbonyl (C=O) stretching vibration of MPS (Sideridou and Karabela, 2009). These suggested that the MPS molecules were presented on RHS surfaces. For MPS0.5-RHS, FTIR spectrum showed single carbonyl stretching vibration at 1717  $\text{cm}^{-1}$  which belonged to the characteristic of the hydrogen bonds between carbonyl groups of MPS with hydroxyl groups of RHS (Stojanovic *et al.*, 2010; Sideridou and Karabela, 2009). With increasing MPS content, FTIR spectra showed overlapped peaks at 1722 and 1718  $\text{cm}^{-1}$ . The peak at 1722  $\text{cm}^{-1}$  was due to the free carbonyl (-C=O) stretching vibration. The peak at 1718  $\text{cm}^{-1}$  was due to the hydrogen bonds between carbonyl groups of MPS with hydroxyl groups of RHS (Sideridou and Karabela, 2009). These indicated that the increase in MPS content seemed to affect molecular arrangement of MPS on RHS surface.

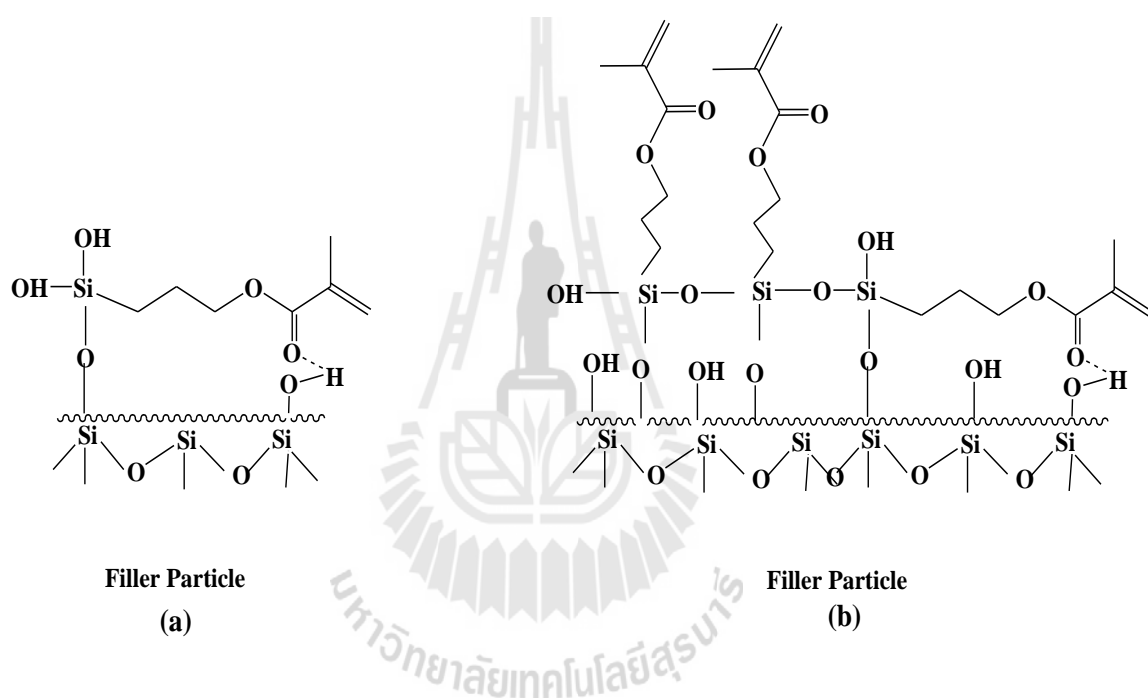




**Figure 4.16** FTIR spectra of U-RHS and MPS-RHS at various MPS contents (a) wavenumber 4000-400  $\text{cm}^{-1}$  and (b) wavenumber 1800-1500  $\text{cm}^{-1}$ .

Sideridou and Karabela (2009) modified surface of  $\text{SiO}_2$  by various MPS contents. They proposed that various arrangements of MPS molecules may appear on  $\text{SiO}_2$  surface according to the treated MPS content. Their proposed molecular orientations of MPS on  $\text{SiO}_2$  surface are shown in Figure 4.17. With using MPS at low content, they observed evidence of hydrogen bonding between carbonyl groups of MPS and hydroxyl groups of  $\text{SiO}_2$  and they proposed the parallel orientation of MPS molecules on RHS surface (Figure 4.17(a)). With increasing MPS content, they proposed random (parallel and perpendicular) orientation of MPS molecular on RHS surface (Figure 4.17(b)). In this present study, the FTIR spectra of the MPS-RHS showed the overlaps bands between free carbonyl ( $\text{-C=O}$ ) and hydrogen bonded carbonyl groups with increasing MPS content.

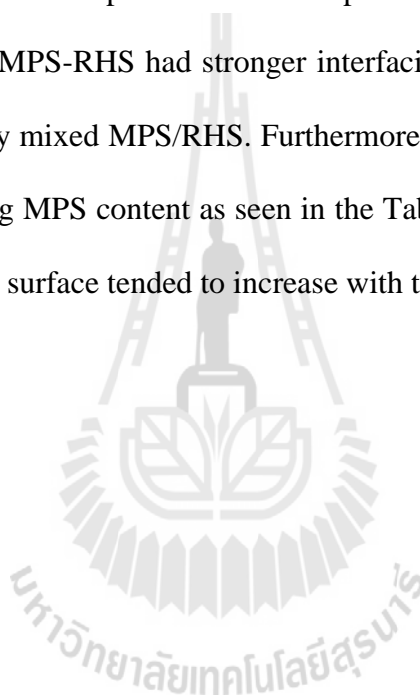
The intensities ratio of the absorption peaks at 1722 to 1632  $\text{cm}^{-1}$  ( $A_{1722}/A_{1632}$ ), *i.e.* the ratio of carbonyl peak to water absorption peak on RHS surface, and the intensities ratio of the absorption peaks at 1722 to 1718  $\text{cm}^{-1}$  ( $A_{1722}/A_{1718}$ ) ratios tended to increase with increasing MPS content. These suggested that the amounts of MPS molecules on RHS surface and the perpendicular orientation of MPS molecular on RHS surface tended to increase with the addition of MPS.



**Figure 4.17** Simplified illustrative molecular structures of (a) random and (b) parallel monomolecular MPS molecules (Sideridou and Karabela, 2009).

TGA thermograms of U-RHS, physically mixed MPS/RHS and MPS-RHS at various MPS contents are shown in Figure 4.18. Their decomposition temperatures ( $T_d$ ) (determined from the temperature corresponding to the maximum rate of decomposition) and residue weights at 600°C are summarized in Table 4.5. All samples demonstrated a slight weight loss around 250°C and below due to the physisorbed water

evaporation and the liberation of water in the RHS particles (above 200°C) (Ma *et al.*, 2010). In comparison, TGA thermograms of MPS-RHS had lower weight loss at this temperature range than that of U-RHS. This indicated that the adsorbed water on RHS surface of MPS-RHS was lower than that of U-RHS. TGA thermograms of physically mixed MPS/RHS in Figure 4.18(b) showed the weight loss at the lower temperature range (around 150°C) as compared with those of MPS-RHS and U-RHS. Additionally, this range of temperature corresponded to the evaporation of adsorbed MPS molecules. This suggested that the MPS-RHS had stronger interfacial interaction between RHS and RHS than the physically mixed MPS/RHS. Furthermore, weight losses of the MPS-RHS increased with increasing MPS content as seen in the Table 4.5. These suggested that the MPS molecules on RHS surface tended to increase with the addition of MPS.



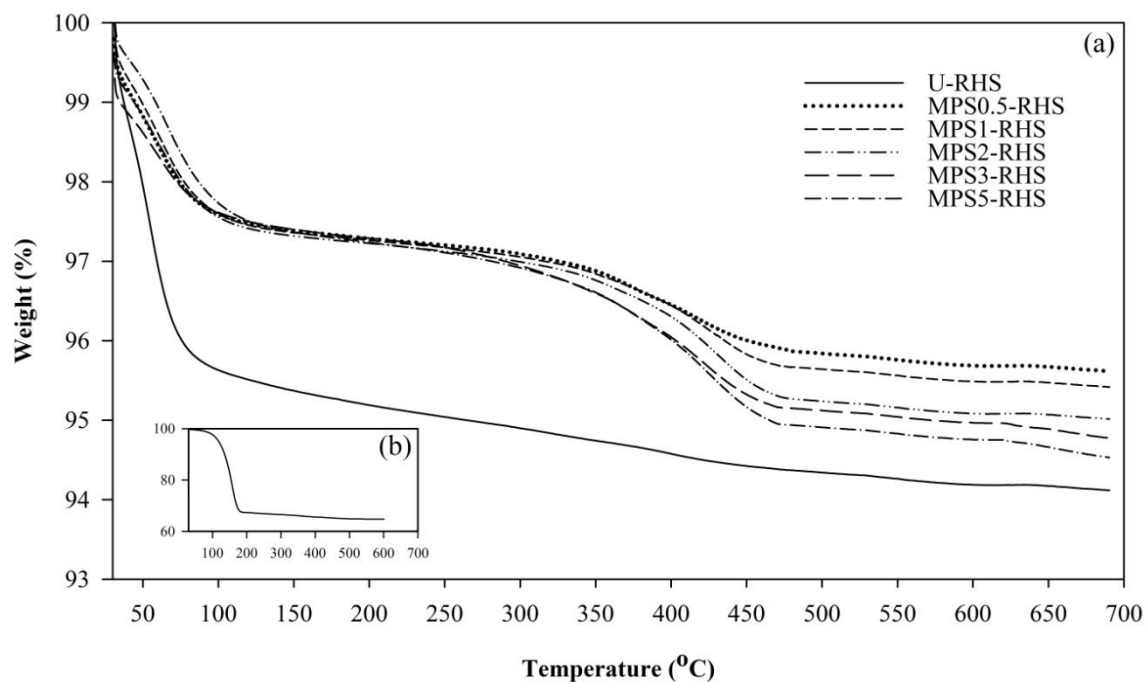


**Figure 4.18** TGA thermograms of (a) U-RHS, MPS-RHS at various MPS contents and (b) physically mixed MPS/RHS.

**Table 4.5** Decomposition temperatures and residue weight at 600°C of physically mixed MPS/RHS, U-RHS and MPS-RHS at various MPS contents.

Sample	$T_d$ (°C)	Residue weight at 600°C (%)
U-RHS	-	94.75
Mixed MPS/RHS	157.91	64.71
MPS0.5-RHS	430.89	96.66
MPS1-RHS	430.49	96.48
MPS2-RHS	428.54	95.98
MPS3-RHS	425.92	95.87
MPS5-RHS	425.63	95.45

#### 4.2.2 Rheological properties of MPS treated RHS/PBAT composites

Figure 4.19 shows shear viscosity as a function of shear rate of neat PBAT, U-RHS/PBAT and MPS-RHS/PBAT composites. The viscosity of neat PBAT and PBAT composites decreased with increasing shear rate. The addition of RHS into PBAT increased the viscosity of neat PBAT. For PBAT composites, shear viscosity of MPS-RHS/PBAT composites were slightly higher than that of U-RHS/PBAT composite. Additionally, shear viscosity of MPS-RHS/PBAT composites slightly increased with increasing MPS content through shear rate ranges. These results implied that the rheological properties of samples not only depended on the addition of RHS filler into PBAT but also MPS molecules on the RHS filler surface modifications. This was presumably because the existence of RHS perturbed the flow of polymer and hindered the mobility of chain segments in melt flow under shear stresses. The enhancement in shear viscosity of MPS-RHS/PBAT composites, as compared with the others like neat PBAT and U-RHS/PBAT composite, was probably because of the good dispersion of the MPS-RHS in PBAT and the strong interfacial adhesion between the filler and the matrix. Bailly and Kontopoulou (2009) studied the rheological property of silane-grafted PP reinforced with SiO<sub>2</sub> and toughened with an elastomeric ethylene–octene copolymer (EOC). They suggested that the improvements in rheological property and the increase in viscosity of the PP composites was attributed to the good dispersion of SiO<sub>2</sub> in the PP matrix and the presence of covalent bonding between the SiO<sub>2</sub> surface and silane grafted PP.

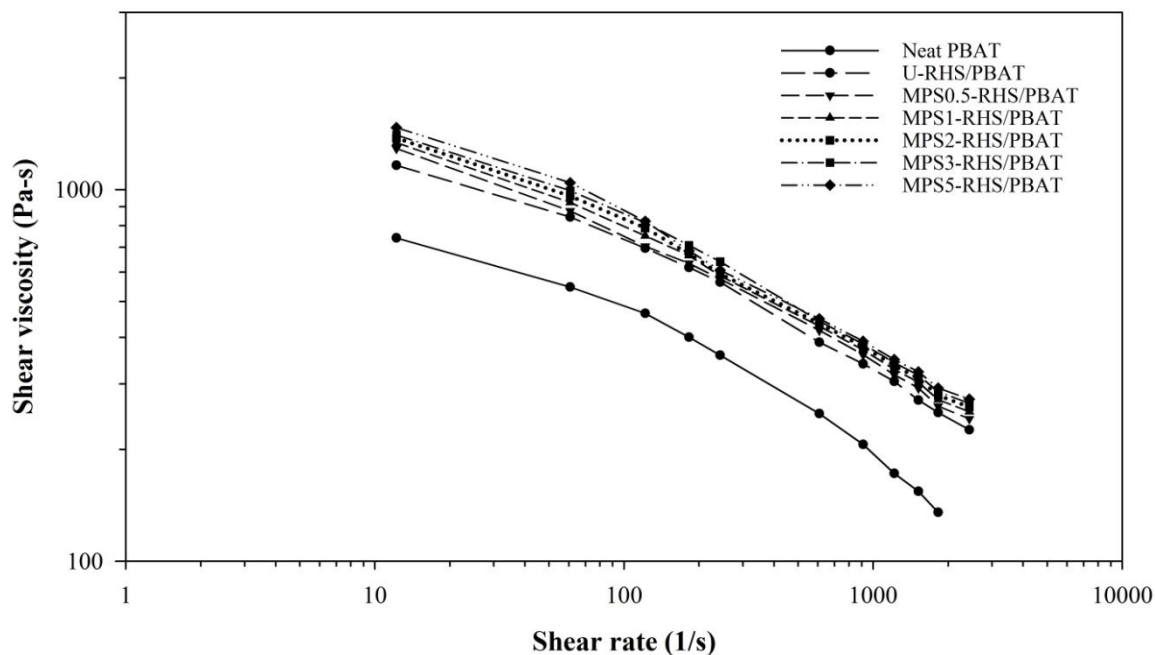


**Figure 4.19** Shear viscosity as a function of shear rate of neat PBAT, U-RHS and MPS-RHS/PBAT composites at various MPS content.

#### 4.2.3 Thermal properties of MPS treated RHS/PBAT composites

TGA thermograms of neat PBAT, U-RHS/PBAT and MPS-RHS/PBAT composites are shown in Figure 4.20. Among the PBAT composites, the  $T_d$  of MPS-RHS/PBAT composites were higher than that of U-RHS/PBAT composite. Additionally, their  $T_d$  and residue weight at 600°C are summarized in Table 4.6. The existence of RHS in PBAT increased  $T_d$  of neat PBAT. Additionally,  $T_d$  of MPS-RHS/PBAT composites increased with increasing MPS content up to 2 wt%. These results indicated that the treating RHS surface with MPS improved thermal properties of PBAT composites. This was probably because of the better dispersion of the MPS-RHS particles and the stronger interfacial adhesion between MPS-RHS and PBAT as compared with those in U-RHS/PBAT composite

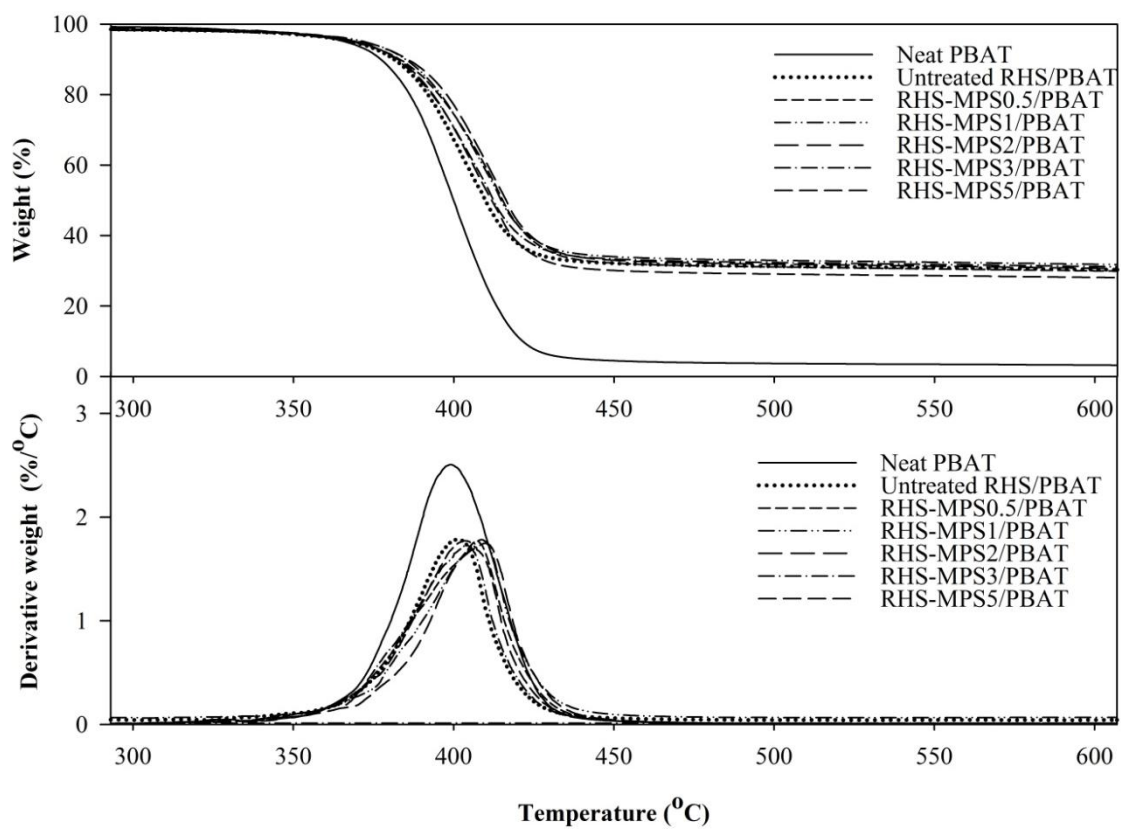


**Figure 4.20** TGA and DTG thermograms of neat PBAT, U-RHS/PBAT and MPS-RHS/PBAT composites at various MPS contents.

**Table 4.6** Decomposition temperatures and residue weight at 600°C of neat PBAT, U-RHS/PBAT and MPS-RHS/PBAT composites at various MPS contents.

Sample	T <sub>d</sub> (°C)	Residue weight at 600°C (%)
Neat PBAT	399.78	2.99
U-RHS/PBAT	401.05	31.20
MPS0.5-RHS/PBAT	405.11	30.77
MPS1-RHS/PBAT	408.30	30.31
MPS2-RHS/PBAT	409.90	31.48
MPS3-RHS/PBAT	407.36	31.58
MPS5-RHS/PBAT	407.08	29.48

#### 4.2.4 Mechanical properties of MPS treated RHS/PBAT composites

From the previous section (4.1), the results revealed that the modulus of the PBAT composites increased with increasing RHS content whereas their tensile and impact strengths decreased. These were because of the incompatibility between hydrophilic RHS filler and hydrophobic PBAT matrix. Therefore, the improvement of compatibility between RHS filler and PBAT matrix was carried out by treating RHS surface with MPS before incorporating in PBAT. In this section, the RHS at 30 wt% was selected for fabricating RHS/PBAT composites, because the composite at this content remained ductile while its modulus was enhanced as compared with that of the neat PBAT. The influence of MPS content on mechanical properties of PBAT composites are displayed in Figure 4.21-4.24.

Tensile modulus of U-RHS/PBAT and MPS-RHS/PBAT composites at various MPS contents is shown in Figure 4.21. Tensile modulus of MPS-RHS/PBAT composites was higher than that of U-RHS/PBAT composite. Moreover, the tensile

modulus of MPS-RHS/PBAT composites increased with increasing MPS content up to the MPS content of 2 wt%. These observations indicated that incorporation of MPS treated RHS in PBAT improved the stiffness of PBAT matrix. According to Nurdina, Mariatti, and Samayamutthirian (2011), treating filler surface with titanate and silane coupling agents significantly improved tensile modulus of the composites as compared with untreated filler. This was because the titanate or the silane treated filler increased the bonding efficiency between the polymer matrix and the filler. However, the decrease in the tensile modulus of MPS-RHS/PBAT composites when MPS content was beyond 2 wt% may be because the adsorbed MPS molecules on the surface of the RHS acted as a plasticizer during the melt-compounding (Ahn, Kim, and Lee, 2004).

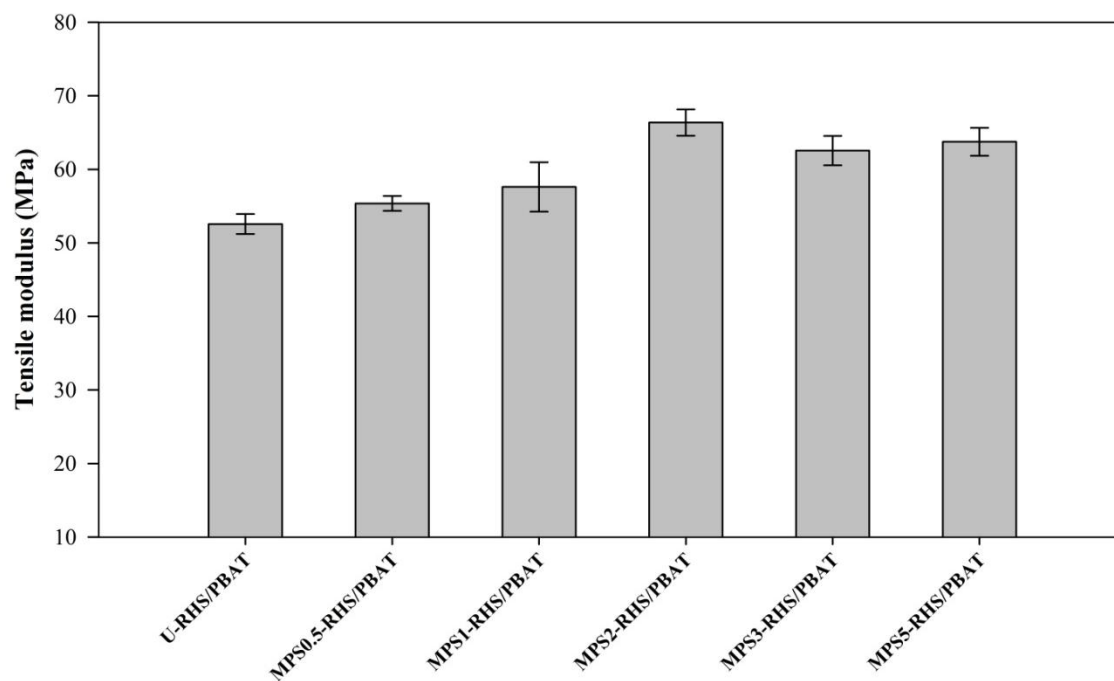


**Figure 4.21** Tensile modulus of U-RHS/PBAT and MPS-RHS/PBAT composites at various MPS contents.

Elongation at break of U-RHS/PBAT and MPS-RHS/PBAT composites at various MPS contents is shown in Figure 4.22. The elongation at break of MPS-RHS/PBAT composites was higher than that of U-RHS/PBAT composite. This was because MPS-RHS had good dispersion in PBAT matrix as compared with U-RHS. With increasing MPS content, the elongation at break of those composites slightly decreased. This result was in contrast to those reported by Metin, Tihminlioglu, Balkose, and Ulku (2004) and Someya, Sugahara, and Shibata (2005). Metin *et al.* studied effect of MPS content on the mechanical properties of zeolite/PP composites while Someya *et al.* studied effect of MPS content on the mechanical properties of MMT/PBAT composites. Both of these groups found the similar results that the elongation at break of the polymer composites reinforced with MPS treated filler was higher than that of untreated filler/polymer composites due to the good dispersion of filler in polymer matrix. Additionally, elongation at break of those composites increased with increasing MPS content. They suggested that MPS probably provided a plasticizing/lubricating effect because of the formation of physically adsorbed layers at the interphase between filler and polymer matrix.

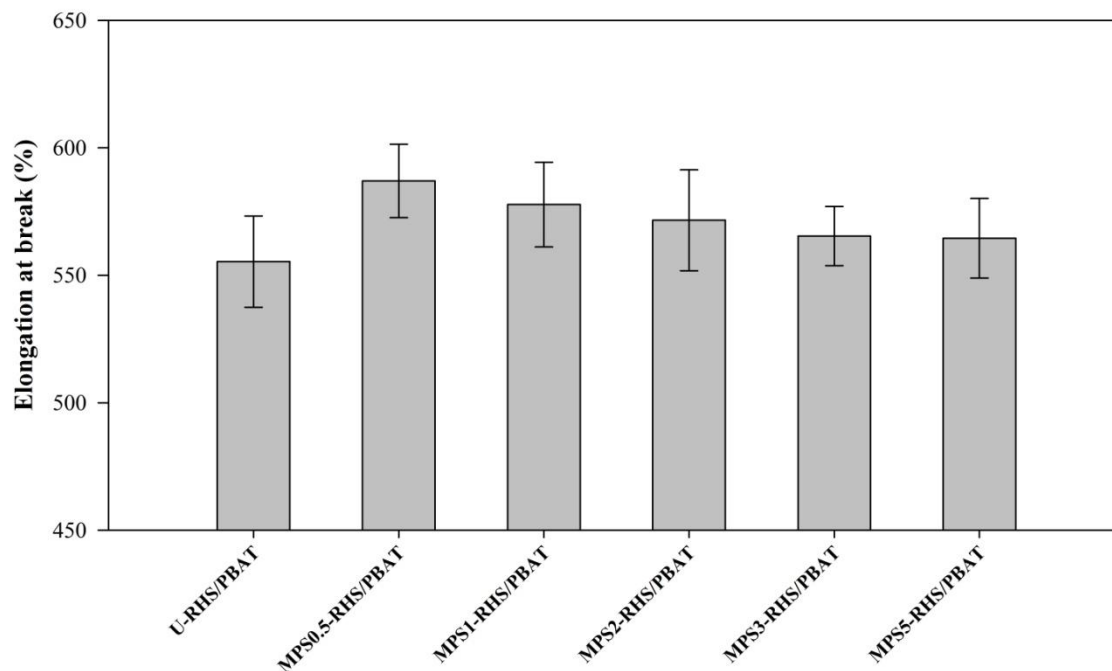


**Figure 4.22** Elongation at break of U-RHS/PBAT and MPS-RHS/PBAT composites at various MPS contents.

Tensile and impact strengths of U-RHS/PBAT and MPS-RHS/PBAT composites at various MPS contents are shown in Figure 4.23 and Figure 4.24, respectively. Both tensile and impact strengths of MPS-RHS/PBAT composites were higher than those of U-RHS/PBAT composite. The increase in tensile and impact strength of the MPS-RHS/PBAT composites was due to the good adhesion between MPS-RHS and PBAT matrix and the good dispersion of MPS-RHS in PBAT matrix as confirmed by their morphologies in Figure 4.26.

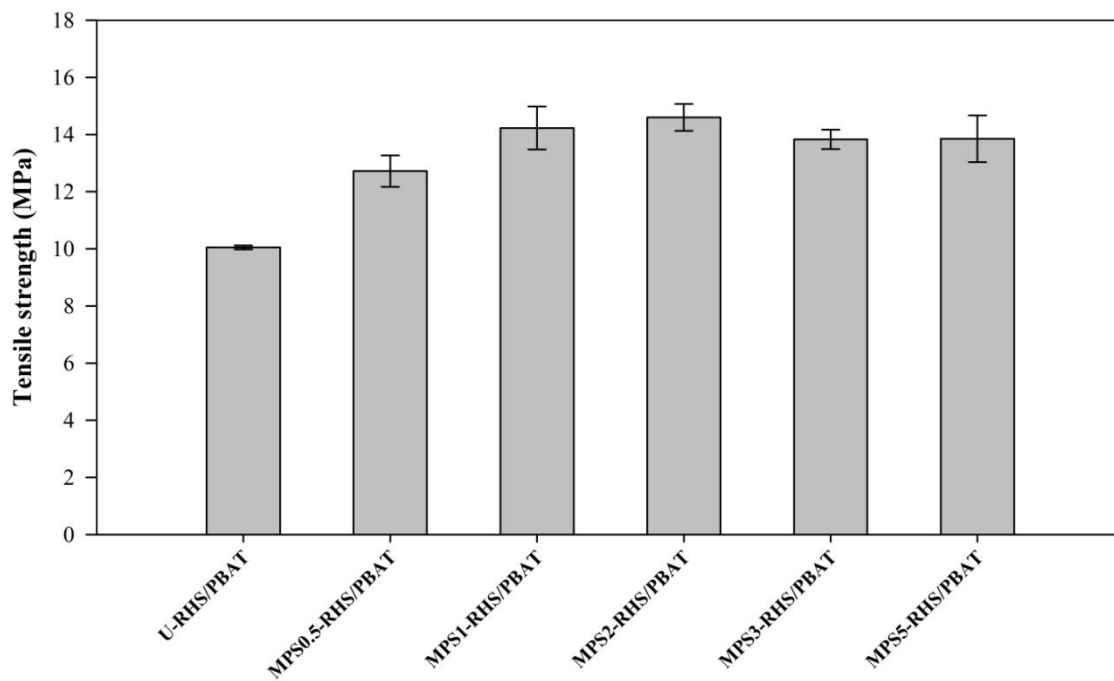


**Figure 4.23** Tensile strength of U-RHS/PBAT and MPS-RHS at various MPS contents.



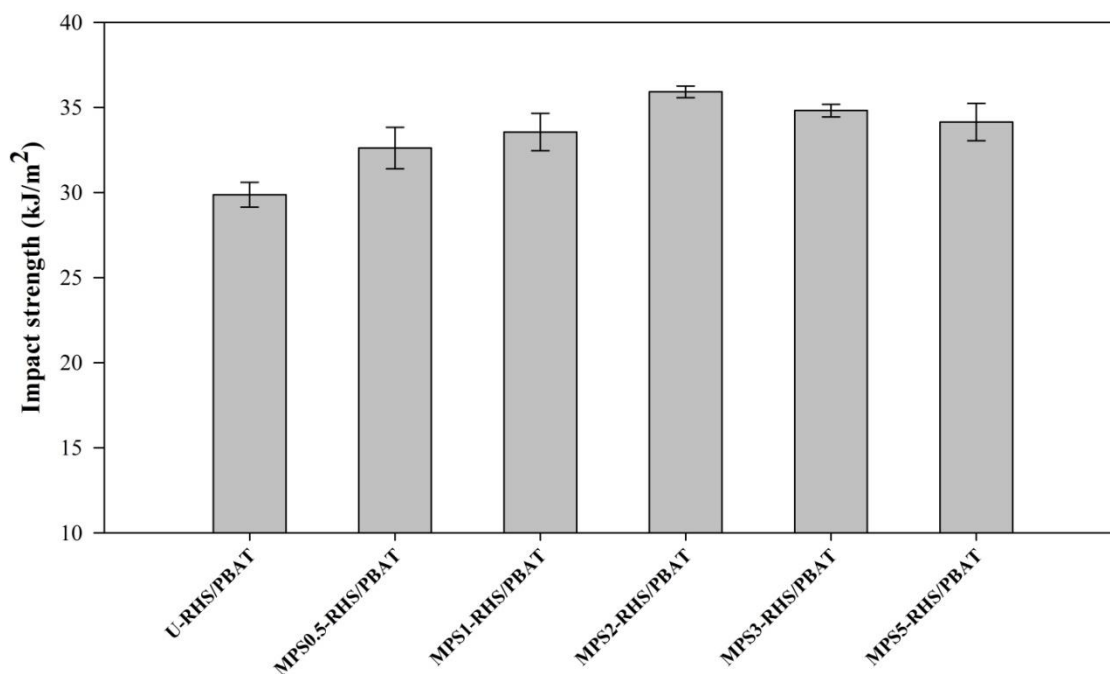


**Figure 4.24** Impact strength of U-RHS/PBAT and MPS-RHS at various MPS contents.

The improvement of mechanical properties of the composites could be related to the presence of MPS molecules treated on RHS surfaces. The first possible reason was that MPS molecules on the RHS surfaces formed a stable hindrance layer between RHS particles inhibiting the RHS agglomeration and thus improving the dispersibility of the RHS in PBAT matrix (Zou, Wu, and Shen, 2008). The second possible reason was that the treated MPS molecules interacted with the PBAT matrix leading to enhanced interfacial adhesion between RHS and PBAT (Matinlinn, Ozcanb, Lassilaa, and Vallittua, 2004).

It should be noted that not only the tensile and the impact strengths of the PBAT composites but also the  $T_d$  of the RHS-MPS2/PBAT composites were the highest. This may be because MPS formed multilayer on RHS surface when MPS was used

beyond 2 wt%. MPS at the first layer was covalent bonded to RHS surface while the second layer was physical interaction with MPS at the first layer. During mechanical and thermal testing, the adhesion at interphase between PBAT and RHS was the critical factor that affected the composite destruction. The weak interaction resulted in the less uses of both thermal and mechanical energy to debond the interphase of RHS and PBAT during the test. The simplified illustrative molecular structure of multilayer MPS molecules, as proposed by Sideridou and Karabela (2009) is shown in Figure. 4.25.

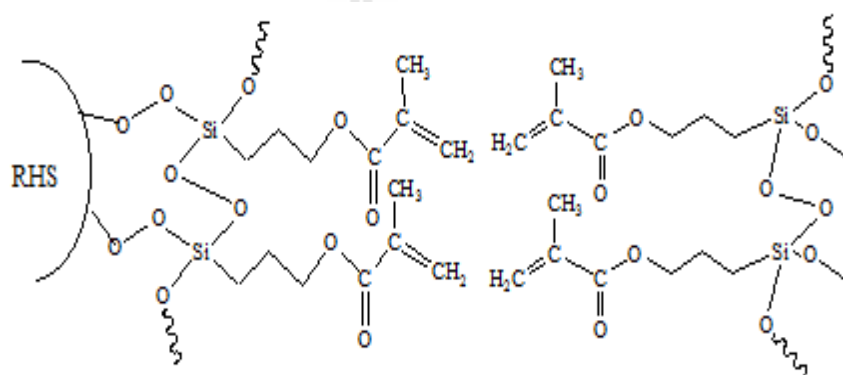


**Figure 4.25** Simplified illustrative molecular structures of multilayer MPS molecules (Sideridou and Karabela, 2009).

#### 4.2.5 Morphological properties of U-RHS/PBAT and MPS-RHS/PBAT composites

SEM micrographs of impact fracture surfaces of U-RHS/PBAT and MPS-RHS/PBAT composites at various MPS contents are shown in Figure 4.26. The U-RHS/PBAT composites in Figure 4.26(a) revealed that the RHS filler tended to expose on the fracture surface, with some cavities surrounding the particles. In addition, the cleaned RHS surface without the adhered PBAT ligaments on the RHS surface was noticed.

These indicated weak adhesion between U-RHS and PBAT matrix. On the other hand, treating RHS surface with MPS (Figure 4.26(b-d)) showed the adhered PBAT matrix on RHS surface. Most of the filler treated with MPS tended to be embedded inside the PBAT matrix. Additionally, the gap between RHS and PBAT matrix was almost disappeared. These suggested that treating RHS surface with MPS improved the adhesion between RHS and PBAT matrix. It can be said that the decrease in the hydrophilicity of RHS filler through surface treatment made RHS fillers more compatible with the hydrophobic PBAT leading to improved surface adhesion and resulting in the higher mechanical properties of PBAT composites.



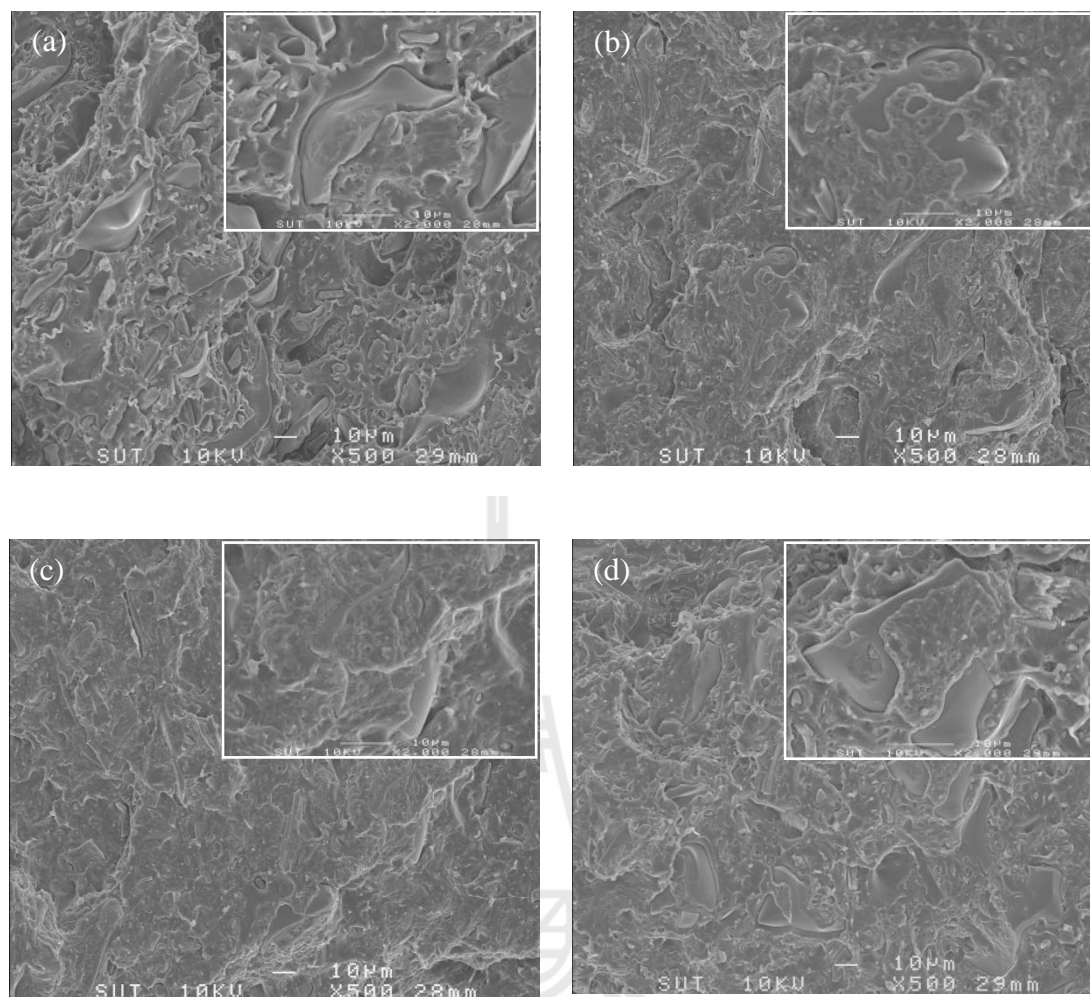


**Figure 4.26** SEM micrographs of tensile fracture surfaces of (a) U-RHS/PBAT composite and MPS-RHS/PBAT composites at various MPS contents: (b) 1 wt%, (c) 2 wt% and (d) 3 wt%.

Treating RHS surface with MPS changed the filler characteristics including filler polarity and filler agglomeration. In addition, the MPS treated RHS at various MPS contents was used to fabricate MPS-RHS/PBAT composites. The results indicated that MPS-RHS improved the mechanical properties of PBAT composites.

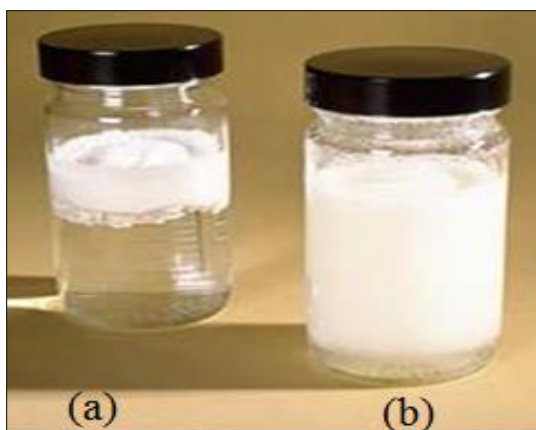
Additionally, the morphology of the composites confirmed that treating RHS surface with MPS improved the adhesion between the MPS-RHS and the PBAT matrix.

### **4.3 Effect of acrylic acid (AA) content on rheological, mechanical, thermal and morphological properties of RHS/PBAT composites**

#### **4.3.1 Characterization of AA treated RHS**

In the order to improve the compatibility between RHS and PBAT matrix and increase in hydrophobicity of the RHS surface, AA was chosen as the functional monomer for modifying RHS surface. AA molecules may be covalently linked onto RHS surface by reaction of the Si-OH groups with the carboxylic acid groups of AA via esterification (Lai, Kuo, Huang, and Chena, 2007).

The photographs of U-RHS and AA treated RHS (AA-RHS) particles immersed in the water at equal time period are shown in Figure 4.27. As seen, U-RHS was the homogeneously dispersed in water while AA-RHS was obviously separated from water. These suggested that the surfaces of AA-RHS had lower hydrophilicity compared with those of U-RHS. The obtained AA-RHS was further characterized before using it as a filler for fabricating RHS/PBAT composites. The results were reported as follows.



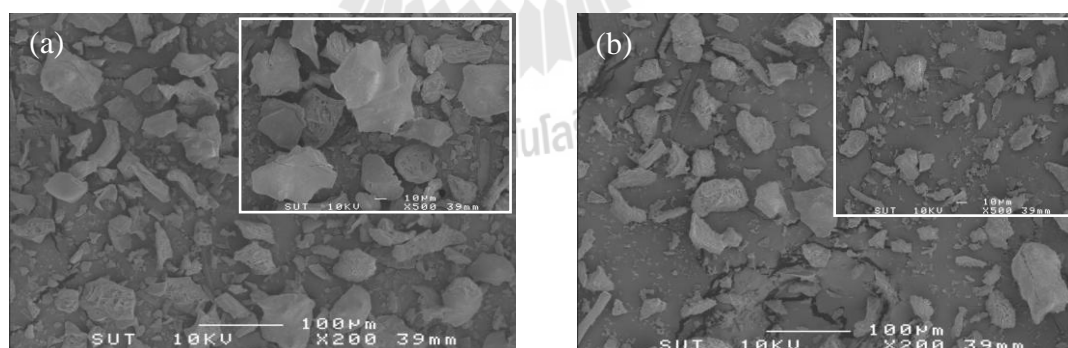
**Figure 4.27** Photographs of (a) AA-RHS particles and (b) U-RHS particles.

Table 4.7 shows the summarized results of particle size distribution, specific surface area and pore characteristic of U-RHS and AA-RHS particles. In comparison between U-RHS and AA-RHS, U-RHS showed the highest particle size distribution while the particle size distribution of AA-RHS decreased with increasing reaction times. This may be due to the breaking up of RHS agglomerates during AA treating process that led to the smaller RHS particles. The specific surface area of U-RHS particles were the highest while the specific surface area of the AA-RHS decreased with increasing reaction time. Also, the pore volumes of U-RHS were the highest while those of the AA-RHS decreased with increasing reaction time. The decrease in specific surface area and pore volumes of AA-RHS particles were because the AA molecules were planted on RHS particles (Wu, Zhang, Rong, and Friedrich, 2005). However, the pore diameters of the U-RHS were the lowest whereas pore diameters of AA-RHS increased with increasing reaction time up to 12 h.

**Table 4.7** Average diameter, surface area and pore characteristics of U-RHS and AA-RHS at various reaction times.

Material	Average diameter, $d(4,3)$ ( $\mu\text{m}$ )	Total pore volume ( $\text{ml/g}$ )	Average pore diameter ( $\text{nm}$ )	BET surface area ( $\text{m}^2/\text{g}$ )
U-RHS	46.20	0.41	0.59	278.76
AA6-RHS	24.54	0.32	0.73	181.67
AA12-RHS	20.62	0.31	0.75	179.72
AA24-RHS	17.25	0.23	0.69	149.68

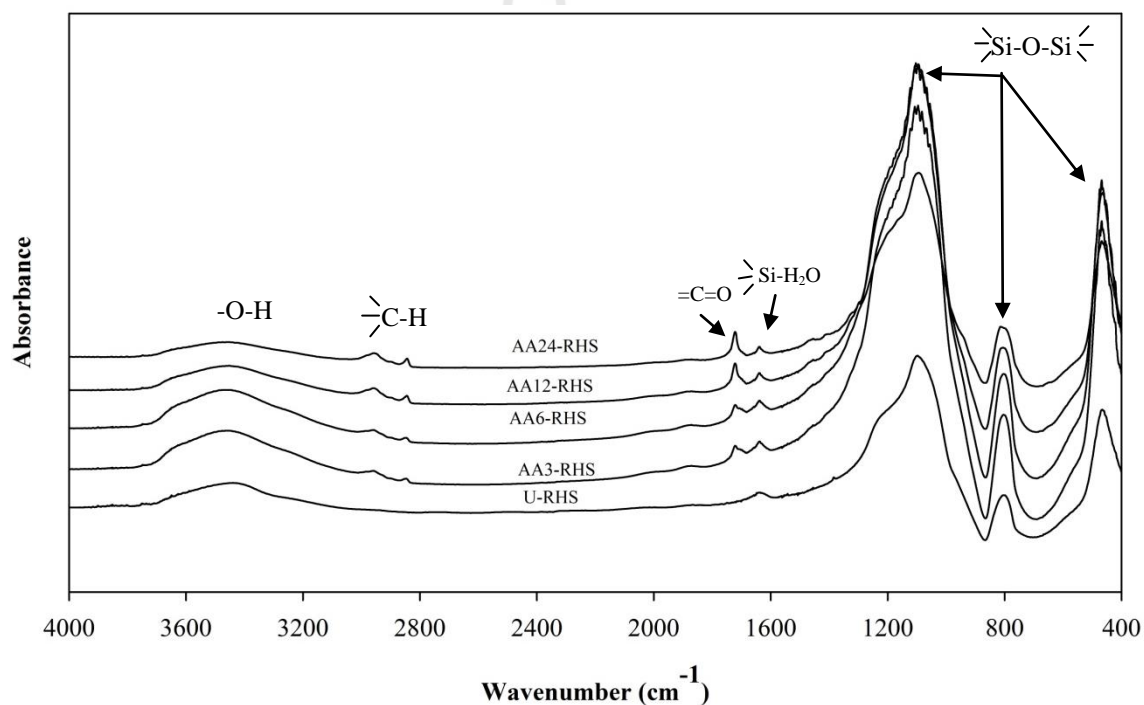
SEM micrographs of U-RHS and AA-RHS particles are shown in Figure 4.28. The micrograph of U-RHS in Figure 4.28(a) showed an irregular geometry and a large scale of particle size distribution. On the other hand, the micrograph of AA-RHS in Figure 4.28(b) showed the reduction in particles size distribution of RHS after treating with AA which was in good agreement with the particle size distribution results shown in Table 4.7.



**Figure 4.28** SEM micrographs of (a) U-RHS particles and (c) AA-RHS particles.

FTIR spectra of U-RHS and AA-RHS at various reaction times are shown in Figure 4.29. The absorption bands of U-RHS were described in section 4.1. The additional absorption bands of AA-RHS were observed around  $2950$ ,  $2845$  and  $1710\text{ cm}^{-1}$

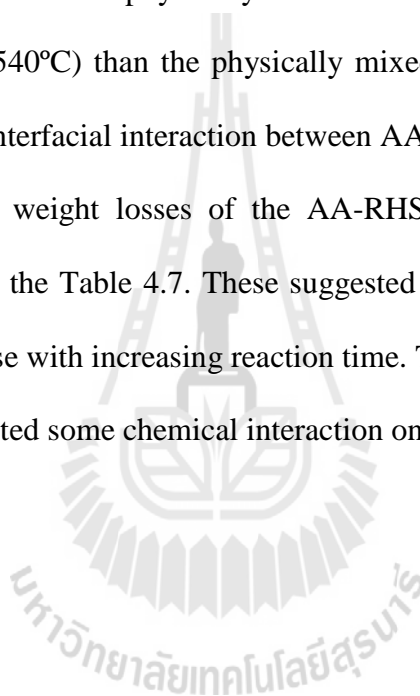
which respectively were attributed to the absorptions of C-H asymmetrical stretching, C-H symmetrical stretching and carbonyl stretching vibration of AA (Suzuki, Siddiqui, Chappell, Siddiqui, and Ottenbrite, 2000; Tang, Lin, Yang, Jiang, and Chen-Yang, 2007). These confirmed that the AA molecules appeared on surface of RHS. In the present results, the intensity ratio of the absorption peaks at 1722 to 1632  $\text{cm}^{-1}$  ( $A_{1710}/A_{1632}$ ), *i.e.* the ratio of carbonyl peak to water absorption peak on RHS surface, tended to increase with increasing reaction time. These suggested that the amounts of AA molecules on RHS surface increased with increasing reaction time.



**Figure 4.29** FTIR spectra of U-RHS and AA-RHS at various reaction times.

TGA thermograms of U-RHS, AA physically mixed AA/RHS and AA-RHS at various reaction times are shown in Figure 4.30. Their  $T_d$  and residue weights at 600°C were summarized in Table 4.7. All samples demonstrated a slight weight loss

around 250°C and below due to the physisorbed water evaporation and the liberation of water in the RHS particles (above 200°C) (Ma *et al.*, 2010). From TGA thermograms, AA-RHS showed lower amount of physisorbed water than U-RHS. These suggested that surfaces of AA-RHS had lower moisture absorption indicating its higher hydrophobicity as compared with that of U-RHS. For physically mixed AA/RHS, the sample showed weight loss around 197.3°C relating to the evaporation of adsorbed AA molecules (Figure 4.30 (b)). In comparison between physically mixed AA/RHS and AA-RHS, the AA-RHS had higher  $T_d$  (around 540°C) than the physically mixed AA/RHS. This suggested that AA-RHS had stronger interfacial interaction between AA-RHS than the physically mixed AA/RHS. Furthermore, weight losses of the AA-RHS increased with increasing the reaction time as seen in the Table 4.7. These suggested that the AA molecules on RHS surface tended to increase with increasing reaction time. TGA and FTIR results suggested that the AA-RHS presented some chemical interaction on RHS surface.



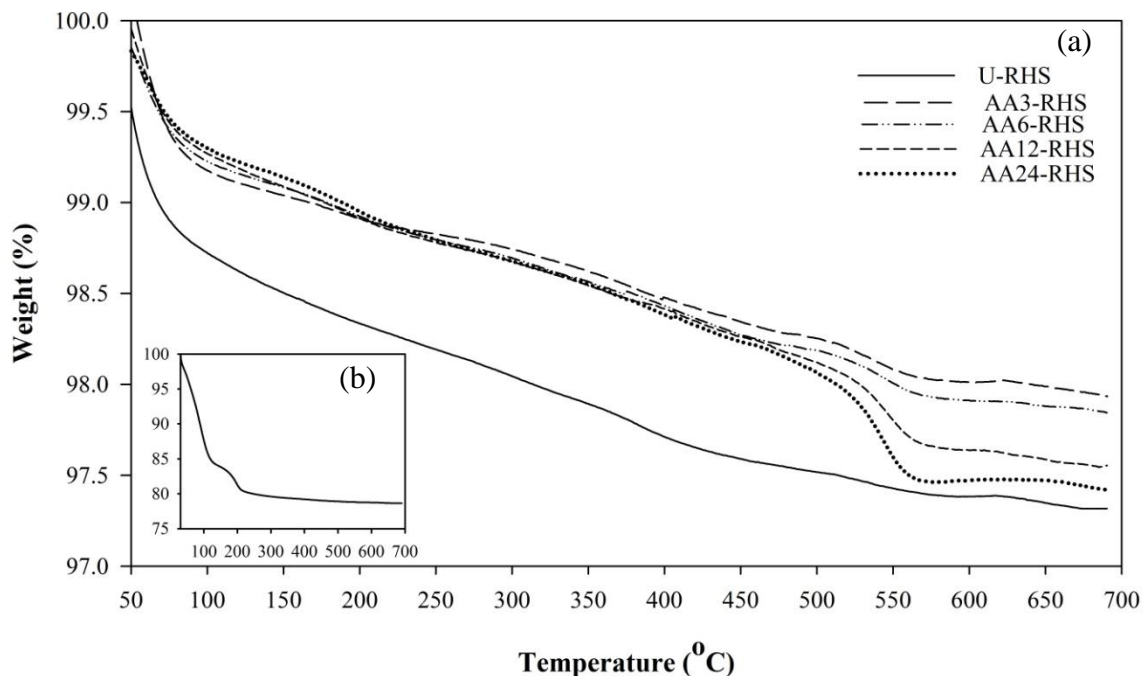


**Figure 4.30** TGA thermograms of U-RHS and AA-RHS at various reaction times.

**Table 4.8** Decomposition temperatures and residue weight at 600°C of physically mixed AA/RHS, U-RHS and AA-RHS at various reaction times.

Sample	$T_d$ (°C)	Residue weight at 600°C (%)
U- RHS		97.31
mixed AA/RHS	197.25	78.88
AA3-RHS	541.02	98.04
AA6-RHS	542.04	97.89
AA12-RHS	544.58	97.61
AA24-RHS	543.63	97.57

### 4.3.2 Rheological properties of AA treated RHS/PBAT composites

Figure 4.31 shows shear viscosity as a function of shear rate of neat PBAT, U-RHS/PBAT and AA-RHS/PBAT composites. The viscosity of neat PBAT and

PBAT composites decreased with increasing shear rate. As a result, the addition of RHS into PBAT increased the viscosity of neat PBAT. This was because the RHS perturbed the flow of polymer and hindered the mobility of chain segments in melt flow under shear stresses. For PBAT composites, shear viscosity of AA-RHS/PBAT composites were slightly higher than that of U-RHS/PBAT composite and negligibly changed with increasing the reaction time. Lee, Kim, M. W., Kim, S. H., and Youn (2008) reported that the increasing of viscosity of composites was due to the combination between the improvement in interfacial bonding between filler and matrix and the improvement in dispersion of filler in matrix.

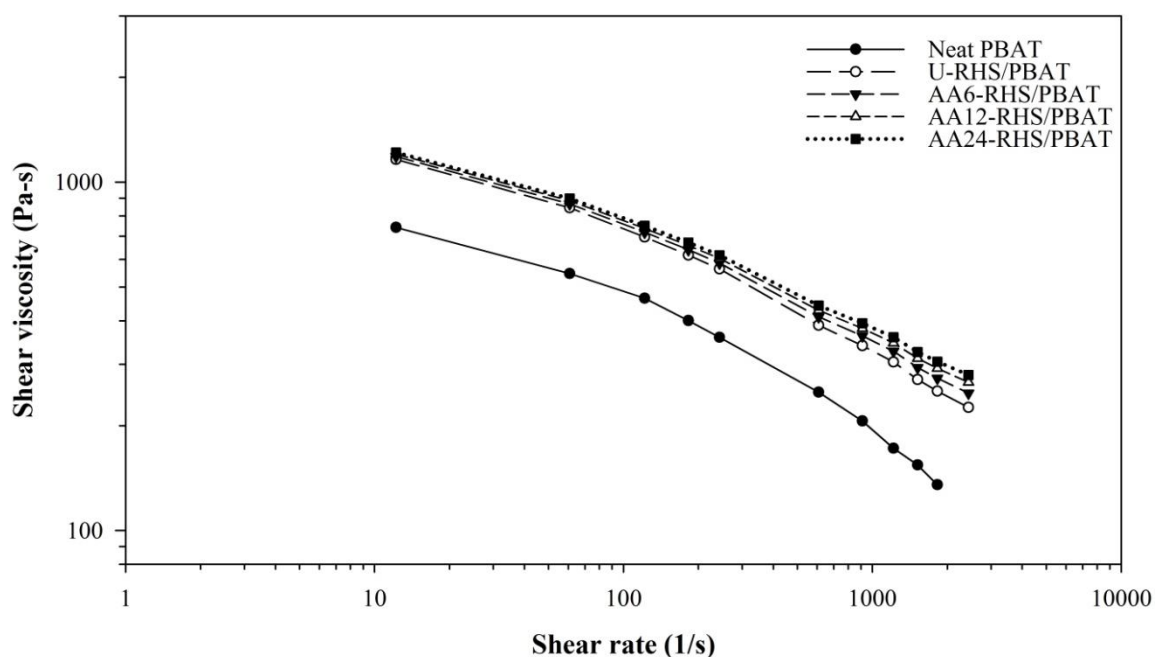


**Figure 4.31** Shear viscosity as a function of shear rate of neat PBAT, U-RHS/PBAT and AA-RHS/PBAT composites at various reaction times.

### 4.3.3 Thermal properties of AA treated RHS/PBAT composites

Figure 4.32 shows TGA thermograms of neat PBAT, U-RHS/PBAT and AA-RHS/PBAT composites at various reaction times. Additionally, their  $T_d$ s and weight losses were summarized in Table 4.8. All samples demonstrated  $T_d$  around 403-410°C. Neat PBAT showed the lowest  $T_d$  (around 403.4°C) compared with the PBAT composites. This suggested that the existence of RHS in PBAT affected the increase in  $T_d$  of PBAT. The existence of RHS particles hindered the PBAT matrix chains mobility. Basically, the incorporation of inorganic particles into the polymer matrix enhanced the thermal stability of the polymer matrix by acting as a superior insulator and mass transport barrier to the volatile products generated during decomposition (Zou, Wu, and Shen, 2008). Among the PBAT composites, the  $T_d$  of AA-RHS/PBAT composites were higher than that of U-RHS/PBAT composite. Furthermore, the  $T_d$  of AA-RHS/PBAT composites increased with increasing reaction time while the weight loss of the AA-RHS/PBAT composites negligibly changed with increasing reaction time. This result suggested that the presence of AA-RHS improved the thermal properties of the PBAT matrix. These phenomena can be explained as follows. Firstly, treating RHS particles with AA reduced the size of the agglomerated RHS particles and thereby improved AA-RHS dispersion in the PBAT matrix as compared with that of U-RHS. Secondly, the AA strengthened the interfacial interaction between RHS and PBAT, which caused an increased restricting strength of RHS in the PBAT chains during decomposition.

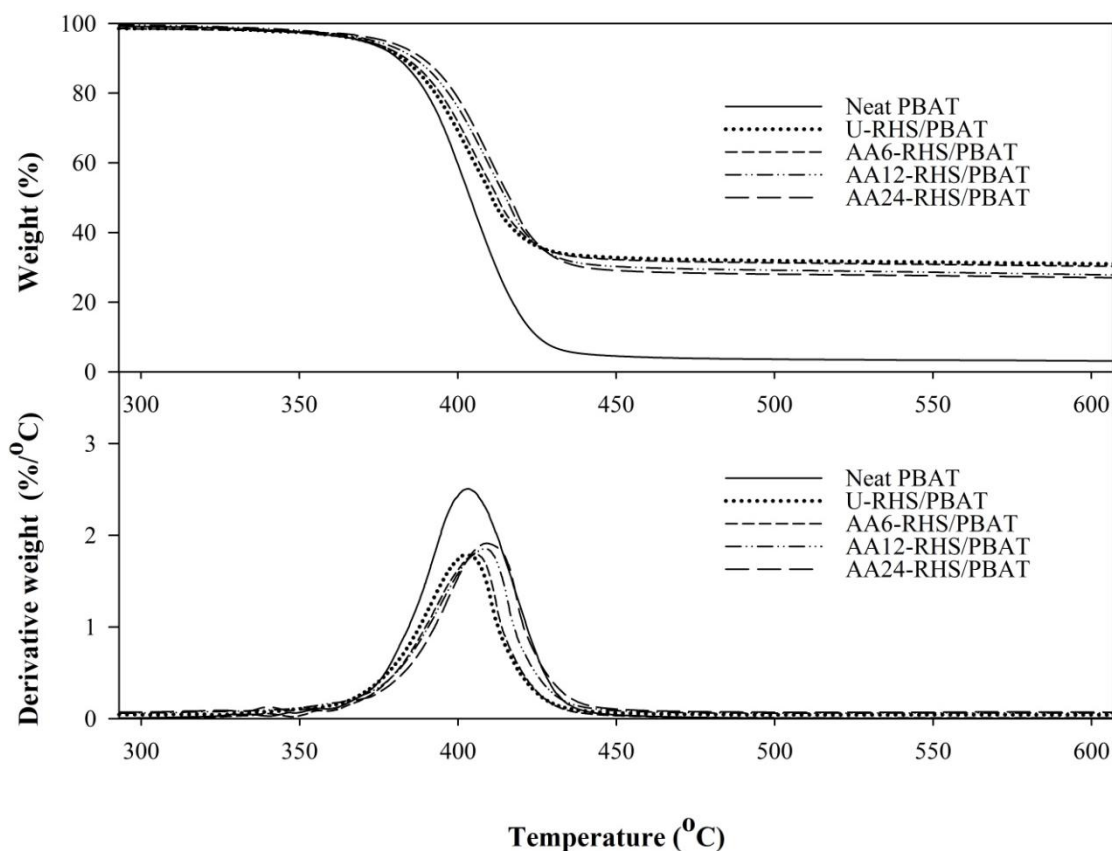


**Figure 4.32** TGA and DTG thermograms of neat PBAT, U-RHS/PBAT and AA-RHS/PBAT composites at various reaction times.

**Table 4.9** Decomposition temperatures and residue weight at 600°C of neat PBAT, U-RHS/PBAT and AA-RHS/PBAT composites at various reaction times.

Sample	T <sub>d</sub> (°C)	Residue weight at 600°C (%)
Neat PBAT	403.35	3.15
U-RHS/PBAT	403.55	31.73
AA6-RHS/PBAT	405.65	31.15
AA12-RHS/PBAT	410.32	28.50
AA24-RHS/PBAT	410.38	27.37

#### 4.3.4 Mechanical properties of AA treated RHS/PBAT composites

From the previous section (4.1), the results revealed that the modulus of the PBAT composites increased with increasing of RHS content whereas their tensile and impact strengths decreased. These were because of the incompatibility between hydrophilic RHS filler and hydrophobic PBAT matrix. Therefore, the improvement of compatibility between RHS filler and PBAT matrix was carried out by treating RHS surface with AA before incorporating in PBAT. In this section, the RHS at 30 wt% was selected for fabricating RHS/PBAT composites because the composite at this content remained flexible while the modulus enhanced as compared with that of neat PBAT. The influences of AA treated RHS at various reaction times on mechanical properties of PBAT composites are displayed in Figure 4.33-4.36.

Tensile modulus of U-RHS/PBAT and AA-RHS/PBAT composites at various reaction times is shown in Figure 4.33. Tensile modulus of AA-RHS/PBAT composites was higher than that of U-RHS/PBAT composite. Moreover, the tensile modulus of AA-RHS/PBAT composites increased with increasing reaction time. These observations indicated that the incorporation of AA-RHS into PBAT matrix improved the stiffness of PBAT matrix. Ahn, Kim, and Lee (2004) studied effect of stearic acid content modified SiO<sub>2</sub> nanoparticles on the properties of SiO<sub>2</sub>/poly(ethylene 2,6-naphthalate) (PEN) composites. They found that the presence of stearic acid treated SiO<sub>2</sub> in PEN matrix improved the modulus of PEN matrix compared with that of untreated SiO<sub>2</sub>. This result was due to the improvement in adhesion between the silica nanoparticles and the PEN matrix.

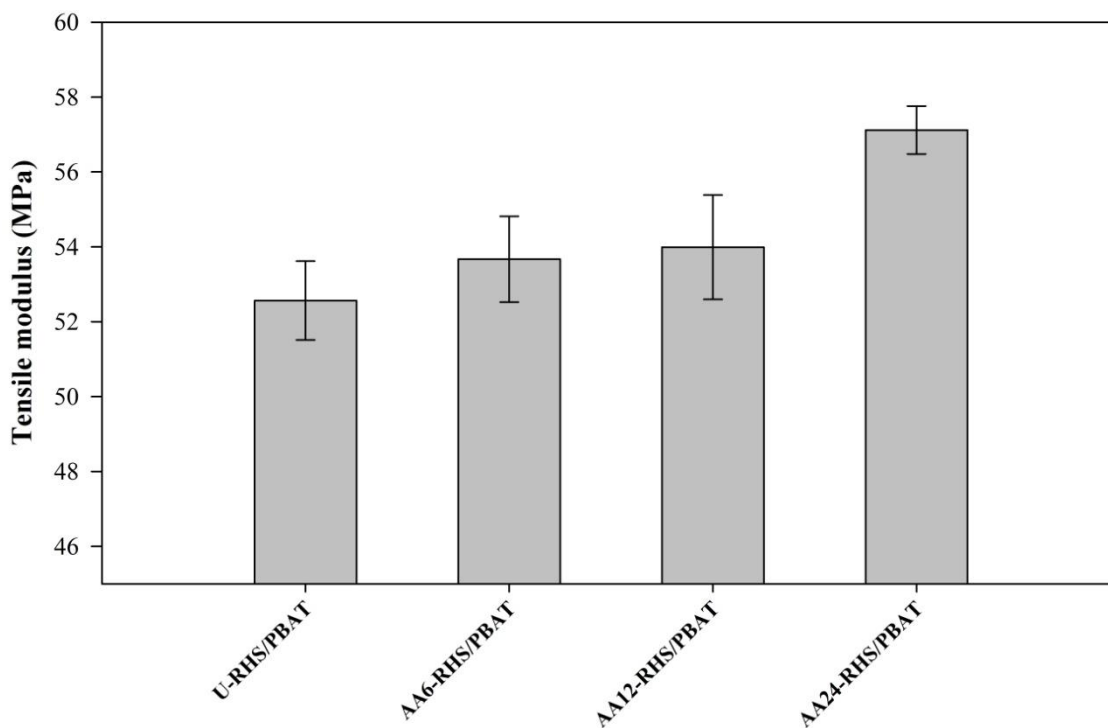


**Figure 4.33** Tensile modulus of U-RHS/PBAT and AA-RHS/PBAT composites at various reaction times.

Elongation at break of U-RHS/PBAT and AA-RHS/PBAT composites at various reaction times is shown in Figure 4.34. The elongation at break of AA-RHS/PBAT composites was higher than that of U-RHS/PBAT composites. The improvement in elongation at break of AA-RHS/PBAT composites represented improved deformation ability of the PBAT composites. This was due to a good dispersion of AA-RHS in PBAT matrix. In addition, the elongation at break of AA-RHS/PBAT composites slightly increased with increasing reaction time. This may be because AA molecules probably provided a plasticizing/lubricating effect via the formation of physically adsorbed layers at the interphase between RHS and PBAT. Wu, Zhang, Rong, and Friedrich (2002) studied effect of treating surface of  $\text{SiO}_2$  with polyethyl acrylate

(PEA) on mechanical properties of SiO<sub>2</sub>/PEA composites. They found the similar results that elongation at break of PP composites can be improved by adding the PEA treated SiO<sub>2</sub> into PP matrix. Additionally, their elongation at break increased with increasing PEA content due to a natural viscoelasticity of PEA at the interphase between filler and matrix.

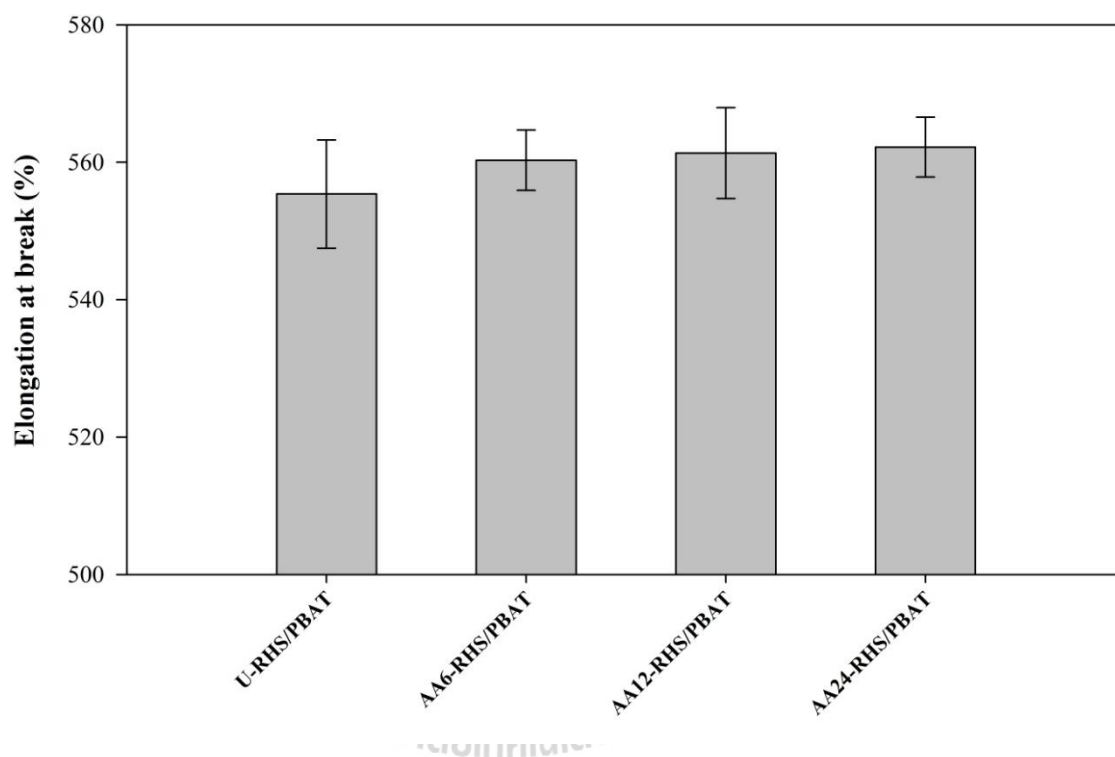


**Figure 4.34** Elongation at break of U-RHS/PBAT and AA-RHS/PBAT composites at various reaction times.

Tensile and impact strengths of U-RHS/PBAT and AA-RHS/PBAT composites at various reaction times are shown in Figure 4.35 and Figure 4.36, respectively. The tensile and impact strengths of AA-RHS/PBAT composites were higher than those of U-RHS/PBAT composites. Moreover, the tensile and the impact strengths

of AA-RHS/PBAT composites increased with increasing the reaction time. This was because the AA-RHS particles had better adhesion and better distribution in PBAT matrix than U-RHS as supported by their SEM morphologies in Figure 4.37.

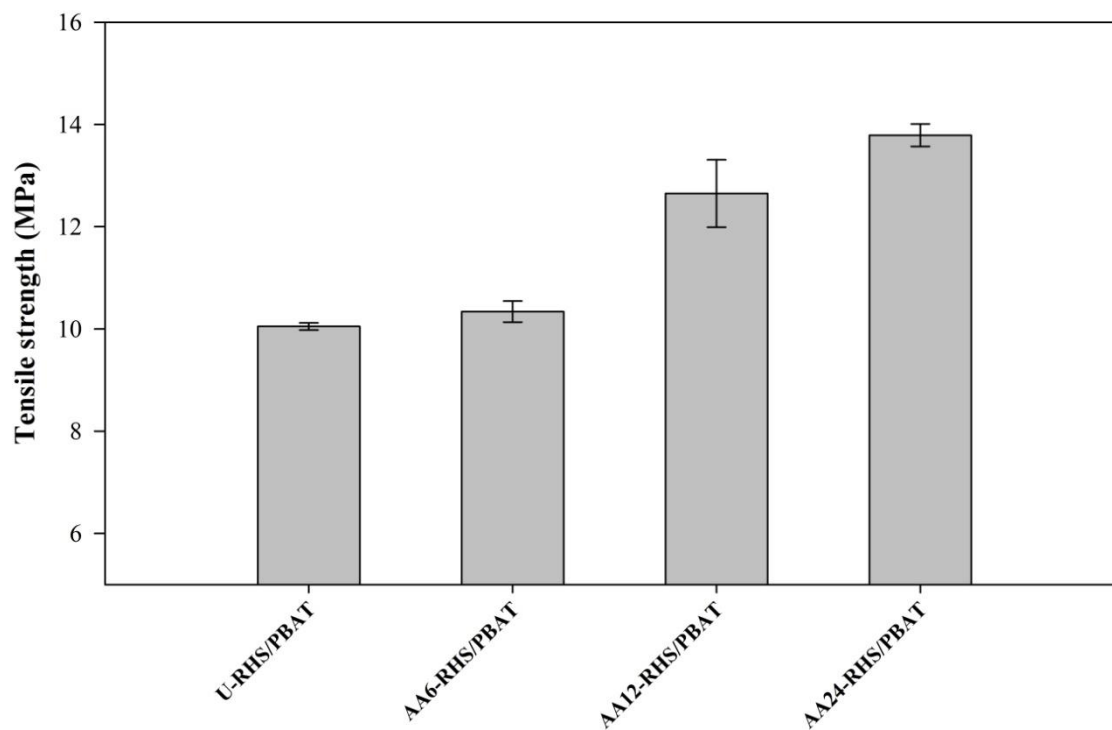


**Figure 4.35** Tensile strength of U-RHS/PBAT and AA-RHS/PBAT composites at various reaction times.

The improvement of mechanical properties of the composites could be related to the presence of AA molecules treated on RHS surfaces. The possible reason was that AA molecules on the RHS surfaces formed a stable hindrance layer between RHS particles inhibiting the RHS agglomeration, reducing RHS moisture absorption and thus improving the dispersibility of the RHS in PBAT matrix (Zou, Wu, and Shen, 2008).

Additionally, the interfacial adhesion of AA-RHS/PBAT composites, according to their SEM morphologies, was improved as compared with that of U-RHS /PBAT composite.

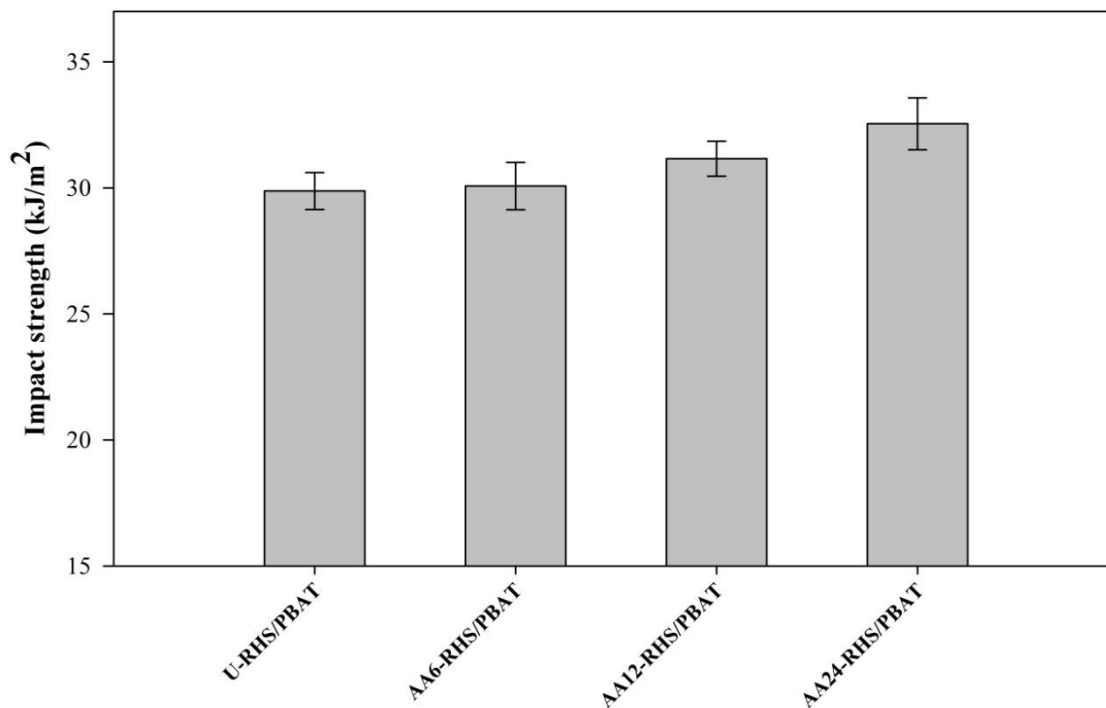
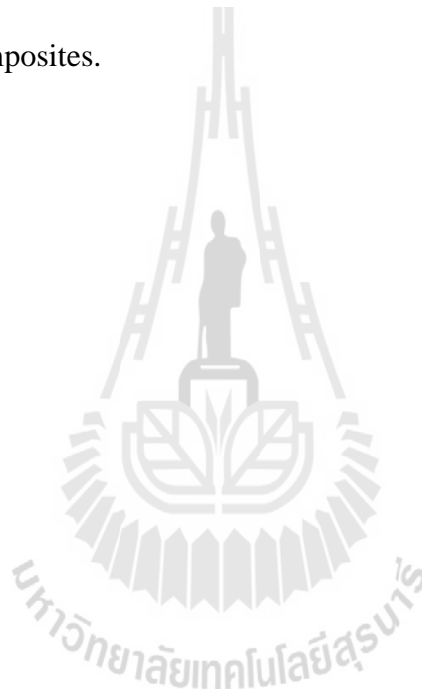


**Figure 4.36** Impact strength of U-RHS/PBAT and AA-RHS/PBAT composites at various reaction times.

#### 4.3.5 Morphological properties of AA treated RHS/PBAT composites

SEM micrographs of impact fracture surfaces of U-RHS/PBAT and AA-RHS/PBAT composites at various reaction times are shown in Figure 4.37. The U-RHS/PBAT composites in Figure 4.37(a) revealed that the RHS filler tended to expose on the fracture surface, with some cavities surrounding the particles. In addition, the cleaned RHS surface without the adhered PBAT ligaments on the RHS surface was noticed. These indicated weak adhesion between U-RHS and PBAT matrix. On the other hand,

treating RHS surface with AA (Figure 4.37(b-d)) showed the adhered PBAT matrix on RHS surface. Most of the RHS treated with AA tended to embed inside the PBAT matrix. Additionally, the gap between RHS and PBAT matrix was almost disappeared. These suggested that treating RHS surface with AA improved the adhesion between RHS and PBAT matrix as obviously shown in their morphologies. It can be said that the decrease in the hydrophilicity of RHS through RHS surface treatment made the fillers more compatible with the hydrophobic PBAT and resulted in the higher mechanical properties of PBAT composites.



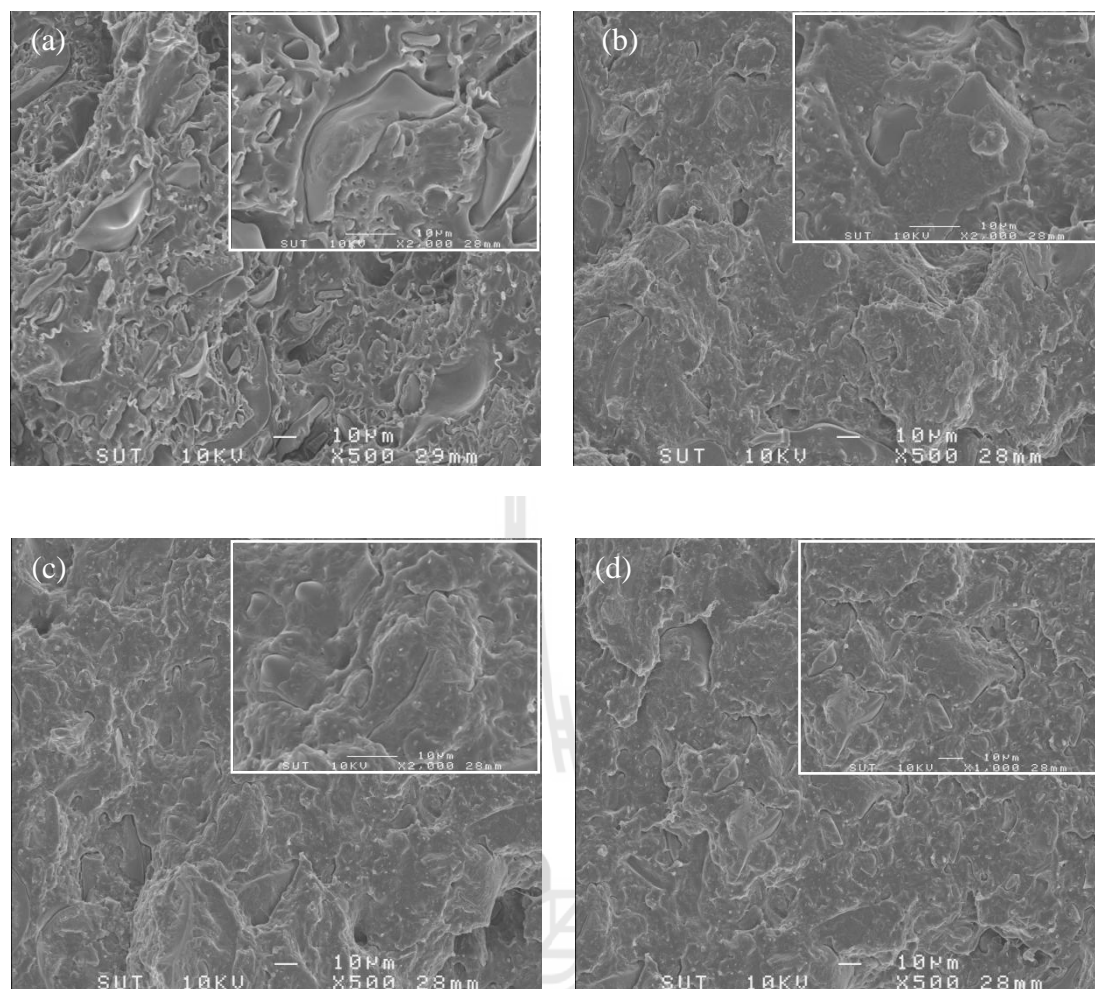


**Figure 4.37** SEM micrographs of impact fracture surfaces of (a) U-RHS/PBAT composite and AA-RHS/PBAT composites at various reaction times: (b) 6 h, (c) 12 h and (d) 24 h.

Treating RHS surface with AA changed the filler characteristics including filler polarity and filler agglomeration. In addition, the AA treated RHS at various reaction times was used to fabricate AA-RHS/PBAT composites. The results indicated that AA-RHS improved the mechanical properties of PBAT composites. Among AA/PBAT composites, the AA24-RHS/PBAT composites provided the optimum

mechanical properties. Additionally, the morphology of the composites confirms that treating RHS surface with AA improved the adhesion between AA-RHS and PBAT matrix.

## **4.4 Water absorption of PBAT and RHS/PBAT composites**

### **4.4.1 Water absorption of PBAT and RHS/PBAT composites**

Plots of percentage of absorbed water against immersion time for neat PBAT, U-RHS/PBAT, MPS-RHS/PBAT and AA-RHS/PBAT composites are shown in Figure 4.38. The amounts of water absorption in samples were obtained from the weight differences of the samples before and after exposing to water. All samples showed similar trends of water absorption. For the first 30 days, water was rapidly absorbed into samples after that the rate of water absorption was slow down. Nevertheless, the water absorption of neat PBAT was lower than those of the PBAT composites. This was due to the hydrophobic character of PBAT matrix. Among the PBAT composites, the highest percentage of water absorption was observed in U-RHS/PBAT composites.

The increased water absorption of U-RHS/PBAT composite was due to the free and reactive hydroxyl groups on the RHS particles which exhibited good affinity to water molecules. Besides, there were micro-voids in between PBAT and RHS caused by the difference in the chemical nature of PBAT and RHS. This phenomenon attributed to poorly bonded area and weak interfacial adhesion between the hydrophilic RHS and the hydrophobic PBAT. Therefore, water molecules could easily penetrate into these micro-voids or accumulated at the RHS-PBAT interface. A similar phenomenon was observed by Yang, Kim, Park, Lee, and Hwang (2006) in LDPE composites containing 30% lignocelluloses filler. They found that the excessive water uptake could cause a

filler-matrix debonding in the presence of porosity and inclusions of filler agglomerates. However, the presence of MPS or AA surface modifier formed a hydrophobic layer on RHS surfaces and the percentages of water uptake of MPS-RHS/PBAT and AA-RHS/PBAT composites were slightly decreased as compared with that of U-RHS/PBAT composites. For MPS-RHS/PBAT composites, the water absorption of PBAT composites decreased with increasing MPS content. For AA-RHS/PBAT composites, the water absorption of PBAT composites decreased with increasing reaction time. The mechanism through which water diffuses into polymeric materials can be explained as either infiltration into the free space (*i.e.* micro voids and other morphological defects) or interaction between polymer matrix and filler which controlled by the available hydrogen bond at hydrophilic sites of filler (Unemori, Matsuya, Matsuya, Akashi, and Akamie, 2003). According to Tang *et al.* (2008), the water diffusion mechanism may be related to the barrier contribution of filler inclusions to water transportation. In addition, Tham, Chow, and Ishak (2010) found that the water absorption of PMMA composites significantly decreased after treating HA surface with MPS. This was because MPS molecules, which were physically or chemically attached to the HA surface, formed a film around HA particles and limited the water absorption.

In this study, the amounts of water absorption in PBAT composites were probably controlled by RHS polarity. The treated RHS with MPS or AA reduced RHS polarity and improved interaction between PBAT and the treated RHS leading to the reduction of micro-voids and water absorption.

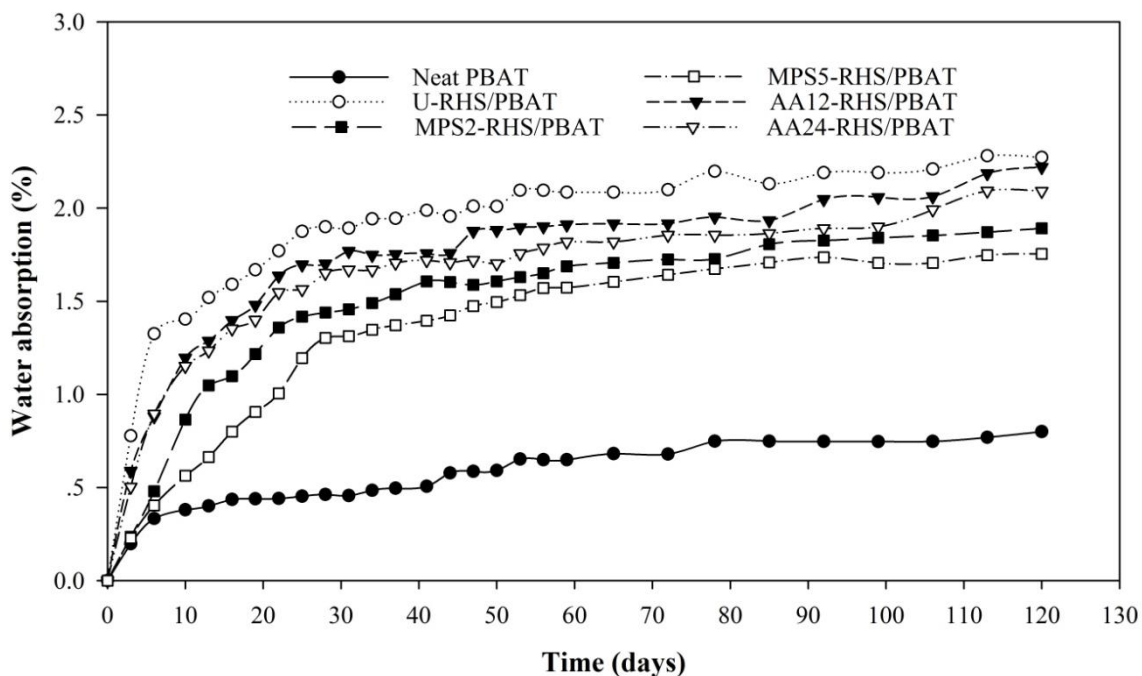
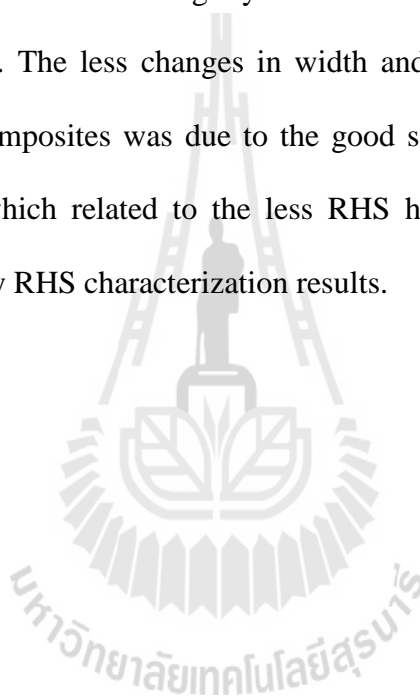


**Figure 4.38** Plots of percentage of absorbed water against immersion time for neat PBAT, U-RHS/PBAT, MPS-RHS/PBAT and AA-RHS/PBAT composites.

#### 4.4.2 Dimension stability of PBAT and RHS/PBAT composites after water absorption

Plots of percentage of width and thickness change against immersion time for neat PBAT, U-RHS/PBAT, MPS-RHS/PBAT and AA-RHS/PBAT composites are shown in Figure 4.39. The changes in width or thickness of samples after water absorption were calculated by the width or the thickness differences between the samples exposed to water and the dried samples. Width and thickness of all samples increased with increasing immersion time. The increase in width and thickness of samples after immersion in water was because the penetrated water molecules inside the sample acted as a force making the distance between the PBAT and RHS (Tham, Chow, and Ishak, 2010). The neat PBAT showed the lowest changes in width and thickness as compared

with those of RHS/PBAT composites. This was due to the hydrophobic character of PBAT. Among RHS/PBAT composites, U-RHS/PBAT composite showed the highest changes in width and thickness. This was due to the good affinity of RHS surface to water molecules and the weak interfacial adhesion between RHS and PBAT. However, the presence of MPS or AA surface modifier formed a hydrophobic layer on RHS surfaces and the percentages of width and thickness changes of MPS-RHS/PBAT and AA-RHS/PBAT composites were slightly decreased as compared with that of U-RHS/PBAT composites. The less changes in width and thickness of MPS-RHS/PBAT and AA-RHS/PBAT composites was due to the good surface adhesion between PBAT and the treated RHS which related to the less RHS hydrophilicity and the less RHS porosity as confirmed by RHS characterization results.



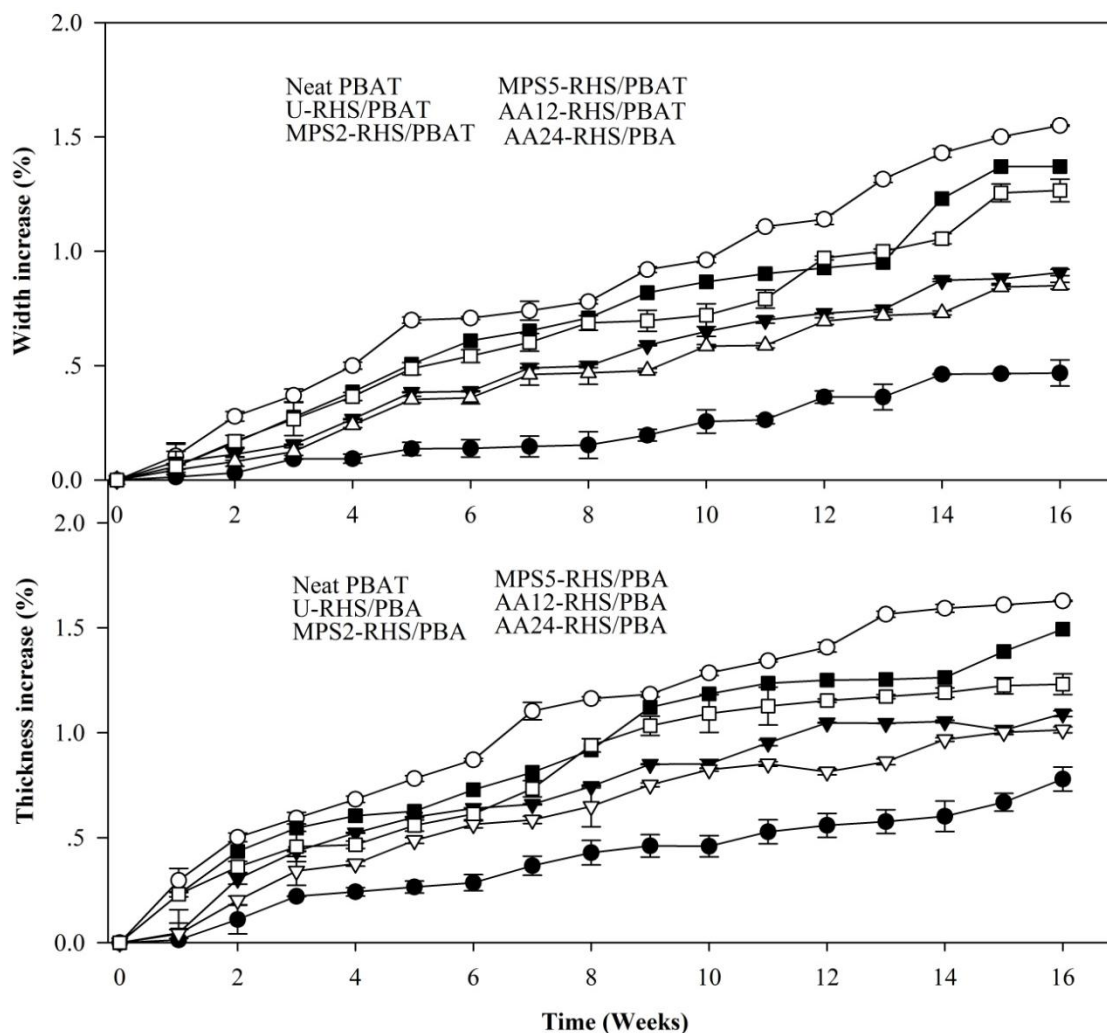


**Figure 4.39** Plots of width and thickness changes against immersion time for neat PBAT, U-RHS/PBAT, MPS-RHS/PBAT and AA-RHS/PBAT composites.

#### 4.4.3 Impact property of PBAT and RHS/PBAT composites after water absorption

Impact strength of neat PBAT, U-RHS/PBAT, MPS-RHS/PBAT and AA-RHS/PBAT composites before and after water absorption are shown in Figure 4.40. All samples revealed the same trends. The impact strength of neat PBAT and PBAT composites after water absorption for 120 days was lower than those before water

absorption. U-RHS/PBAT composites showed the lowest impact strength. This was due to the weak interfacial bonding between PBAT and RHS which induced transportation of water molecules into the sample when soaking in an aqueous environment (Tang *et al.*, 2008). In addition, Espert, Vilaplana, and Karlsson (2004) also reported that a reduction of the impact strength of materials after the water absorption may be due to weak adhesion between matrix and filler under wet conditions.

After water absorption, impact strength of MPS-RHS/PBAT composites and AA-RHS/PBAT composites was slightly higher than that of U-RHS/PBAT composites. In comparison, the impact strength of MPS-RHS/PBAT composites was higher than those of AA-RHS/PBAT composites. According to those reported by Tham, Chow, and Ishak (2010), they studied effect of water absorption on properties of HA/PMMA composites. The mixing of untreated HA particles with polymer showed the poor surface adhesion between HA and PMMA with presence of micro-voids. The micro-voids assented the relaxation of polymer chains and induced transportation of water molecules into the HA/PMMA composites. The flexural strength of the HA/PMMA composites decreased due to the weak interfacial bonding between PMMA and HA. Besides, they suggested that the reduction of flexural strength of the HA/PMMA composites after water absorption could be attributed to the plasticizing effect of water molecules. The diffused water molecules induced volumetric expansion between the matrix and the filler. When the stress exceeded the strength of the interphase region, debonding may take place between the filler and the matrix resulting in an irreversible damage to the composites.

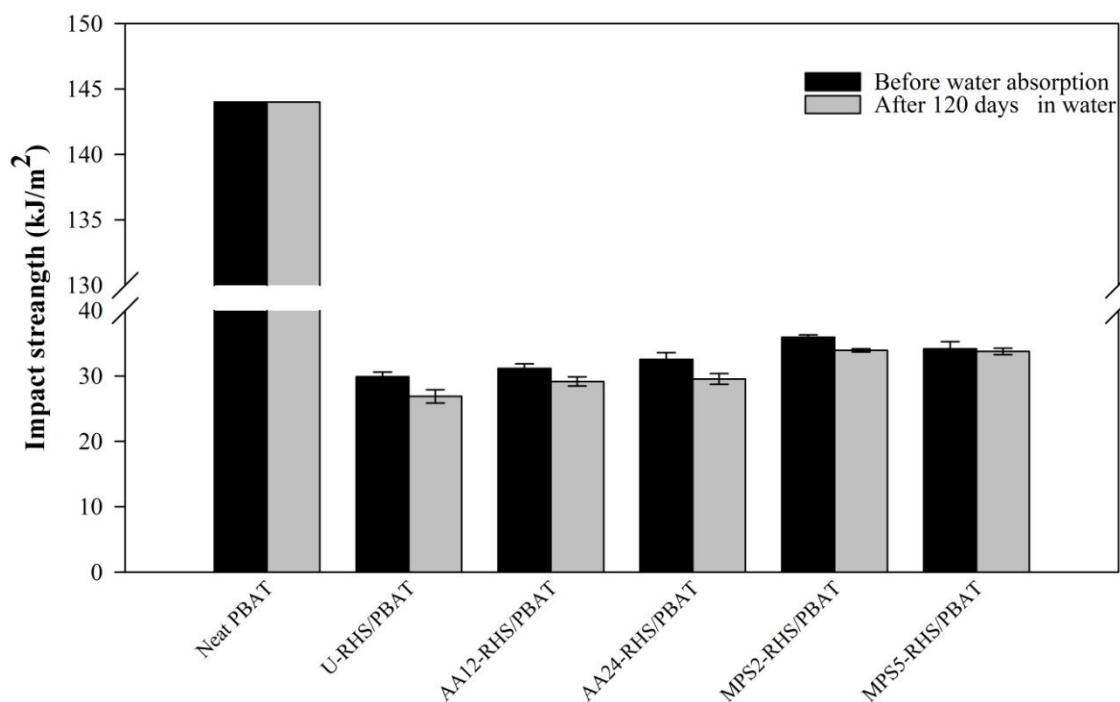


**Figure 4.40** Impact strength of neat PBAT, U-RHS/PBAT, MPS-RHS/PBAT and AA-RHS/PBAT composites.

The changes in physical and mechanical properties including percentage of water absorption, dimension stability and impact property of the PBAT composites after water absorption were characterized. The addition of RHS into PBAT induced the transportation of water into the PBAT matrix leading to the decrease in the dimension stability and the impact strength of the neat PBAT and the PBAT composited after water immersion. The percentages of water absorption in MPS-RHS/PBAT and AA-RHS/PBAT composites were less than that of U-RHS/PBAT composite. On the other hand, their dimension stability and impact strength after water absorption were higher than those of U-RHS/PBAT composite.

## 4.5 Biodegradability of PBAT and RHS/PBAT composites

Biodegradability of PBAT, U-RHS/PBAT, and MPS-RHS/PBAT and AA-RHS/PBAT composites was determined by measuring and comparing their weight, tensile properties and morphological properties before and after soil burial tests as follows.

### 4.5.1 Weight loss of PBAT and RHS/PBAT composites

Weight losses of neat PBAT, U-RHS/PBAT, MPS-RHS/PBAT and AA-RHS/PBAT composites after soil burial tests are plotted against burial time as shown in Figure 4.41. All samples showed the increase in weight loss with increasing soil burial time. It was observed that the rate of weight loss was rapidly increased after burial the samples for 60 days. The weight loss of neat PBAT was lower than those of the RHS/PBAT composites. This meant that the addition of RHS enhanced the biodegradability of PBAT matrix under this composting condition. In contrast, Lee *et al.* (2002) found a decrease in biodegradability of aliphatic unsaturated polyester nanocomposites under composting. They assumed that this was due to the high aspect ratio and the good dispersion of clay in the matrix. Besides, the nano clay formed a more tortuous path which hindered the penetration and the diffusion of microorganisms into the samples. Similarly, Maiti, Batt, and Giannelis (2003) suggested that adding clays into PHB matrix increased crystallinity of PHB matrix, which played a barrier role to reduce the rate of water absorption, leading to the decrease in biodegradation of PHB nanocomposites. However, Han, Lim, Kim, D. K., Kim, M. N., and Im (2008) revealed that the incorporating SiO<sub>2</sub> not only increased crystallinity of PBS matrix but also increased biodegradability of PBS matrix. Thus may be the hydroxyl groups on the

fumed  $\text{SiO}_2$  increased hydrophilicity of the composites resulting in enhanced susceptibility to microbial attack.

Basically, the degradation of biodegradable polymers in compost environment starts with water absorption, ester cleavage and formation of oligomer fragments (Pavlidou and Papispyridesb, 2008). In addition, the presence of hydroxyl groups on filler surface is a responsible factor for degradation of polymer composites since those hydroxyl groups result in preferential water absorption and initiate hydrolysis of the polymer matrix (Ray *et al.*, 2002). So, the increase in biodegradation of PBAT composites as compared with that of neat PBAT in this study was due to the presence of hydroxyl groups of the RHS. These hydroxyl groups on RHS surface initiated hydrolysis of the PBAT matrix after absorbing water from the compost. For this reason, the weight loss of neat PBAT had the lowest while that of U-RHS/PBAT showed the highest among all PBAT composites.

Treating RHS surface with MPS or AA led to the decrease in percentages of weight loss of MPS-RHS/PBAT and AA-RHS/PBAT composites as compared with that of U-RHS/PBAT composites. For MPS-RHS/PBAT composites, the weight loss of PBAT composites decreased with increasing MPS content. For AA-RHS/PBAT composites, the weight loss of PBAT composites decreased with increasing reaction time. The treated MPS or the treated AA molecules decreased the hydrophilicity of RHS. This led to the better dispersion of RHS in PBAT matrix and the increase in interfacial adhesion between PBAT and treated RHS resulting in the decrease in the weight loss compared with U-RHS/PBAT composites. Similar results were reported by Ray *et al.* (2002). They suggested that the biodegradability of organically modified layered silicate/

PLA nanocomposites depended on the presence of terminal hydroxyl groups of the silicate layers. They confirmed this assumption by preparing PLA reinforced with two types of silicates, *i.e.* layered silicate surface without surface modification and organically modified layered silicate which had no terminal hydroxyl edge group. As a result, the degradation of the organically modified layered silicate/PLA nanocomposite was almost the same as that of neat PLA matrix and lower than that of unmodified silicate/PLA nanocomposite.

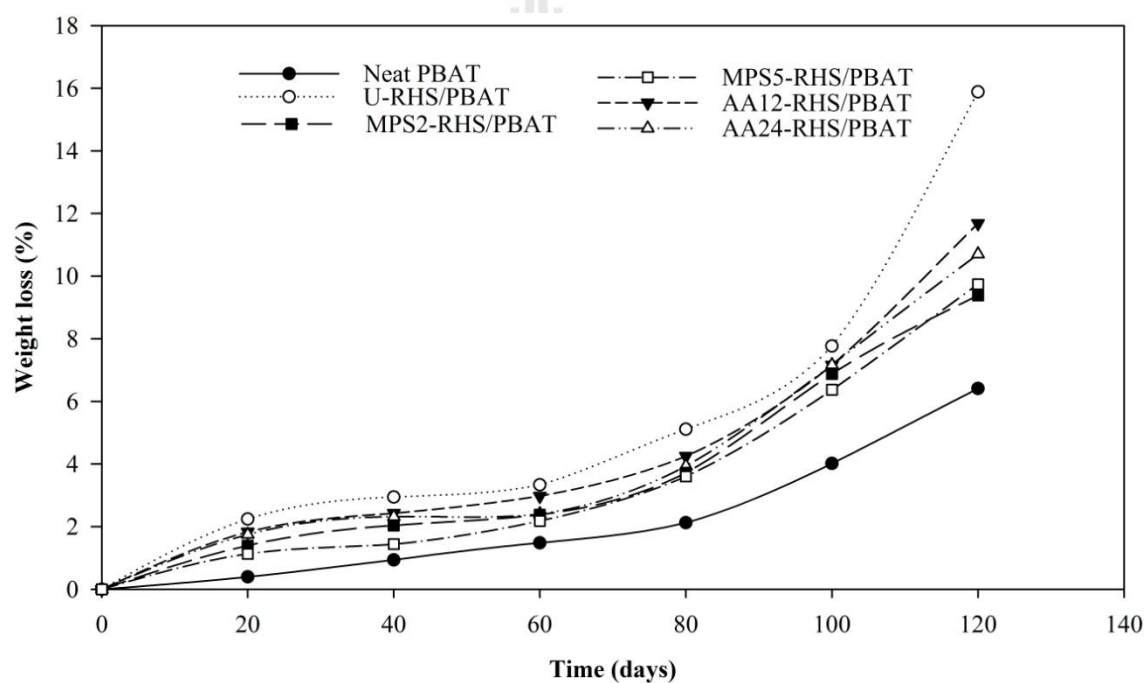


**Figure 4.41** Plots of weight loss after soil-burial tests against burial time for neat PBAT, U-RHS/PBAT, MPS-RHS/PBAT and AA-RHS/PBAT composites.

#### **4.5.2 Tensile properties of PBAT and PBAT composites after soil-burial tests**

The tensile properties, including tensile modulus, tensile strength and elongation at break, of neat PBAT, U-RHS/PBAT, MPS-RHS/PBAT and AA-RHS/PBAT composites without soil-burial tests and after soil-burial tests are shown in Figure 4.42-4.44.

In Figure 4.42, tensile modulus of all samples decreased with increasing burial time. The decrease in tensile modulus of samples after burial under composting environment was because the penetrated water molecules inside the sample acted as a force making the distance between the PBAT and RHS (Tham, Chow, and Ishak, 2010). As compared with PBAT composites, the neat PBAT showed the lowest tensile modulus which linearly decreased with increasing composting time up to 40 days. Among PBAT composites, U-RHS/PBAT composites showed the lowest tensile modulus which linearly decreased with increasing composting time. However, tensile modulus of PBAT composites illustrated indifference after composting of 80 days. Tensile modulus of all PBAT composites seemed to decrease under composting environment more rapidly than that of neat PBAT as seen from their slopes in Figure 4.42. This suggested that the addition of RHS into PBAT induced the increase in PBAT biodegradation rate. After composting, the losses of tensile modulus were approximate 80% in the PBAT composites and 55% in neat PBAT.

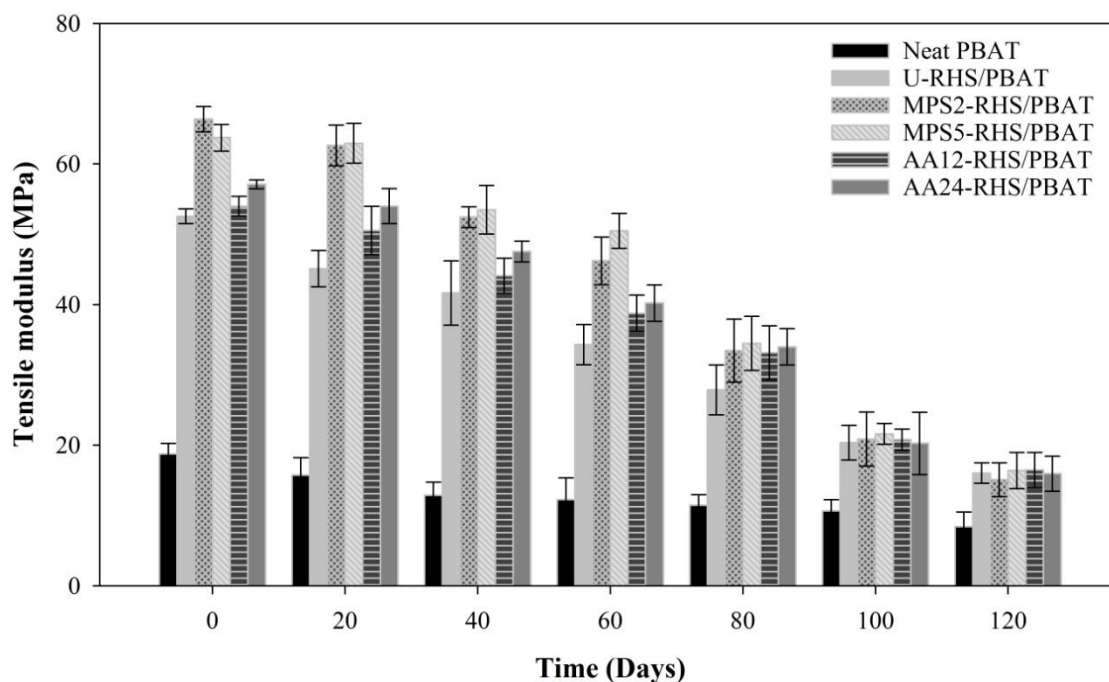


**Figure 4.42** Tensile modulus of neat PBAT, U-RHS/PBAT, MPS-RHS/PBAT and AA-RHS/PBAT composites at various composting times.

In Figure 4.43, elongation at break of all samples decreased with increasing burial time. The decrease in elongation at break of samples after burial under composting environment was because the penetrated water molecules inside the sample acted as a plasticizing and induced the degradability of the composites (Tham, Chow, and Ishak, 2010). Before and after composting test, the neat PBAT showed the highest of elongation at break as compared with those of PBAT composites. Besides, the elongation at break of neat PBAT sharply decreased (more than 50%) after 20-day composting. Among PBAT composites, U-RHS/PBAT composites showed the lowest elongation at break after composting test. After composting, the loss of elongation at break was approximately 90% in RHS/PBAT composites and 98% in neat PBAT.

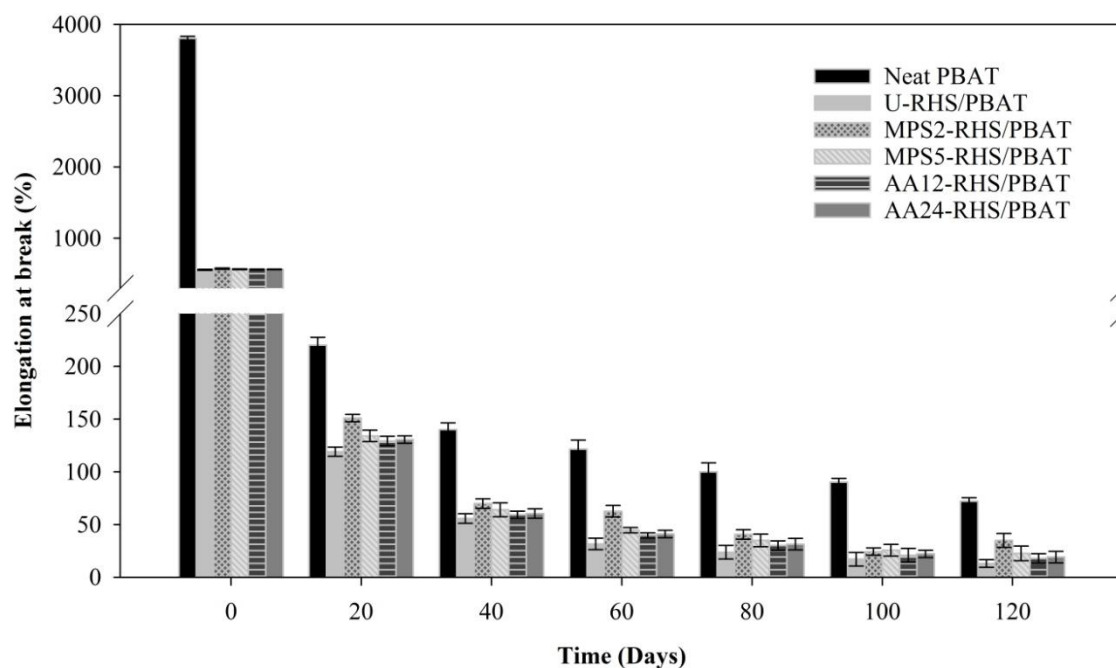


**Figure 4.43** Elongation at break of neat PBAT, U-RHS/PBAT, MPS-RHS/PBAT and AA-RHS/PBAT composites at various composting times.

In Figure 4.44, tensile strength of all samples decreased with increasing burial time. The neat PBAT showed the highest tensile strength. After 20-day composting, tensile strength of neat PBAT significantly decreased (40%). The U-RHS/PBAT composite showed the lowest tensile strength. After composting, the loss of tensile strength was approximately 55% in RHS/PBAT composites and 75% in neat PBAT.

The losses of elongation and tensile strength of neat PBAT were higher than those of RHS/PBAT composites after composting due to the chains scission and the oligomer fragments formation of PBAT matrix (Pavlidou and Papaspyridesb, 2008; Witt *et al.*, 2001).

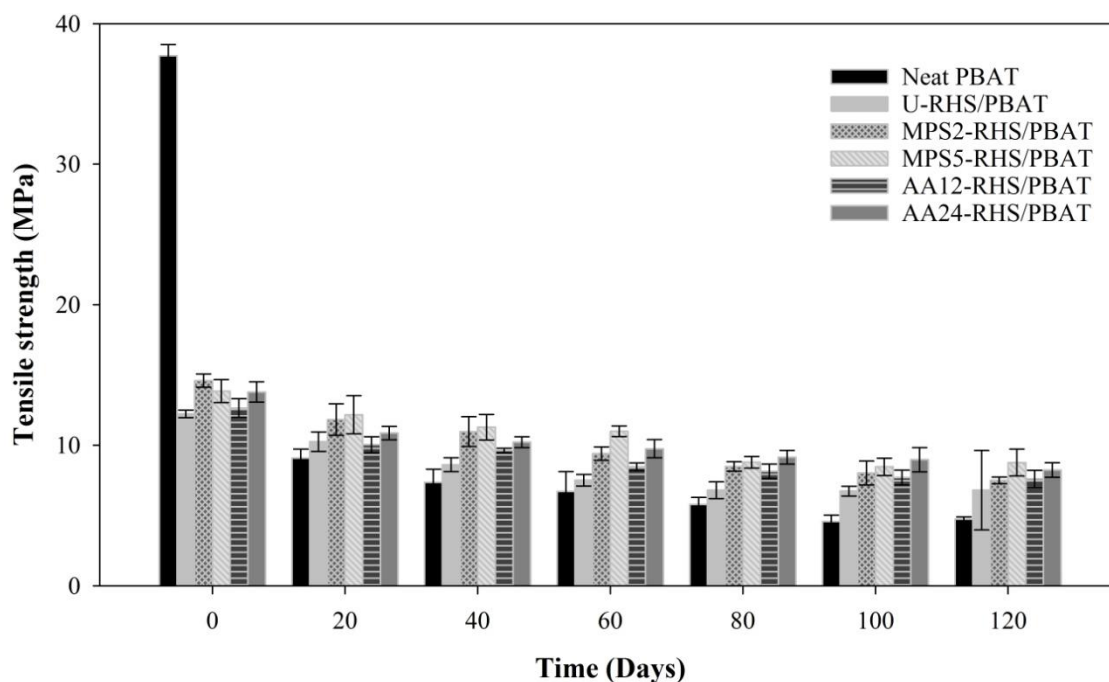


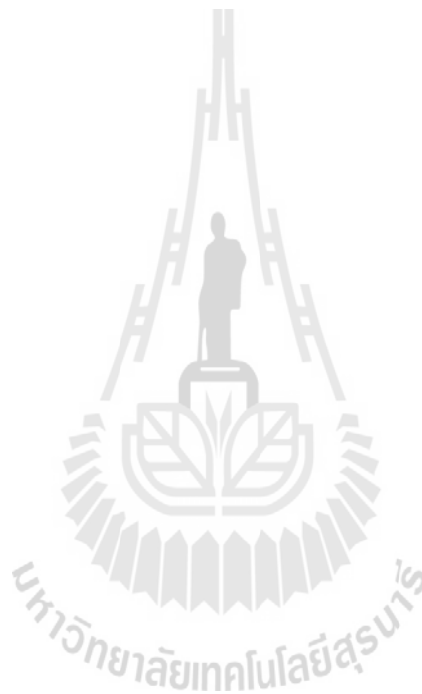
**Figure 4.44** Tensile strength of neat PBAT, U-RHS/PBAT, MPS-RHS/PBAT and AA-RHS/PBAT composites at various composting times.

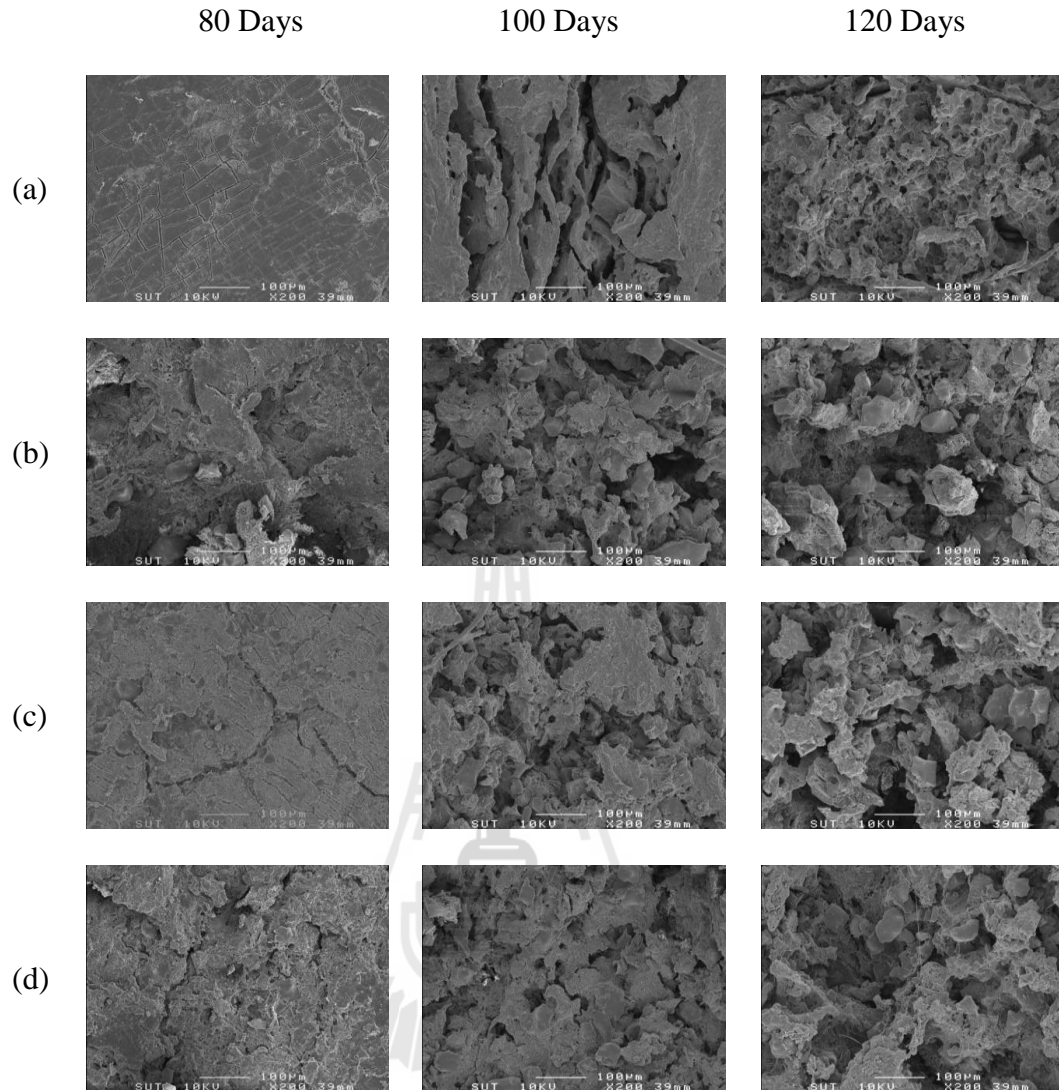
In comparison between MPS-RHS/PBAT and AA-RHS/PBAT composites, the mechanical properties of MPS-RHS/PBAT composites both before and after composting were higher than those of AA-RHS/PBAT composites. From the characterization results of MPS-RHS and AA-RHS, MPS-RHS showed the smaller in size relating to better dispersion of RHS particle in PBAT matrix as compared with AA-RHS. The SEM micrographs also showed that MPS-RHS/PBAT composites had smooth fracture surfaces than that of AA-RHS/PBAT composites. Additionally, the interfacial adhesion between MPS-RHS and PBAT seemed to be stronger than that of AA-RHS and PBAT. As seen in Figure 4.47, the gap between MPS-RHS and PBAT was less than that of AA-RHS and PBAT. This result might be due to high reactivity between MPS and PBAT chain ends (Zou, Wu, and Shen, 2008).

### 4.5.3 Morphological properties of PBAT and RHS/PBAT composites after soil-burial tests

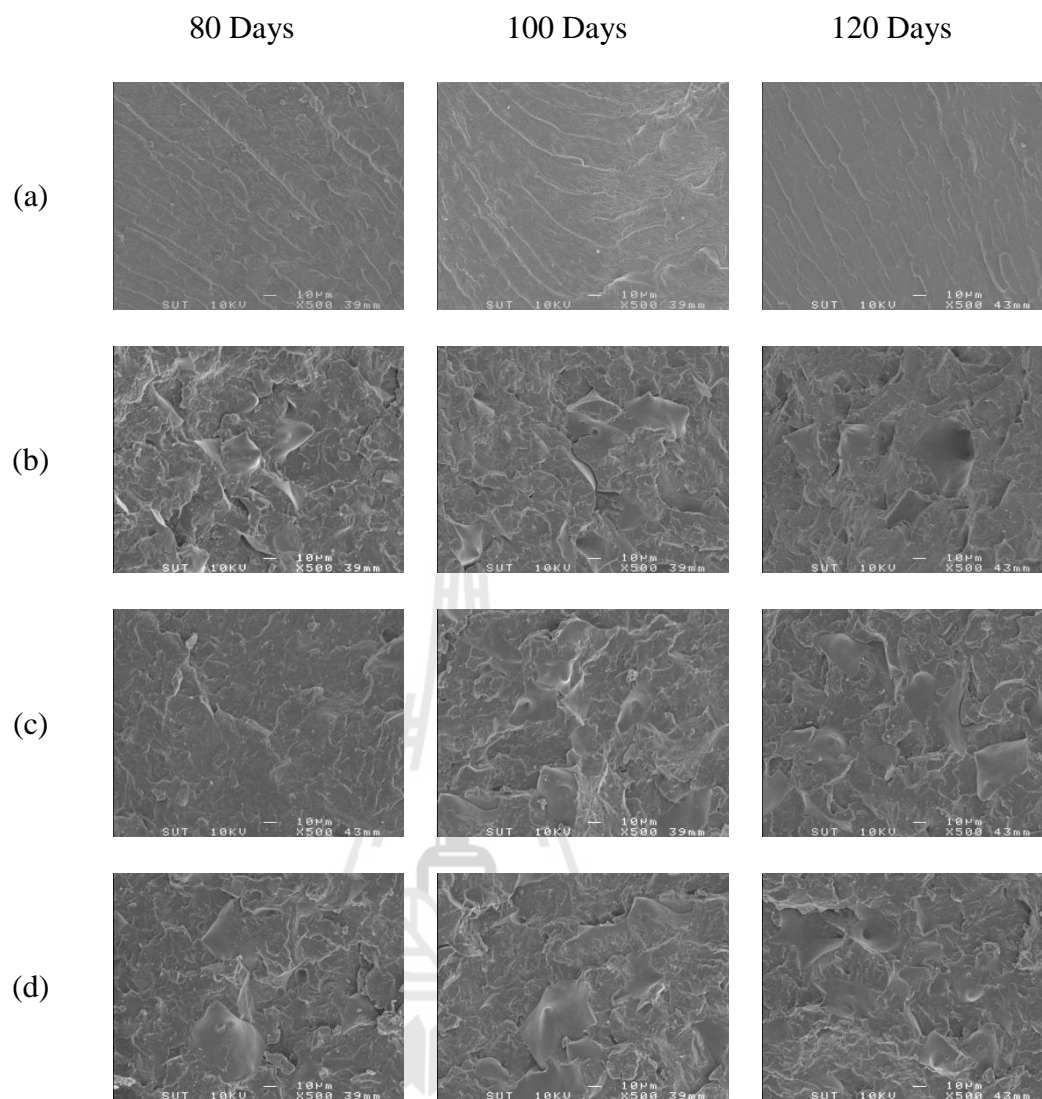
SEM micrographs of outer surface and cryofracture surface of neat PBAT, U-RHS/PBAT, MPS-RHS/PBAT and AA-RHS/PBAT composites after burial under composting condition are shown in Figure 4.45-4.46, respectively. For neat PBAT and PBAT composites, the cracks were observed on the sample surfaces (Figure 4.45) after 80 burial days and continued growing deeper. The outer surface of neat PBAT in Figure 4.45(a) was less severe than those of the RHS/PBAT composites. Also the cryofracture surface of neat PBAT (Figure 4.46(a)) insignificantly changed after 120-day composting. This suggested that neat PBAT had the lowest biodegradability. Additionally, it was also observed that neat PBAT had the lowest weight loss as compared with PBAT composites (section 4.4.2-4.4.5). The U-RHS/PBAT composites in Figure 4.45(b) presented the most severe surface. The cryofracture surface of U-RHS/PBAT composites (Figure 4.46(b)) also showed the worst adhesion between RHS and PBAT compared with other PBAT composites. This suggested that U-RHS/PBAT composite had the highest biodegradation. In addition, U-RHS/PBAT composite had the highest weight loss compared with other PBAT composites. The biodegradation of U-RHS/PBAT composite caused from the rapid absorption of water into the sample. The absorbed water molecules created the crack and generated the degradation at interphase of PBAT composites. Then, micro organism easily penetrated into the PBAT composites. On the other hand, the outer surface of MPS-RHS/PBAT and AA-RHS/PBAT composites (Figure 4.45(c) and 4.45(d)) after 80-day burial time showed relatively mild degradation as compared with that of U-RHS/PBAT composite. After 100-day burial time, the outer surface of all

PBAT composites become relatively severed and their outer surface did not change at that time. Moreover, the cryofracture surface micrographs of MPS-RHS/PBAT (Figure 4.46(c)) and AA-RHS/PBAT (Figure 4.46(d)) composites showed better surface adhesion between RHS and PBAT than that of U-RHS/PBAT because of the improvement of interfacial adhesion between RHS filler and PBAT matrix. Therefore, the penetration of water or micro-organism through RHS-PBAT interface was restrained.

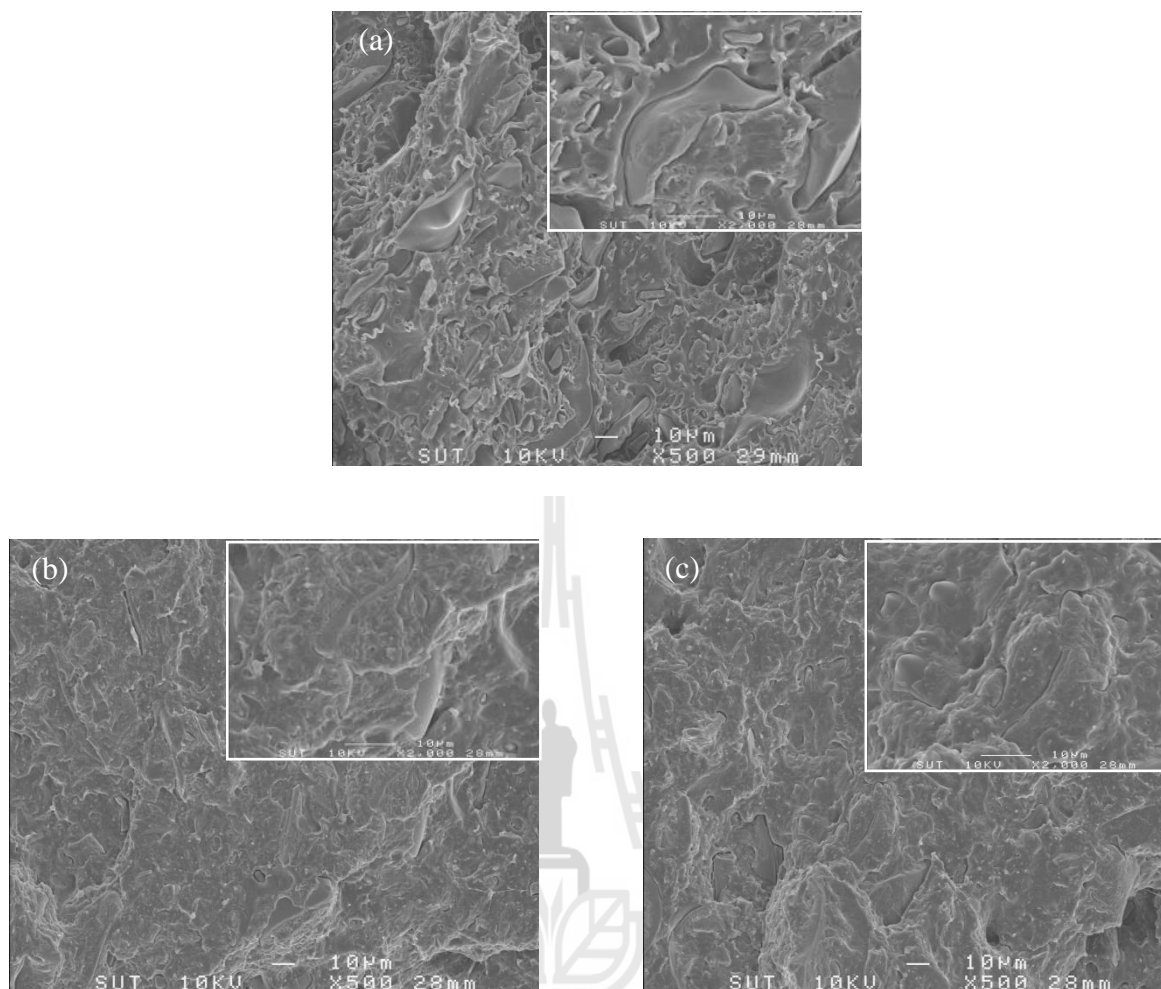




**Figure 4.45** SEM micrographs of surfaces fragmentation of (a) neat PBAT, (b) U-RHS/PBAT, (c) MPS2-RHS/PBAT and (d) AA24-RHS/PBAT composites after soil-burial tests.



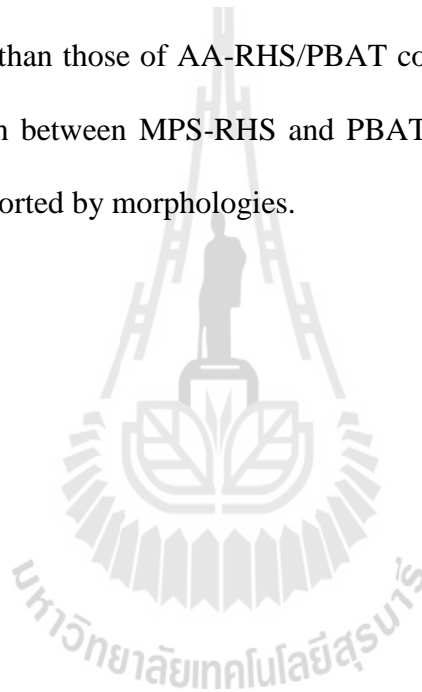
**Figure 4.46** SEM micrographs of cryofracture of (a) neat PBAT, (b) U-RHS/PBAT, (c) MPS2-RHS/PBAT and (d) AA24-RHS/PBAT composites after soil-burial tests.

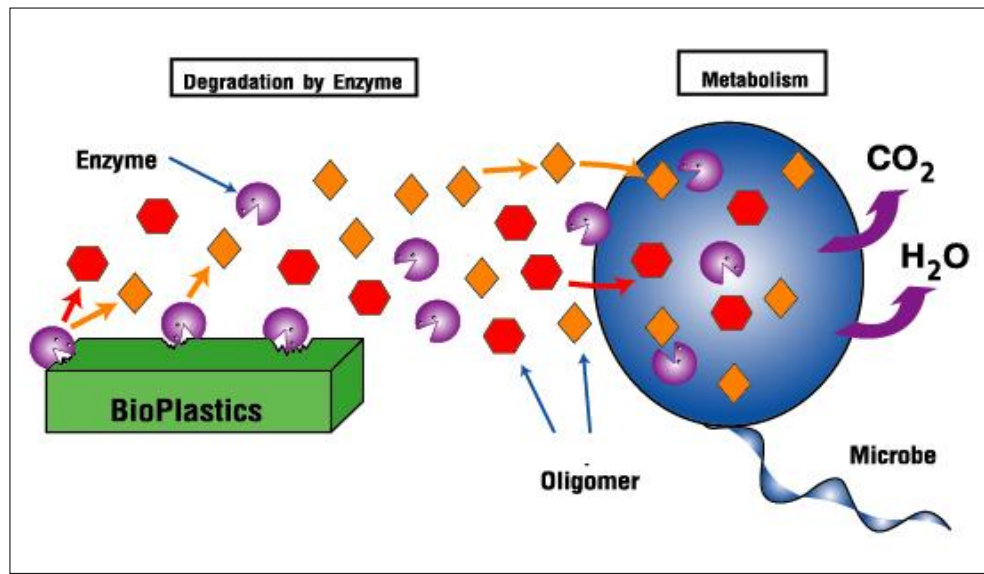


**Figure 4.47** SEM micrographs of impact fracture surfaces of (a) U-RHS/PBAT, (b) MPS2-RHS/PBAT and (c) AA24-RHS/PBAT composites before soil-burial tests.

For the soil burial test, the incorporation of RHS into PBAT matrix tended to increase biodegradability of PBAT under composting. Nonetheless, the biodegradability of MPS-RHS/PBAT and AA-RHS/PBAT composites was less than that of U-RHS/PBAT composites. It was expected that the presence of terminal hydroxyl groups of the RHS might be one of the factors that was responsible for biodegradability

of PBAT under composting. The hydroxyl groups of RHS surface preferentially absorbed water from the composting and started heterogeneous hydrolysis of aliphatic ester linkage of the PBAT matrix. In comparison between MPS-RHS/PBAT and AA-RHS/PBAT composites, the percentage of water absorption, width and thickness changes after water absorption as well as biodegradation after soil burial in compost environment of MPS-RHS/PBAT composites were lower than those of AA-RHS/PBAT composites. However, the impact strength and the tensile properties of MPS-RHS/PBAT composites after water absorption were higher than those of AA-RHS/PBAT composites. This observation may be because the adhesion between MPS-RHS and PBAT was stronger than that of AA-RHS and PBAT as supported by morphologies.





# CHAPTER V

## CONCLUSIONS

RHS was prepared from rice husk by acid leaching and calcination. The RHS was in form of amorphous silica with approximate purity of 97 wt%. The obtained RHS was used as a filler for fabricating poly (butylene adipate-*co*-terephthalate) (PBAT) composites.

Effect of RHS content on properties of RHS/PBAT composites was studied. Various RHS contents (10-60 wt%) were mixed with PBAT in an internal mixer. The incorporation of RHS into PBAT increased crystallinity and viscosity of PBAT composites. In addition, tensile modulus and yield strength of the PBAT composites increased with increasing RHS content while elongation at break and impact strength of PBAT composites decreased with addition of RHS. Additionally, SEM morphologies of PBAT composites revealed a weak surface adhesion between RHS and PBAT. So, RHS surface was modified by two different types of surface modifier, *i.e.* MPS or AA before fabricating the PBAT composites.

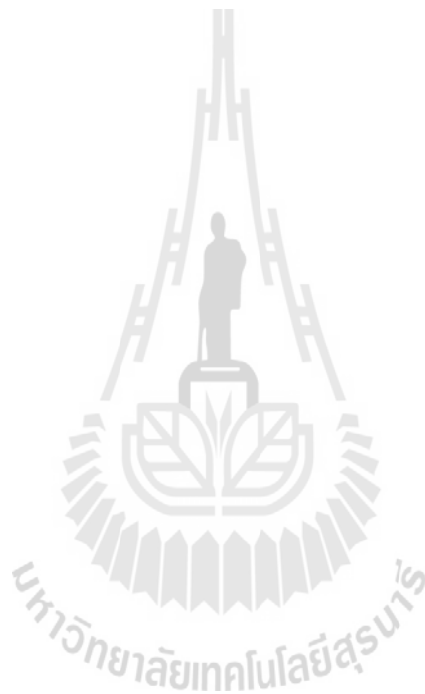
Effect of MPS contents on the properties of MPS-RHS/PBAT composites was studied. MPS-RHS at various MPS contents improved mechanical properties of MPS-RHS/PBAT composites and slightly changed their  $T_d$  and viscosity. In addition, the tensile strength, the impact strengths and the  $T_d$  of the MPS2-RHS/PBAT composites were the highest. Moreover, morphologies of PBAT composites revealed that the surface

adhesion between MPS-RHS and PBAT were better than that of U-RHS and PBAT matrix.

For treating RHS surface with AA, various reaction times, *i.e.* 6, 12 and 24 h were used for the AA-RHS reaction. The AA-RHS/PBAT composites at various times were fabricated. AA-RHS at various reaction times improved mechanical properties of AA-RHS/PBAT composites and slightly changed their  $T_d$  and viscosity. Among the AA-RHS/PBAT composites, the mechanical properties of AA24-RHS/PBAT composites were the highest. Additionally, the SEM morphologies of the composites confirmed that the surface adhesion between AA-RHS and PBAT were better than that of U-RHS and PBAT.

Water absorption, dimension stability and impact property of neat PBAT, and PBAT composites after immersion into water were studied. The addition of RHS into PBAT increased water absorption of PBAT matrix. However, the dimension stability and the impact strength of the PBAT composite after water immersion were decreased. The presence of MPS or AA on RHS surface slightly decreased water absorption of PBAT composites resulting in the increase in dimension stability and impact strength of PBAT composites as compared with those of U-RHS/PBAT composites. Moreover, biodegradability of PBAT and PBAT composites after soil burial tests were determined. The results showed that the addition of U-RHS, MPS-RHS and AA-RHS into the PBAT matrix increased biodegradability of PBAT matrix after composting. However, the biodegradability of MPS-RHS/PBAT and AA-RHS/PBAT composites was delayed as compared with U-RHS/PBAT composites.

In comparison between MPS-RHS/PBAT and AA-RHS/PBAT composites, the mechanical properties of MPS-RHS/PBAT composites were higher than those of AA-RHS/PBAT composites. However, water absorption and biodegradability of MPS-RHS/PBAT composites were lower than those of AA-RHS/PBAT composites.



## REFERENCES

- Abdelmouleh, M., Boufi, S., Belgacem, M. N., and Dufresne, A. (2007). Short natural-fibre reinforced polyethylene and natural rubber composites: Effect of silane coupling agents and fibres loading. **Compos. Sci. Technol.** 67: 1627-1639.
- Ahn, S. H., Kim, S. H., and Lee, S. G. (2004). Surface-modified silica nanoparticle-reinforced poly(ethylene 2,6-naphthalate). **J. Appl. Polym. Sci.** 94: 812-818.
- Arencon, D. and Velasco, J. I. (2009). Fracture toughness of polypropylene-based particulate composites. **Materials.** 2: 2046-2094.
- Bailly, M. and Kontopoulou, M. (2009). Preparation and characterization of thermoplastic olefin/nanosilica composites using a silane-grafted polypropylene matrix. **Polymer.** 50: 2472-2480.
- Bikiaris, D. N., Papageorgiou, G. Z., Pavlidou, E., Vouroutzis, N., Palatzoglou, P., and Karayannidis, G. P. (2006). Preparation by melt mixing and characterization of isotactic polypropylene/sio<sub>2</sub> nanocomposites containing untreated and surface-treated nanoparticles. **J. Appl. Polym. Sci.** 100: 2684-2696.
- Castel, C. D., Jr., T. P., Barbosa, R. V., Liberman, S. A., and Mauler, R. S. (2010). Properties of silane grafted polypropylene/montmorillonite nanocomposites. **Composites Part A.** 41: 185-191.
- Chandrasekhar, S., Pramada, P. N., and Praveen, L. (2005). Effect of organic acid treatment on the properties of rice husk silica. **J. Mater. Sci.** 40: 6535-6544.

- Chen, J.-H., Chen, C.-C., and Yang, M.-C. (2011). Characterization of nanocomposites of poly(butylene adipate-co-terephthalate) blending with organoclay. **J. Polym. Res.** 41: 185-191.
- Chuayjuljit, S., Eiumnoh, S., and Potiyaraj, P. (2001). Using silica from rice husk as a reinforcing filler in natural rubber. **J. Sci. Res. Chula. Univ.** 26: 127-138.
- Della, V. P., Kuhn, I., and Hotza, D. (2002). Rice husk ash as an alternate source for active silica production. **Mater. Lett.** 57: 818–821.
- Dorigato, A., Pegoretti, A., and Penati, A. (2010). Linear low-density polyethylene/silica micro- and nanocomposites: dynamic rheological measurements and modelling. **Polym. Lett.** 4: 115-129.
- Espert, A., Vilaplana, F., and Karlsson, S. (2004). Comparison of water absorption in natural cellulosic fibres from wood and one-year crops in polypropylene composites and its influence on their mechanical prope. **Composites: Part A.** 35: 1267-1276.
- Fu, S.-Y., Feng, X.-Q., Lauke, B., and Mai, Y.-W. (2008) Effects of particle size, particle/matrix interface adhesion and particle loading on mechanical properties of particulate-polymer composites. **Composites: Part B.** 39: 933–961.
- Fuad, M. Y. A., Ismail, Z., Ishak, Z. A. M., and Omar, A. K. M. (1995). Application of rice husk ash as fillers in polypropylene: effect of titanate, zirconate and silane coupling agents. **Eur. Polym. J.** 31: 885-893.
- Galeski, A. (2003). Strength and toughness of crystalline polymer systems. **Prog. Polym. Sci.** 28: 1643-1699.

- Han, S.I., Lim, J. S., Kim, D. K., Kim, M. N., and Im, S. S. (2008). In situ polymerized poly(butylene succinate)/silica nanocomposites: Physical properties and biodegradation. **Polym. Degrad. Stab.** 93: 889-895.
- Hong, Z., Qiu, X., Sun, J., Deng, M., Chen, X., and Jing, X. (2004). Grafting polymerization of L-lactide on the surface of hydroxyapatite nano-crystals. **Polymer.** 45: 6699-6706.
- Hsiang, H. I., Chang, Y. L., Chen, C. Y., and Yen, F. S. (2009). Silane functional effects on the rheology and abrasion resistance of transparent SiO<sub>2</sub>/UV-curable resin nano-composites. **Mater. Chem. Phys.** 120: 476-479.
- Ismail, H., Mega, L., and Khalil, H. A. (2001) Effect of a silane coupling agent on the properties of white rice husk ash–polypropylene/natural rubber composites. **Polym. int.** 50: 606-611.
- Ismail, H., Nasaruddin, M. N., and Ishiaku, U. S. (1999). White rice husk ash filled natural rubber compounds: the effect of multifunctional additive and silane coupling agents. **Polym. Test.** 18: 287-298.
- Ismail, H., Nasaruddin, M. N., and Rozman, H. D. (1999). The effect of multifunctional additive in white rice husk ash filled natural rubber compounds. **Eur. Polym. J.** 35: 1429-1437.
- Ismail, H., Nizam, J. M., and Abdul Khalil, H. P. S. (2001). The effect of a compatibilizer on the mechanical properties and mass swell of white rice husk ash filled natural rubber/linear low density polyethylene blends. **Polym. Test.** 20: 125-133.

- Jiang, L., Zhang, J., and Wolcott, M. P. (2007). Comparison of polylactide/nano-sized calcium carbonate and polylactide/montmorillonite composites: Reinforcing effects and toughening mechanisms. **Polymer**. 48: 7632-7644.
- Kalapathy, U., Proctor, A., and Shultz, J. (2000). A simple method for production of pure silica from rice hull ash. **Bioresour. Technol.** 73: 257-262.
- Lai, Y. H., Kuo, M. C., Huang, J. C., and Chena, M. (2007) On the PEEK composites reinforced by surface-modified nano-silica. **Mater. Sci. Eng. A**. 458: 158-169.
- Lee, S. H., Kim, M. W., Kim, S. H., and Youn, J. R. (2008). Rheological and electrical properties of polypropylene/MWCNT composites prepared with MWCNT masterbatch chips. **Eur. Polym. J.** 44: 1620-1630.
- Lin, J. C. (2008). Investigation of impact behavior of various silica reinforced polymeric matrix nanocomposites. **Compos. Struct.** 84: 125-131.
- Lin, O. H., Akil, H. M., and Mohd Ishak, Z. A. (2009). Characterization and properties of activated nanosilica/polypropylene composites with coupling agents. **Polym. Compos.** 30: 1693-1700.
- Liou, T.H. (2004). Preparation and characterization of nano-structured silica from rice husk. **Mater. Sci. Eng., A**. 364: 313-323.
- Liu, W., Tian, X., Cui, P., Li, Y., Zheng, K., and Yang, Y. (2004). Preparation and characterization of PET/silica nanocomposites. **J. appl. Polym. Sci.** 91 : 1229-1232.
- Lu, H., Hu, Y., Li, M., Chen, Z., and Fan, W. (2006). Structure characteristics and thermal properties of silane-grafted-polyethylene/clay nanocomposite prepared by reactive extrusion. **Compos. Sci. Technol.** 66: 3035-3039.

- Ma, X.k., Lee, N.H., Oh, H.J., Kim, J.W., Rhee, C.K., Park, K.S., and Kima, S.J. (2010). Surface modification and characterization of highly dispersed silica nanoparticles by a cationic surfactant. *Colloids. Surf. A : Physicochem. Eng. Aspects.* 358: 172–176.
- Madera-Santana, T. J., M. Misra, Drzal, L. T., Robledo, D., and Freile-Pelegrin, Y. (2009). Preparation and characterization of biodegradable agar/poly(butylene adipate-co-terephthalate) composites. *Polym. Eng. Sci.* 49: 1117-1126.
- Maiti P., Batt CA., and Giannelis EP. (2003). Renewable plastics: synthesis and properties of PHB nanocomposites. *Polym. Mater. Sci. Eng.* 88: 58-59.
- Marten, E., Muller, R. J., and Deckwer, W. D. (2005). Studies on the enzymatic hydrolysis of polyesters. II. Aliphatic-aromatic copolyesters. *Polym. Degrad. Stab.* 88: 371-381.
- Martin, O. and Averous, L. (2001). Poly (lactic acid): plasticization and properties of biodegradable multiphase systems. *Polymer.* 42: 6209-6219.
- Matinlinn, J. P., Ozcanb, M., Lassilaa, L. V. J., and Vallittua, P. K. (2004). The effect of a 3-methacryloxypropyltrimethoxysilane and vinyltriisopropoxysilane blend and tris(3-trimethoxysilylpropyl)isocyanurate on the shear bond strength of composite resin to titanium metal. *Dent. Mater.* 20: 804-813.
- Metun, D., Tihminlioglu, F., Balkose, D., and Ulku, S. (2004). The effect of interfacial interactions on the mechanical properties of polypropylene/natural zeolite composites. *Composites: Part A.* 35: 23-32.
- Muller, R.-J., Kleeberg, I., and Deckwer, W.-D. (2001). Biodegradation of polyesters containing aromatic constituents. *J. Biotechnol.* 86: 87–95.

- Nabar, Y., Raquez, J. M., Dubois, P., and Narayan, R. (2005). Production of starch foams by twin-screw extrusion: effect of maleated pol (butylene adipate-co-terephthalate) as a compatibilizer. **Biomacromolecules**. 6: 807-817.
- Nurdina, A. K., Mariatti, M., and Samayamutthirian, P. (2011). Effect of filler surface treatment on mechanical properties and thermal properties of single and hybrid filler-filled pp composites. **J. Appl. Polym. Sci.** 120: 857-865.
- Pavlidou, S. and Papaspyridesb, C. D. (2008). A review on polymer-layered silicate nanocomposites. **Prog. Polym. Sci.** 33: 1119-1198.
- Ray, S. S., Yamada, K., Okamoto, M., Akinobu Ogami and Ueda, K. (2003). New Polylactide/Layered Silicate Nanocomposites. **Chem. Mater.** 15: 1456-1465.
- Shumigin, D., Tarasova, E., Krumme, A., and Meier, P. (2011). Rheological and mechanical properties of poly(lactic) acid/cellulose and LDPE/cellulose composites. **Mater. Sci.** 17: 1392-1320.
- Sideridou, I. D. and Karabela, M. M. (2009). Effect of the amount of 3-methacyloxypropyltrimethoxysilane coupling agent on physical properties of dental resin nanocomposites. **Dent. Mater.** 25: 1315-1324.
- Signori, F., Coltelli, M. B., and Bronco, S. (2009). Thermal degradation of poly (lactic acid) (PLA) and poly (butylenes adipate-co-terephthalate) (PBAT) and their blends upon melt processing. **Polym. Degrad. Stab.** 94: 74-82.
- Someya, Y., Kondo, N., and Shibata, M. (2007). Biodegradation of poly(butylene adipate-co-butylene terephthalate)/layered-silicate nanocomposites. **J. Appl. Polym. Sci.** 106: 730-736.

- Someya, Y., Sugahara, Y., and Shibata, M. (2005). Nanocomposites based on poly(butylene adipate-coterephthalate) and montmorillonite. **J. Appl. Polym. Sci.** 95: 386-392.
- Stojanovic, D., Orlovic, A., Glisic, S. B., Markovic, S., Radmilovic, V., Uskokovic, P. S., and Aleksic, R. (2010). Preparation of MEMO silane-coated SiO<sub>2</sub> nanoparticles under high pressure of carbon dioxide and ethanol. **J. Supercrit. Fluids.** 52: 276-284.
- Sun, S., Li, C., Zhang, L., Du, H. L., and Burnell-Gray, J. S. (2006). Effects of surface modification of fumed silica on interfacial structures and mechanical properties of poly(vinyl chloride) composites. **Eur. Polym. J.** 42: 1643-1652.
- Suzuki, K., Siddiqui, S., Chappell, C., Siddiqui, J. A., and Ottenbrite, R. M. (2000). Modification of porous silica particles with poly(acrylic acid). **Polym. Adv. Technol.** 11: 92-97.
- Tan, F. T., Cooper, D. G., Maric, M., and Nicell, J. A. (2008). Biodegradation of a synthetic co-polyester by aerobic mesophilic microorganisms. **Polym. Degrad. Stab.** 93: 1479-1485.
- Tan, X., Xu, Y., Cai, N., and Jia, G. (2009). Polypropylene/silica nanocomposites prepared by in-situ melt ultrasonication. **Polym. Compos.** 30: 835 - 840.
- Tang, J. C., Lin, G. L., Yang, H. C., Jiang, G. J., and Chen-Yang, Y. W. (2007). Polyimide-silica nanocomposites exhibiting low thermal expansion coefficient and water absorption from surface-modified silica. **J. Appl. Polym. Sci.** 104: 4096-4105.

- Tang, J. C., Yang, H. C., Chen, S. Y., and Chen-Yang, Y. W. (2007). Preparation and properties of polyimide/silica hybrid nanocomposites. **Polym. Compos.** 28: 575-581.
- Tham, W. L., Chow, W. S., and Mohd Ishak, Z. A. (2010). Simulated body fluid and water absorption effects on poly(methyl methacrylate)/hydroxyapatite denture base composites. **Exp. Polym. Lett.** 4: 517-528.
- Unemori M., Matsuya Y., Matsuya S., Akashi A., and Akamie A. (2003). Water absorption of poly(methyl methacrylate) containing 4-methacryloxyethyl trimellitic anhydride. **Biomaterials.** 24: 1381-1387.
- Velde, K. V. D. and Kiekens, P. (2002). Thermal degradation of flax: The determination of kinetic parameters with thermogravimetric analysis. **J. Appl. Polym. Sci.** 83: 2634-2643.
- Wang, K., Wu, J., Ye, L., Zeng, H., and Cai, A. (2003). Mechanical properties and toughening mechanisms of polypropylene/barium sulfate composites. **Composites: Part A.** 34: 1199-1205.
- Witt, U., Einig, T., Yamamoto, M., Kleeberg, I., Deckwer, W. D., and Muller, R. J. (2001). Biodegradation of aliphatic aromatic copolyesters: evaluation of the final biodegradability and ecotoxicological impact of degradation intermediates. **Chemosphere.** 44: 289-299.
- Wittayakun, J., Khemthong, P., and Prayoonpokarach, S. (2008). Synthesis and characterization of zeolite NaY from rice husk silica. **Korean J. Chem. Eng.** 25: 861-864.

- Wu, C. L., Zhang, M. Q., Rong, M. Z., and Friedrich, K. (2002). Tensile performance improvement of low nanoparticles filled polypropylene composites. **Compos. Sci. Technol.** 62: 1327-1340.
- Wu, L., Cao, D., and Huang, Y. (2008). Poly (L-lactic acid)/SiO<sub>2</sub> nanocomposites via in situ melt polycondensation of L-lactic acid in the presence of acidic silica sol: Preparation and characterization. **Polymer.** 49: 742-748.
- Yalcin, N. and Sevinc, V. (2001). Studies on silica obtained from rice husk. **Ceram. Int.** 27: 219-224.
- Yan, S., Yin, J., Yang, Y., Dai, Z., Ma, J., and Chen, X. (2007). Surface-grafted silica linked with L-lactic acid oligomer: a novel nanofiller to improve the performance of biodegradable poly(L-lactide). **Polymer.** 48: 1688-94.
- Yang, H. S., Kim, H. J., Park, H. J., Lee, B. J. and Hwang, T. S. (2007). Effect of compatibilizing agents on rice husk flour reinforced polypropylene composites. **Compos. Struct.** 77: 45-55.
- Yao, X., Tian, X., Xie, D., Zhang, X., Zheng, K., Xu, J., G., Zhang, and Pi., Cui (2009). Interface structure of poly (ethylene terephthalate)/silica nanocomposites. **Polymer.** 50: 1251-1256.
- Zou, H., Wu, S., and Shen, J. (2008). Polymer/silica nanocomposites: preparation, characterization, properties, and applications. **Chem. Rev.** 108: 3893-3957.





**APPENDIX A**

**PARTICLE SIZE DISTRIBUTION OF U-RHS**

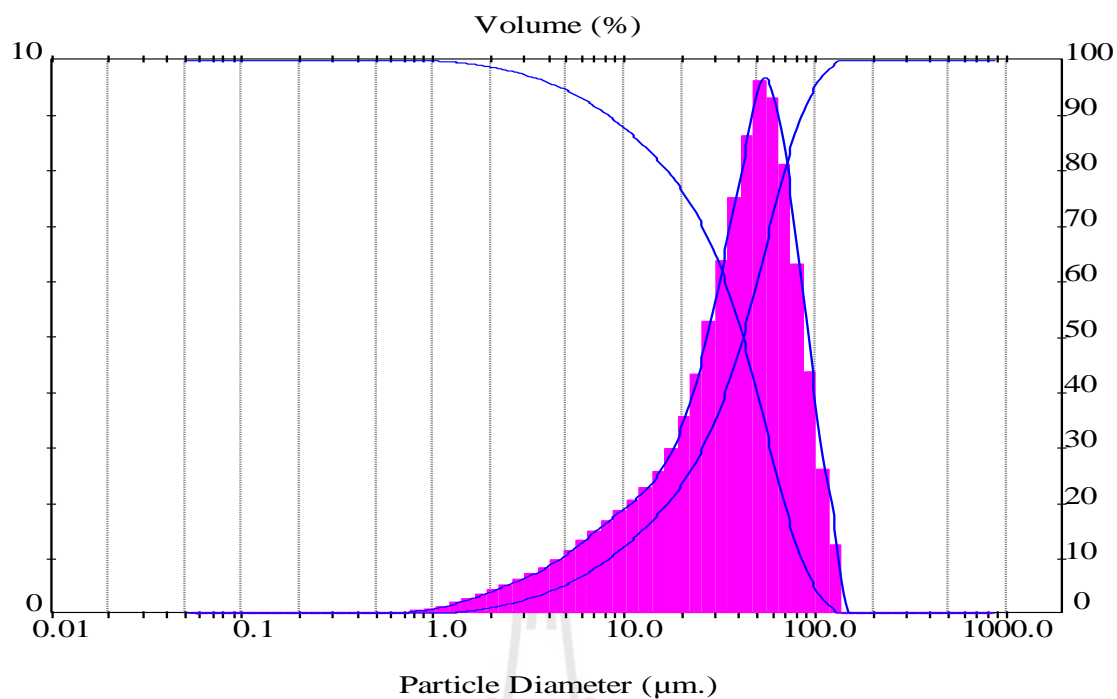
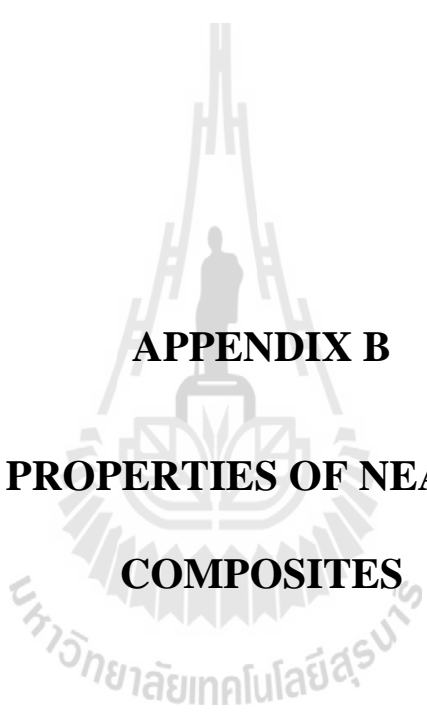


**Figure A.1** Particle size distribution of U-RHS particles.

**Table A.1** Particle size distribution of U-RHS particles.

Particle size distribution	Value (μm)
d (4,3)	46.20
d (v,0.1)	8.80
d (v,0.5)	44.48
d (v,0.9)	84.87



**APPENDIX B**

**MECHANICAL PROPERTIES OF NEAT PBAT AND PBAT  
COMPOSITES**

**Table B.1** Mechanical properties of neat PBAT and PBAT composites at various RHS contents.

Sample	Tensile modulus (Mpa)	Elongation at break (%)	Tensile strength (Mpa)	Yield strength (Mpa)	Impact Strength (kJ/m <sup>2</sup> )
Neat PBAT	18.76±1.49	3801.44±30.35	37.72±0.80	8.71±0.34	>144.00
RHS10/PBAT	29.72±0.68	2101.17±62.80	25.25±0.66	10.62±0.12	>144.00
RHS20/PBAT	42.39±0.26	1172.29±85.45	17.39±0.73	12.12±0.43	>144.00
RHS30/PBAT	52.56±0.86	555.37±7.87	10.05±0.07	12.23±0.22	29.09±0.32
RHS40/PBAT	104.06±6.10	83.92±4.19	13.57±0.74	17.15±0.75	28.20±0.59
RHS50/PBAT	220.06±8.06	47.66±6.59	20.15±0.30	21.30±0.83	27.16±0.65
RHS60/PBAT	414.15±6.90	27.44±3.11	24.51±0.55	24.80±0.72	24.98±0.29

**Table B.2** Mechanical properties of neat PBAT, U-RHS/PBAT and MPS-RHS/PBAT composites at various MPS contents.

Sample	Tensile modulus (Mpa)	Elongation at break (%)	Tensile Strength (Mpa)	Yield strength (Mpa)	Impact Strength (kJ/m <sup>2</sup> )
Neat PBAT	18.76±1.49	3801.44±30.35	37.72±0.80	8.71±0.34	>144.00
U-RHS/PBAT	52.57±0.86	555.37±7.87	10.05±0.07	12.12±0.43	29.09±0.32
MPS0.5-RHS/PBAT	55.37±1.00	587.03±4.39	12.72±0.55	17.23±0.32	32.62±1.22
MPS1-RHS/PBAT	57.61±3.36	577.73±6.61	14.23±0.75	19.99±0.15	33.56±1.10
MPS2-RHS/PBAT	66.37±1.79	571.59±9.78	14.60±0.47	21.99±0.39	35.92±0.34
MPS3-RHS/PBAT	62.55±1.99	565.39±1.62	13.83±0.34	20.24±0.45	34.82±0.36
MPS5-RHS/PBAT	63.75±1.90	564.53±5.60	13.85±0.82	18.91±0.40	34.14±1.09

**Table B.3** Mechanical properties of neat PBAT, U-RHS/PBAT and AA-RHS/PBAT composites at various reaction times.

Sample	Tensile modulus (Mpa)	Elongation at break (%)	Tensile strength (Mpa)	Yield strength (Mpa)	Impact Strength (kJ/m <sup>2</sup> )
Neat PBAT	18.76±1.49	3801.44±30.35	37.72±0.80	8.71±0.34	>144.00
U-RHS/PBAT	52.56±0.86	555.37±7.87	10.05±0.07	12.12±0.43	29.09±0.32
AA6-RHS/PBAT	53.67±1.15	560.29±4.39	10.34±0.27	12.62±0.30	30.07±0.93
AA12-RHS/PBAT	53.99±1.39	561.33±6.61	12.65±0.66	15.55±0.39	31.15±0.69
AA24-RHS/PBAT	57.12±0.63	562.20±4.35	13.79±0.23	17.43±0.21	32.54±1.03

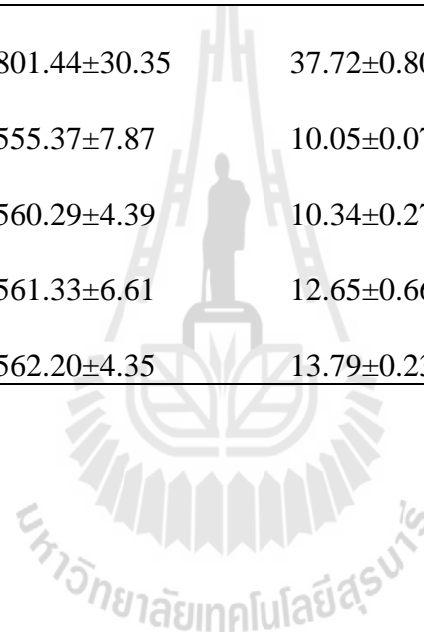


**Table B.4** Tensile strength (Mpa) of neat PBAT, U-RHS/PBAT, MPS-RHS/PBAT and AA-RHS/PBAT composites at various composting times.

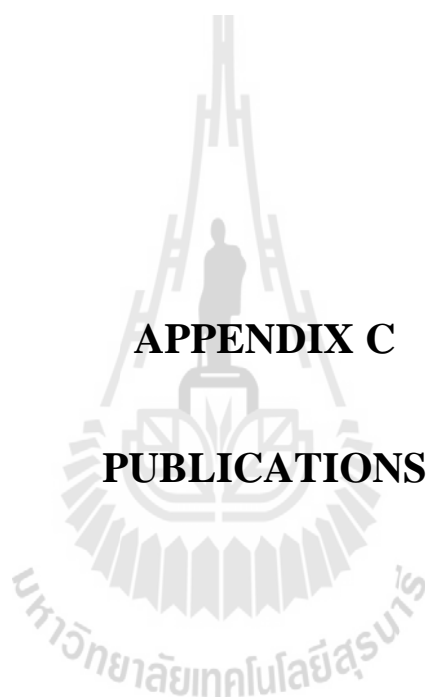
days	PBAT	U-RHS/PBAT	RHS-MPS2/BPAT	RHS-MPS5/BPAT	RHS-AA12/BPAT	RHS-AA24/BPAT
0	37.72±0.80	10.05±0.07	14.60±0.47	13.85±0.82	12.65±0.67	13.79±0.73
20	9.09±0.64	10.26±0.69	11.83±1.12	12.17±1.35	10.04±0.57	10.87±0.48
40	7.36±0.94	8.61±0.49	10.97±1.06	11.29±0.91	9.63±0.16	10.22±0.39
60	6.71±1.42	7.51±0.41	9.41±0.48	11.00±0.37	8.46±0.28	9.75±0.65
80	5.80±0.49	6.80±0.59	8.49±0.33	8.79±0.42	8.14±0.52	9.15±0.49
100	4.58±0.45	6.73±0.34	8.02±0.85	8.47±0.62	7.69±0.53	8.97±0.86
120	4.74±0.17	6.80±2.83	7.49±0.24	8.77±0.96	7.60±0.61	8.23±0.52

**Table B.5** Elongation at break (%) of neat PBAT, U-RHS/PBAT, MPS-RHS/PBAT and AA-RHS/PBAT composites at various composting times.

days	PBAT	U-RHS/PBAT	RHS-MPS2/BPAT	RHS-MPS5/BPAT	RHS-AA12/BPAT	RHS-AA24/BPAT
0	3801.44±30.35	555.38±7.87	571.59±9.79	564.53±5.60	561.33±6.62	562.20±4.35
20	220.07±7.46	119.00±4.45	150.88±3.55	134.00±5.45	129.18±4.46	130.48±3.46
40	140.00±6.45	55.58±4.50	69.77±4.46	63.92±6.50	59.09±3.58	60.39±4.46
60	121.51±8.45	31.51±5.46	62.52±5.46	44.44±2.55	39.62±2.50	40.92±3.49
80	100.00±8.46	23.63±6.55	40.51±4.44	34.81±5.99	29.98±4.50	31.28±5.49
100	90.23±3.49	17.09±6.46	24.33±3.45	25.58±5.50	20.76±6.50	22.06±3.49
120	71.92±3.50	12.95±3.55	34.81±6.50	22.55±6.88	17.72±4.49	19.02±5.49

**Table B.6** Tensile strenmodulus (Mpa) of neat PBAT, U-RHS/PBAT, MPS-RHS/PBAT and AA-RHS/PBAT composites at various composting times.

days	PBAT	U-RHS/PBAT	RHS-MPS2/BPAT	RHS-MPS5/BPAT	RHS-AA12/BPAT	RHS-AA24/BPAT
0	18.76±1.50	52.57±1.05	66.37±1.80	63.75±1.90	53.99±1.39	57.12±0.64
20	15.73±2.48	45.09±2.58	62.65±2.89	62.95±2.84	50.55±3.43	54.01±2.48
40	12.88±1.85	41.64±4.58	52.45±1.48	53.48±3.46	44.10±2.50	47.56±1.48
60	12.26±3.08	34.31±2.85	46.22±3.38	50.48±2.48	38.76±2.58	40.22±2.58
80	11.46±1.48	27.87±3.55	33.44±4.48	34.48±3.85	33.12±3.84	33.98±2.58
100	10.66±1.58	20.34±2.46	20.86±3.84	21.61±1.48	20.80±1.48	20.26±4.44
120	8.42±2.08	16.03±1.44	15.08±2.39	16.38±2.59	16.49±2.48	15.94±2.48



**APPENDIX C**

**PUBLICATIONS**

## List of publications

Phosee, J., Wittayakun, J., and Suppakarn, N. (2010). Mechanical Properties and Morphologies of Rice Husk Silica (RHS)/Poly (butylene adipate-co-terephthalate) (PBAT) Composites : Effect of Filler Content. **In Proceedings of Pure and Applied Chemistry International Conference 2010**, (p.515-519). Ubon Ratchathani, Thailand.

Phosee, J., Wittayakun, J., and Suppakarn, N. (2010). Mechanical Properties and Morphologies of Rice Husk Silica (RHS)/ Poly(butylene adipate-co-terephthalate) (PBAT) Composites: Effect of Silane Coupling Agent. **Adv. Mater. Res.** 123-125 :141-144.

Phosee, J., Wittayakun, J., and Suppakarn, N. (2012). Effect of Acrylic Acid Treated Rice Husk Silica on Properties of Poly (butylene adipate-co-terephthalate) (PBAT) Composites. **Adv. Mater. Res.** 410: 81-85.

## Mechanical properties of rice husk silica (RHS)/ poly (butylene adipate-*CO*-terephthalate) (PBAT): effect of filter content

J. Phosee<sup>1,2</sup>, J. Wittayakun<sup>3</sup>, N. Suppakarn<sup>1,2\*</sup>

<sup>1</sup> School of Polymer Engineering, Institute of Engineering, Suranaree University of Technology,  
Nakhon Ratchasima, Thailand 30000

<sup>2</sup> Center of Excellence for Petroleum, Petrochemicals and Advanced materials,  
Chulalongkorn University, Bangkok, Thailand 10330

<sup>3</sup> School of Chemistry, Institute of Science, Suranaree University of Technology,  
Nakhon Ratchasima, Thailand 30000

\*E-mail: nitinat@sut.ac.th

**Abstract:** Poly (butylene adipate-*co*-terephthalate) (PBAT) is an interesting biodegradable polymer but it is expensive compared to other plastics with similar properties. To encourage the uses of PBAT and other biodegradable plastics, properties such as mechanical properties has to be improved to suit applications at the competitive cost. This work aimed to prepare a composite between PBAT and rice husk silica (RHS), PBAT/RHS. Amorphous silica with 97% purity was obtained after refluxing and burning rice husk. The amount of RHS in the range of 10-60 %wt was used as a reinforcing filler in the PBAT composites. Stress-strain curves of PBAT composites indicated the changes from ductile to brittle behaviors at the RHS content beyond 30%wt. Incorporation of the RHS into PBAT increased the modulus while decreased elongation at break, tensile strength and impact strength of PBAT composites. SEM micrographs of tensile fracture surfaces of the composites showed poor distribution of RHS and weak adhesion between RHS and PBAT matrix.

### Introduction

Plastics materials are used vastly for various applications in daily basis but not many of them are biodegradable leading to environmental problems. Thus, it is necessary to develop biodegradable polymers with acceptable properties and reasonable cost.

Polyesters are good candidates because they consist of potentially hydrolyzable ester bonds. The aromatic polyesters exhibit excellent properties but are resistant to microbial attack. On the other hand, aliphatic polyesters are biodegradable but lack of important properties for applications [1-4]. To combine good material properties with biodegradability, a special type of biodegradable aliphatic-aromatic copolyester, poly (butylene adipate-*co*-terephthalate) (PBAT), was developed by BASF. PBAT is an alternative form of petrochemical plastics used mainly in biodegradable packaging [5-7]. Although PBAT is compostable, good water and tear resistant, high elongation at break, properties such as modulus of elasticity, thermal stability and gas barrier properties have to be improved to suit the applications. The mechanical properties of PBAT can be enhanced

by either blending it with other biodegradable or non-biodegradable polymers [7] such as poly (lactic acid) (PLA) or mixing with a reinforcing filler such as montmorillonite (MMT), silica (SiO<sub>2</sub>) to fabricate filler/polymer composites [7-9].

Rice husk, considered as an agricultural waste and abundantly available in Thailand, can be used as a silica source with high purity and low cost. [10-11]. Silica is widely used in various products in electronics, ceramic, and polymer material industries because it has good abrasion resistance, electrical insulation and high thermal stability. Silica has been proposed as an attractive filler for biodegradable polymer matrices because it can improve thermal and mechanical properties and increase gas barrier properties [12-14]. Such properties can be achieved by a homogeneous dispersion in polymer matrix and high interfacial adhesion between the filler and PBAT matrix due to micrometer size of silica [15].

The objective of this study is to improve properties of PBAT matrix by using rice husk silica (RHS) as a filler. Effect of RHS content on mechanical properties of the RHS/PBAT composite was studied.

### Materials and Methods

Rice husk was obtained from a local rice mill in Nakhon Ratchasima, Thailand. Poly(butylene adipate-*co*-terephthalate) (PBAT, Ecoflex F111 BX 7011) was purchased from BASF. Hydrochloric acid (37%wt HCl) for RHS extraction was purchased from Carlo-Erba.

Rice husk was washed thoroughly with water to remove the adhered soil and dust, and dried in open air. The dried rice husk was refluxed in 3M HCl solution for 3 h, filtered and washed repeatedly with water until the filtrate was neutral. After the acid treatment, the rice husk was dried at 100 °C overnight and burned in furnace muffle at 550 °C for 5 h to remove organic contents.

PBAT / RHS composites were prepared using an internal mixer (Hakke Rheomix 3000P). The mixing temperature was 150 °C, the rotor speed was 50 rpm and the mixing time was 15 min. PBAT pellets and

## Mechanical Properties and Morphologies of Rice Husk Silica (RHS)/ Poly (butylene adipate-co-terephthalate) (PBAT) Composites: Effect of Silane Coupling Agent

Jirapa Phosee<sup>1, 2, a</sup>, Jatuporn Wittayakun<sup>3, b</sup>, Nitinat Suppakarn<sup>1, 2, c\*</sup>

Corresponding to: Nitinat Suppakarn (nitinat@sut.ac.th)

<sup>1</sup> School of Polymer Engineering, Institute of Engineering,  
 Suranaree University of Technology, Nakhon Ratchasima, Thailand

<sup>2</sup> Center of Excellence for Petroleum, Petrochemicals and Advanced Materials,  
 Chulalongkorn University, Bangkok, Thailand

<sup>3</sup> School of Chemistry, Institute of Science, Suranaree University of Technology,  
 Nakhon Ratchasima, Thailand

<sup>a</sup>yoyo\_yok7217@hotmail.com, <sup>b</sup>jatuporn@sut.ac.th, <sup>c</sup>\*nitinat@sut.ac.th

**Keywords:** Rice husk silica, Poly (butylene adipate-co-terephthalate) (PBAT), Silane coupling agent, Composites, Mechanical properties.

**Abstract.** In this work, rice husk silica (RHS), obtained from rice husk waste, was used as a reinforcing filler for preparing PBAT composites. The RHS surface was modified using a silane coupling agent, *i.e.*  $\gamma$ -methacryloxypropyltrimethoxysilane (MPS), in order to facilitate interfacial adhesion between PBAT matrix and RHS filler. The contents of MPS were varied between 0.5 - 5.0 % based on weight of RHS. FTIR spectra indicated the appearance of MPS molecules on RHS surface. Untreated RHS and MPS treated RHS were used to produce RHS/PBAT composites containing 30%wt RHS. The results showed that mechanical properties of the PBAT composites can be enhanced by treating RHS surface with 2 %wt MPS.

### Introduction

Plastics materials are used in various applications in daily basis but not many of them are biodegradable leading to environmental problems. Thus, it is necessary to develop biodegradable polymers with acceptable properties and reasonable cost [1]. Poly (butylene adipate -co-terephthalate) (PBAT) is a biodegradable polymer extensively used to produce fibers, films, and packaging materials due to its good resistance to creep fracture and fatigue. To encourage the uses of PBAT as well as other biodegradable plastics, their properties such as modulus of elasticity and gas barrier properties still need to be improved to suit applications at a competitive cost [2-4]. The mechanical properties of PBAT can be enhanced by either blending with other polymers or mixing with a reinforcing filler such as montmorillonite (MMT), silica (SiO<sub>2</sub>) [5].

Rice husk, considered as an agricultural waste and abundantly available in Thailand, can be used as a silica source with high purity and low cost [6]. Rice husk silica (RHS) has been proposed as an attractive filler for biodegradable polymer matrices because it can improve thermal and mechanical properties and increase gas barrier properties of the polymer composites [7]. So, the RHS was used as a filler for producing PBAT composites in this study. However, adhesion between RHS and PBAT are rather poor. The direct mixing of RHS with PBAT leads to the RHS agglomeration within PBAT matrix and deterioration of mechanical properties of the composites [8]. This limits load bearing application of the composites. In order to introduce appropriate interfacial interaction between surface of inorganic particles and organic matrix, the particles have to be modified before use [9].

## Effect of Acrylic Acid Treated Rice Husk Silica on Properties of Poly (butylene adipate-co-terephthalate) (PBAT) Composites

Jirapa Phosee<sup>1,2,a</sup>, Jatuporn Wittayakun<sup>3,b</sup> and Nitinat Suppakarn<sup>1,2,c\*</sup>

<sup>1</sup>School of Polymer Engineering, Institute of Engineering,  
 Suranaree University of Technology, Nakhon Ratchasima, 30000 Thailand

<sup>2</sup>Center for Petroleum, Petrochemicals and Advanced Materials,  
 Chulalongkorn University, Bangkok, 10330 Thailand

<sup>3</sup>School of Chemistry, Institute of Science,  
 Suranaree University of Technology, Nakhon Ratchasima, 30000 Thailand

<sup>a</sup>jirapa.polymer@gmail.com, <sup>b</sup>jatuporn@sut.ac.th, <sup>c</sup>nitinat@sut.ac.th

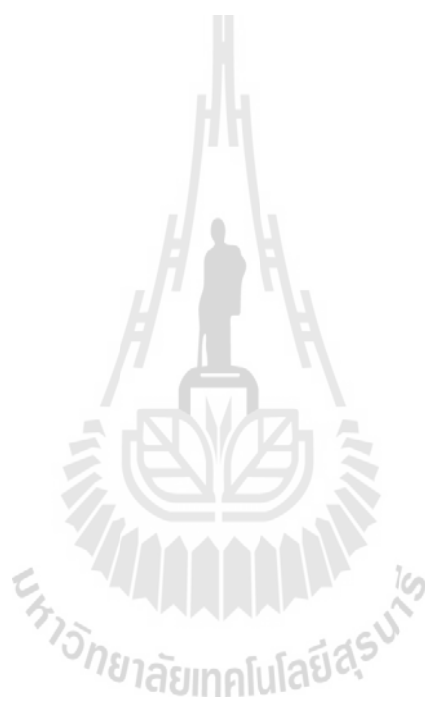
**Keywords:** rice husk silica, poly (butylene adipate-co-terephthalate) (PBAT), acrylic acid, composites.

**Abstract.** In this work, rice husk silica (RHS), obtained from rice husk waste, was used as a reinforcing filler for preparing PBAT composites. In order to facilitate interfacial adhesion between PBAT matrix and RHS filler, the RHS surface was treated with acrylic acid (AA) at a reaction temperature of 140°C. The RHS to AA weight ratio was fixed while the reaction times were varied between 3-24 h. TGA results and FTIR spectra indicated the appearance of AA molecules on RHS surface. Untreated RHS (U-RHS) and AA treated RHS (AA-RHS) were used to produce PBAT composites. The filler content was 30 wt%. Tensile properties and impact strength of AA-RHS/PBAT composites were higher than those of U-RHS/PBAT composite. As revealed by SEM micrographs, AA-RHS was well dispersed in PBAT matrix and the interfacial adhesion between RHS surface and PBAT matrix was improved.

### Introduction

Plastics materials are used in various applications in daily basis but not many of them are biodegradable leading to environmental problems. Thus, it is necessary to develop biodegradable polymers with acceptable properties and reasonable cost [1]. Poly (butylene adipate-co-terephthalate) (PBAT) is a biodegradable polymer extensively used to produce fibers, films, and packaging materials due to its good resistance to creep fracture and fatigue. To encourage the uses of PBAT as well as other biodegradable plastics, their properties such as modulus of elasticity and gas barrier properties still need to be improved to suit applications at a competitive cost [2-4]. The mechanical properties of PBAT can be enhanced by either blending with other polymers or mixing with a reinforcing filler such as montmorillonite (MMT), silica (SiO<sub>2</sub>) [5].

Rice husk, considered as an agricultural waste and abundantly available in Thailand, can be used as a silica source with high purity and low cost [6]. Rice husk silica (RHS) has been proposed as an attractive filler for biodegradable polymer matrices because it can improve thermal and mechanical properties of polymer composites [7]. In our previous work, RHS was used as a filler for producing PBAT composites [8]. It was found that the direct mixing of RHS with PBAT led to the RHS agglomeration within PBAT matrix and the deterioration of mechanical properties of the composites since their interfacial adhesion were rather poor [8]. This limits load bearing application of the composites. In order to introduce appropriate interfacial interaction between surface of inorganic particles and organic matrix, the particles have to be modified before use [9]. This work proposed an approach to enhance interfacial adhesion between RHS and PBAT. We modified RHS surface using acrylic acid (AA) at various reaction times before adding into PBAT. Then we investigated effect of reaction times on mechanical and morphological properties of RHS/PBAT composites.



## BIOGRAPHY

Ms. Jirapa Phosee was born on June 27, 1985 in Sisaket, Thailand. She earned her Bachelor's Degree in Polymer Engineering from Suranaree University of Technology (SUT) in 2008. After graduation, she continued her Master's degree in Polymer Engineering at School of Polymer Engineering, Institute of Engineering at Suranaree University of Technology. During her master's degree study, she presented two oral and three poster presentations entitled: **“Mechanical Properties and Morphologies of Rice Husk Silica (RHS)/Poly(butylene adipate-co-terephthalate) (PBAT) Composites: Effect of Silane Coupling Agent”** at the 3<sup>rd</sup> International Conference on Multi-Functional Materials and Structures (MFMS 2010) in Jeonju, Korea, **“Effect of Filler Surface Modification on Mechanical Properties and Morphologies of Rice Husk Silica/Poly (butylene adipate-co-terephthalate) (PBAT) Composites”** in the 2<sup>nd</sup> Congress on Research symposium on Petroleum, Petrochemicals and Advance materials, Bangkok, Thailand, **“Effect of Acrylic Acid Treated Rice Husk Silica on Properties of Poly (butylene adipate-co-terephthalate) (PBAT) Composites”** in the processing and Fabrication of Advanced materials (PFAM 2011) in Hong Kong and **“Effect of Filler Content on Mechanical Properties and Morphologies of Rice Husk Silica (RHS)/ Poly (butylene adipate-co-terephthalate) (PBAT) Composites”** in the 1<sup>st</sup> Congress on Research symposium on Petroleum, Petrochemicals and Advance materials, Bangkok, Thailand, respectively.

